University of Genova- Fondazione Istituto Italiano di Tecnologia (IIT)

MAPPING LOW-FREQUENCY FIELD POTENTIALS IN BRAIN CIRCUITS WITH HIGH-RESOLUTION CMOS ELECTRODE ARRAY RECORDINGS

Ph.D. Thesis

in partial fulfilment of the requirements for the doctoral school:
"NEUROSCIENCES AND NEUROTECHNOLOGIES (5519)"
at University of Genova and the Italian Institute of Technology (IIT)
(XXXII-cycle)

Candidate: Zordan Stefano

Supervisor: Dr. Luca Berdondini

Referee(s): Stefano Vassanelli, Associate professor of Physiology

Department of Biomedical Sciences of the University of Padova

Michele Giugliano, Assistant professor and Principal investigator

Neuronal Dynamics Laboratory at SISSA, Trieste

Date of submission of the thesis: 31st January 2020

Herewith I declare, that I prepare my Ph.D. Thesis for the tentative project “Mapping low-frequency field potentials in brain circuits with high-resolution CMOS electrode array recordings" on my own and with no other sources and aids than quoted.

Genova, 31.01.2020 **signature** 

Table of Contents

1 Introduction 5

1.1 The motivation of this PhD thesis 5

1.2 From memory to the hippocampus: a short overview of a long journey 5

1.3 Objectives and structure of this PhD thesis 8

2 Physiological and technological principles 9

2.1 Anatomy of Hippocampus 9

2.1.1 The dentate gyrus 10

2.1.2 The CA subfields 11

2.1.3 The subiculum proper 11

2.1.4 The entorhinal cortex 11

2.1.5 Organization of local circuit connections 12

2.2 Synaptic plasticity 13

2.3 Oscillations: behavioral neural correlates 15

2.3.1 SPW-Rs supported memory consolidation 15

2.4 Electrode neurotechnologies for recording brain signals 17

2.4.1 Passive multielectrode arrays (MEA) 17

2.4.2 Active multielectrode arrays based on CMOS technology (CMOS-MEAs) 18

3 High-resolution CMOS-MEAs recordings of electrically evoked responses in cortico-hippocampal slices and applications for compound testing 20

3.1 Introduction 20

3.2 Materials and methods 23

3.2.1 Brain slices preparation for acute electrophysiology 23

3.2.2 Recording of electrically evoked field-potential responses with high-resolution CMOS-MEA 23

3.2.3 Monitoring the execution of the experiment, data extraction and analysis 24

3.2.4 Shape- and temporal-based waveform classification 24

3.2.5 Statistical analysis of the data from multiple samples and conditions 26

3.3 Results 28

3.3.1 Spatially-resolved LTP with multielectrode high-resolution recordings and waveforms clustering 28

3.3.2 Quantifying compound effects on LTP by clustering responses based on time-delay 29

3.3.3 Identification of highly potentiated “silent” regions 30

3.4 Discussion 31

4 Mapping *in vitro* sharp wave ripples with high resolution electrode array recordings 33

4.1 introduction 33
4.2 Material and methods 35
4.2.1 Brain slices preparation for acute electrophysiology 35
4.2.2 Recording of SPW-R events with high-resolution CMOS-MEA: spontaneous and electrically induced events 35
4.2.3 Anatomical reconstruction and immunostaining 36
4.2.4 Data analysis 36
4.3 Results 40
4.3.1 Revealing different spatiotemporal patterns of SPW-Rs from high-resolution recordings 40
4.3.2 Spatial synchronization maps reveal anatomical layers from electrical recordings 42
4.4 Discussion 43
4.5 Perspectives 47
5 Software development for SiNAPS probe 50
5.1 Introduction 50
5.2 SiNAPS probes 50
5.3 SiNAPS acquisition system architecture 51
5.4 Preliminary experiments 52
5.4.1 Surgical procedures and acute *in vivo* recordings 52
5.5 Control Software development 54
5.5.1 Low level Libraries 54
5.5.2 The GUI Interface 54
5.5.3 Future implementations and improvements 56
5.6 Perspectives 56
6 Overall Conclusion 58
7 Publications 60
7.1 Papers 60
7.2 Conferences 60
8 Cited References 63

1 INTRODUCTION

You have to begin to lose your memory, if only in bits and pieces, to realize that memory is what makes our lives. Life without memory is no life at all (…). Our memory is our coherence, our reason, our feeling, even our action. Without it, we are nothing (…). (I can only wait for the final amnesia, the one that can erase an entire life, as it did my mother's (…)).

Luis Buñuel

1.1 THE MOTIVATION OF THIS PHD THESIS

Neuroscience can nowadays take advantage of recent progress in neurotechnologies that are on the way to provide unprecedented spatial and temporal resolution to record and modulate brain activity. In particular, recent developments of planar multielectrode arrays (MEAs) for *in vitro* electrophysiology based on complementary metal-oxide semiconductor (CMOS) technology allowed scaling the recording capabilities of these devices from a few tens of electrodes to several thousands of densely integrated microelectrodes. Following similar technological concepts, this shift to CMOS-based devices very recently allowed realizing high-resolution implantable electrode array probes for *in vivo* electrophysiology. However, despite providing unprecedented recording performances, these new generations of neurotechnologies are on the way to drastically increase the volume of experimental data that is acquired from each *in vitro* sample or animal model. This challenges the development of experimental methodologies that can exploit these new electrode-based devices as well as of computational tools that can manage such volume of experimental data.

This emerging challenge defines the overall motivations of this PhD thesis. Indeed, in my work, I mainly focused on studying the experimental use of planar CMOS-MEAs on brain tissue and in exploring the potential advantages of this technique by developing dedicated computational tools to analyze the acquired experimental data. As described in the next section, I rather focused on the acquisition and analysis of low-frequency field potentials in the cortico-hippocampal circuit because of their relevance for the process of memory. I also had the chance to contribute to the development of implantable active dense probes under development in the laboratory of IIT in which I developed my PhD. In this respect, my overall motivation was to contribute in setting the ground in computational methods that might be adapted to *in vivo* high-resolution electrophysiological studies.

1.2 FROM MEMORY TO THE HIPPOCAMPUS: A SHORT OVERVIEW OF A LONG JOURNEY

The accumulation of experiences, collectively called memory, is responsible for shaping the individual identity. The emergence of an individual and personal identity is therefore linked to mechanisms that enable mammals and us to recollect the past and to predict future behavior based on these recollections (Buzsáki 2004).

A fundamental question that has driven (and still drives) many studies in neuroscience is "what are these experiences and where are they stored?". Experiences stored in the brain are typically considered to be divided into two major categories: implicit and explicit memories. An engineer would call them unsupervised (or automatic) and supervised storage of data. For a psychologist, the term explicit (or declarative) refers to those experiences that have "conscious" recollections and that can be declared verbally. They include lifetime episodes unique to an individual, such as the date of births of our children, or learning arbitrary facts related to the world we live in. These latter factual or semantic memories lack a unique personal link. In contrast to these consciously experienced

memories, implicit memories represent, for instance, the habituation to the annoying sound of the traffic when living next to a highway, and do not require that we are aware of the memory process (Cave and Squire 1992).

Forming and storing arbitrary associations requires a suitable structure with a large number of connections randomly organized. The six-layer neocortex with its regular modular architecture and mostly local wiring is far from being ideal for such a task. As far as we know, a large part of the modularly organized neocortex is tuned to extract statistical regularities of the world conveyed by our sensors. But there is another piece of cortex, buried deep within the medial temporal lobe of the human brain, where lies a group of many millions of neurons organized into a network that is quite different from what can be found anywhere else in the nervous system. It is a structure whose bulb-like shape, protruding into the lateral ventricles, has captivated anatomists since the first dissections already at the time of classical Egypt. Nowadays defined as the hippocampus, this circuit is composed of a group of brain areas consisting of the dentate gyrus, the hippocampus, the subiculum, the presubiculum, the parasubiculum, and the entorhinal cortex. Interestingly, the basic layout of cells and fiber pathways of the hippocampal formation is quite similar in all mammals, thus denoting its ancestral evolution.

Despite anatomical differences among individual's brain areas, the brain is so heavily interconnected that it is misleading to think about the function of one small part of it in isolation. Rather, all brain regions work together to give rise to the implementation and execution of brain functions. It is nowadays generally recognized that there are multiple types of memory and that the hippocampus is one of the most important circuits, but participate in only in some forms of memory.

Over the centuries, the hippocampus has been proposed as the seat of many functions, ranging from olfaction to motor function and even reason, stubbornness, and inventiveness. The bolognese anatomist Giulio Cesare Aranzi (in 1564) was the first to coin the name "hippocampus" for this deep brain area, undoubtedly because of its shape similarity to the tropical fish. After the advent of microscopy, the hippocampus delivered fascinating pictures of its characteristic, neatly regimented cellular arrangements. Although the hippocampal formation is organized in a very different way from other cortical areas, its study has played an important role to set the ground for unraveling some of the basic principles of cortical organization.

During the last 30 years, the most widely studied cell in the nervous system is the pyramidal neuronal cell of the hippocampus. One reason for this interest has been the peculiar anatomy of the hippocampus, with all principal cells in a single layer and synaptic inputs to the well defined dendritic lamina. A striking example is Camillo Golgi's picture from 1886, where he used his revolutionary new technique to illustrate the unique organization of the hippocampus.

Once formed, hippocampal circuits are not immutable, as synapses throughout the various components of the hippocampal formation show both short-term and long-term changes. The latter includes the intensively studied phenomenon of long-term potentiation (LTP). Research on this form of synaptic plasticity has revealed a range of properties that are highly suggestive of a potential cellular

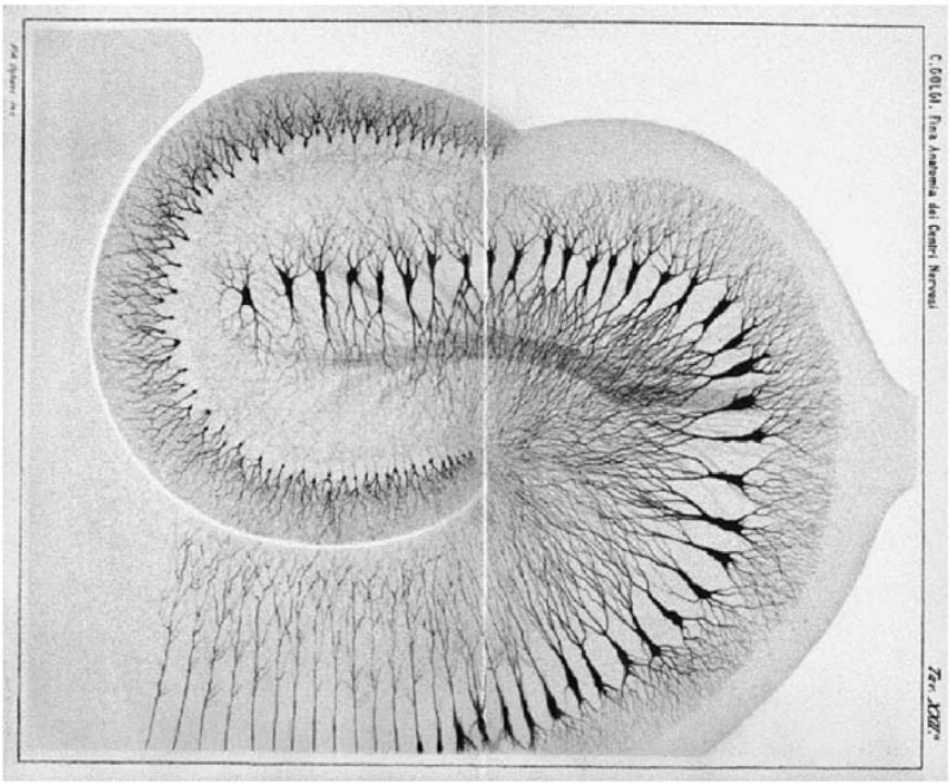

Figure 1.1 Section of the hippocampus stained with the original golgi method *(1886) (from: Andersen, Morris, Amaral, Bliss, & O'Keefe, 2007)*

memory mechanism. The idea that the hippocampal formation is intimately associated with memory is due to observations made on brain-damaged patients by William Scoville and Brenda Milner in 1957. Scoville removed the mesial aspects of the temporal lobes from several patients in an attempt to relieve a variety of neurological and psychiatric conditions. The most famous these, H.M., was a severely epileptic patient whose seizures were resistant to antiepileptic drug treatment. Following surgery, his seizures were reduced, but he was left with profound global amnesia. H.M.'s memory deficit is observable as an inability to remember material or episodes experienced after the surgical intervention (anterograde amnesia); it also includes an inability to recall information experienced for some period of time prior to the surgical intervention (retrograde amnesia). H.M. could remember items for brief periods, provided he was allowed to rehearse and was not distracted. Upon distraction, however, H.M. is rapidly forgetting (Andersen et al. 2007).

An important development in the study of hippocampal functions was the use of implanted microelectrodes to monitor single-neuron activity in the hippocampus of the awake intact animal (Hirano, Best, and Olds 1970; O'Keefe and Dostrovsky 1971; Ranck 1973). Correlating the spiking activity with the animal's location in the environment gave rise to the cognitive map theory, which has fostered research into the spatial functions of the hippocampus (O'Keefe and Dostrovsky 1971). This theory suggested that the hippocampus in animals was dedicated to spatial memory and allows animals to navigate in familiar environments. Extension of this theory to humans envisaged the addition of a temporal signal, allowing the hippocampus to act as a spatiotemporal context-dependent (episodic) memory circuit.

1.3 OBJECTIVES AND STRUCTURE OF THIS PHD THESIS

In my PhD, I aim at studying the application of high-resolution recording technologies and at investigating computational methods adapted to electrophysiological data generated by these devices for the study, as a first step, of the hippocampal circuit. A major technological advance for hippocampal research, and also for the field of neurobiology, was the development of the *in vitro* hippocampal slice preparation. Neurobiological principles that have been discovered from work on *in vitro* hippocampal preparations include, for instance, the identification of excitatory and inhibitory synapses and their localization, transmitters, and receptors, the discovery of long-term potentiation (LTP) and long-term depression (LTD) and oscillations in neuronal networks.

In this context, the initial aim of my work was to optimize the preparation and maintenance of acute cortico-hippocampal brain slices on planar CMOS-MEAs. At first, I focused on experimental methods and computational data analysis tools for drug-screening applications on brain slices based on LTP quantifications. Long-term potentiation (LTP) has been extensively studied with the belief that the mechanisms involved in its generation are essentially the same as those that underlie the synaptic basis of memory (Volianskis et al. 2015). Although the majority of standard protocols still use two electrodes platforms for quantifying LTP, nowadays we can record the electrical activity from many electrodes using recent advancements in large-scale CMOS-MEA devices.

In the second part of my work, I aimed at exploiting the recording resolution of these devices to study the generation of sharp wave ripples (SPW-Rs) in the hippocampal circuit. This research activity was carried out also by visiting the laboratory of Prof. A. Sirota (Ludwig Maximilians University, Munich). In addition to set-up the experimental conditions to record SPW-Rs from planar CMOS-MEAs integrating 4096 microelectrodes, I also explored the implementation of a data analysis pipeline to identify spatiotemporal features that might characterize a different type of SPW-R events.

Finally, I also contributed to the initial implementation of high-density implantable CMOS-probes with the aim of evaluating *in vivo* the algorithms that I investigated for my first's studies on brain slices. With this aim, in the last period of my PhD I worked on the development of a Graphical User Interface for controlling the SiNAPS probes under development in our laboratory (Angotzi et al. 2019), and I participated to preliminary experimental recordings using 4-shank CMOS-probes featuring 1024 simultaneously recording electrodes.

This thesis is structured in 5 chapters. Following Chapter 1 that is aimed at providing an overall introduction to this PhD thesis, the next chapter (Chapter 2) will provide a background on the basic principles of the physiology of the hippocampal circuit and of the electrode-based devices. This will be followed by three chapters reporting on the outcomes of the studies described above, namely Chapter 3 on "High-resolution CMOS-MEAs recordings of electrically evoked responses in cortico-hippocampal slices and applications for compound testing", Chapter 4 on "Mapping *in vitro* sharp wave ripples with high resolution electrode array recordings" and Chapter 5 on "Software development for SiNAPS probes".

2 PHYSIOLOGICAL AND TECHNOLOGICAL PRINCIPLES

The aim of this Chapter is to introduce some basic notions on the physiology of the hippocampal circuit and on neurotechnologies used to functionally investigate this brain circuit. This ground will be further developed toward the specific topics reported in the next Chapters, namely on long-term potentiation (LTP) and on Sharp-Wave-Ripples (SPW-Rs) in Chapters 3 and 4, respectively.

2.1 ANATOMY OF HIPPOCAMPUS

The term hippocampus (derived from the Greek word for the sea horse) was first coined during the sixteenth century by the anatomist Arantius (1587). De Garengeot (1742) named the hippocampus "cornu ammonis" or "Ammon's horn" after the mythological Egyptian god Amun Kneph, whose symbol was a ram.

The hippocampus is a deep brain structure. One of the most captivating features of the hippocampus is its neuroanatomy (**Figure 2.1**). The relatively simple organization of its principal cell layers coupled with the highly organized laminar distribution of many of its inputs has encouraged its use as a model system for modern neurobiology. The hippocampus has three subdivisions: the CA3, CA2, and CA1. (CA comes from cornu ammonis). The other regions of the hippocampal formation include the dentate gyrus, subiculum, presubiculum, parasubiculum, and the entorhinal cortex. Remarkably, the hippocampus is one of the few brain regions that receives highly processed, multimodal sensory information from a variety of neocortical sources (Andersen et al. 2007).

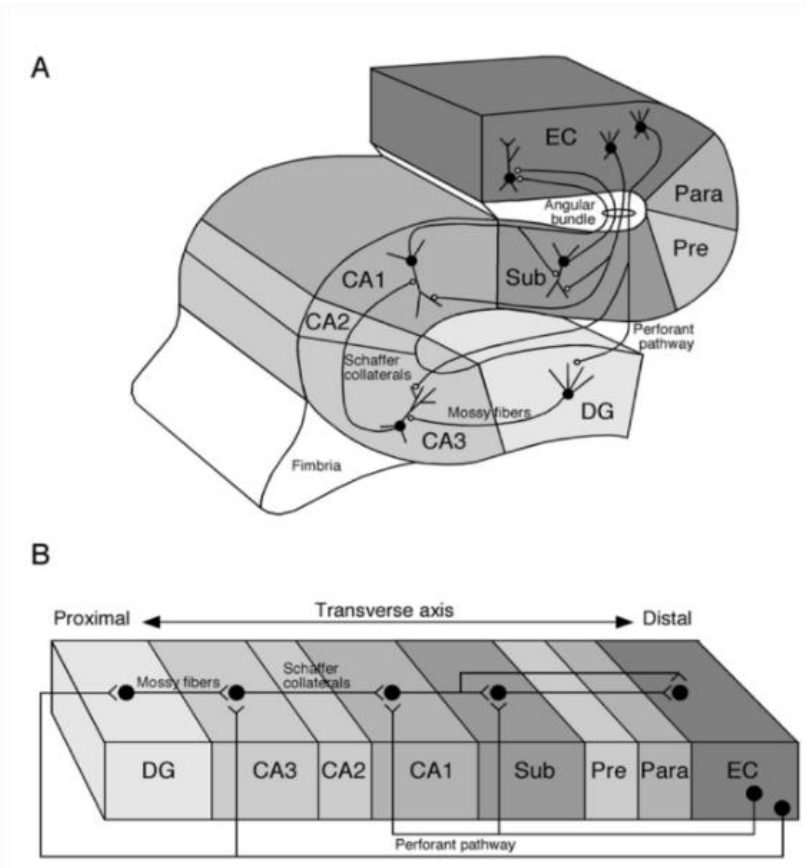

Figure 2.1 Schematic view of the principal pathway of the hippocampus formation *(**A**) Perforant and alvear pathway : EC Layer II to DG and CA3;EC Layer III to CA1 and Sub. Mossy fibers from granule cells of Dg to CA3; Schaffer collaterals from Pyramidal cell in CA3 to CA1 (from Andersen et al. 2007). (**B**) Projection along the transverse axis.*

The entorhinal cortex can be considered as the first input component of the hippocampal circuit. Indeed, much of the neocortical input reaching the hippocampal formation does so through the entorhinal cortex. Cells in the superficial layers of the entorhinal cortex give rise to axons that project, among other destinations, to the dentate gyrus. These projections from the entorhinal cortex to the dentate gyrus define part of the major hippocampal input pathway called the perforant path. Although the entorhinal cortex provides the major input to the dentate gyrus, the dentate gyrus does not project back to the entorhinal cortex. This pathway is therefore unidirectional. The principal cells of the dentate gyrus, the granule cells, give rise to axons called mossy fibers that connect with pyramidal cells of the CA3 field of the hippocampus. The CA3 cells, however, do not project back to the granule cells. The pyramidal cells of CA3, in turn, are the source of the major input to the CA1 hippocampal field (the Schaffer Collateral axons). Following the pattern of its predecessors, CA1 does not project back to CA3. The CA1 field of the hippocampus then projects uni-directionally to the subiculum, providing its major excitatory input. Again, the subiculum does not project back to CA1.

Once reaching the CA1 and the subiculum, the pattern of intrinsic connections becomes more elaborated. The CA1, for example, projects not only to the subiculum, but also to the entorhinal cortex. Furthermore, whereas the subiculum does project to the presubiculum and the parasubiculum, its more prominent cortical projection is directed to the entorhinal cortex. Through these connections both CA1 and the subiculum close the hippocampal processing loop that begins in the superficial layers of the entorhinal cortex and ends in its deep layers. Three major fiber systems are associated with the hippocampal formation. The first is the angular bundle, which carries fibers between the entorhinal cortex and the other fields of the hippocampal formation. The second is the fimbria-fornix pathway through which the hippocampal formation is interconnected with the basal forebrain, hypothalamic, and brain stem regions. The third comprises the dorsal and ventral commissures, through which the hippocampal formation of one hemisphere is connected with the hippocampal formation of the contralateral hemisphere. Unlike the mostly locally organized neocortical neurons, the distribution of the contacts in the recursive and feed-forward projections in the hippocampus is reminiscent of a random graph. Interestingly, the basic hippocampal architecture is common to many species. Yet there are some striking species differences. For example, the compact pyramidal cell layer in the CA1 region of the rat, for example, becomes thicker and more heterogeneous in monkeys and humans.
In the next paragraphs, I will shortly introduce the different sub-circuits forming the hippocampus.

2.1.1 The dentate gyrus

The dentate gyrus (DG) comprises three major layers. Superficially, closest to the hippocampal fissure there is a relatively cell-free layer called the molecular layer. The principal cell layer (granule cell layer) lies deep to the molecular layer and is made up of a densely packed layer that is four to eight granule cells thick. The granule cell and molecular layers (which together are sometimes referred to as the fascia dentata) form a V (or U) shaped structure (depending on the septotemporal position) that encloses a cellular region, the polymorphic cell layer, which constitutes the third layer of the dentate gyrus. The dentate gyrus receives its major input from the entorhinal cortex via the so-called perforant pathway (Ramón y Cajal, 1893). The projection to the dentate gyrus arises mainly from cells located in layer II of the entorhinal cortex, although a minor component of the projection also comes from layers V and VI(Steward and Scoville 1976). It also receives inputs from the septal nuclei, cells, the supramammillary area and prominent noradrenergic input from the pontine nucleus locus coeruleus. The dentate gyrus does not project to any brain region other than the CA3 field of the hippocampus. The axons that project to CA3, the mossy fibers, arise exclusively from the granule cells and terminate in a relatively narrow zone mainly located just above the CA3 pyramidal cell layer(Blackstad et al. 1970; Gaarskjaer 1978; Swanson, Wyss, and Cowan 1978; Claiborne, Amaral, and Cowan 1986)

2.1.2 The CA subfields

The principal cellular layer in the hippocampus is the pyramidal cell layer. The pyramidal cell layer is tightly packed in CA1 and more loosely packed in CA2 and CA3. The narrow, relatively cell-free layer located deep to the pyramidal cell layer is called the stratum oriens. This layer contains the basal dendrites of the pyramidal cells and several classes of interneurons. Deep to the stratum oriens is the thin, fibercontaining alveus. In the CA3 field, but not in CA2 or CA1, a narrow acellular zone, the stratum lucidum, is located just above the pyramidal cell layer and is occupied by the mossy fibers. There is a slight thickening of the stratum lucidum at its distal end, where, at least at septal levels of the hippocampus, the mossy fibers bend temporally and travel longitudinally. The stratum radiatum can be defined as the suprapyramidal region in which the CA3 to CA3 associational connections and the CA3 to CA1 Schaffer collateral connections are located. The most superficial layer of the hippocampus is called the stratum. lacunosum-moleculare. It is in this layer that fibers from the entorhinal cortex terminate. Afferents from other regions, such as the nucleus reuniens of the midline thalamus, also terminate in the stratum lacunosum-moleculare. Both the stratum radiatum and the stratum lacunosum-moleculare contain a variety of interneurons.

Pyramidal neurons are by far the most numerous neurons in the hippocampus. As in the dentate gyrus, however, there is a fairly heterogeneous group of interneurons that are scattered through all layers. Most types of interneuron are found in all the hippocampal subfields. The pyramidal basket cell resides in or close to the pyramidal cell layer, and its dendrites extend into the stratum oriens, stratum radiatum, and stratum lacunosummoleculare. A second type of hippocampal interneuron is the chandelier, or axo-axonic, cell. Their cell bodies, like those of the basket cells, are located in or adjacent to the pyramidal cell layer, and their dendrites span all the hippocampal strata. One class of cells (Lacaille et al. 1987) has been called the O-LM cell (oriens lacunosum-moleclare) and has as its defining feature a dense axonal arbor that is confined to the stratum lacunosum-molecolare.

2.1.3 The subiculum proper

The subiculum is the major output of the hippocampus and receives projections from the CA1 region and EC layer III neurons. This region is subdivided into parasubiculum, presubiculum, postsubiculum, and prosubiculum.

2.1.4 The entorhinal cortex

The entorhinal cortex (EC) provides the major interface of other neocortical areas to the hippocampus. The EC is part of the neocortex with the typical 6-layered structure. Principal neurons are the stellate cells which populate layer II, and the pyramidal neurons, which populate layers II, III, and V. As mentioned above, principal cells from layer II of EC are projecting to the dentate gyrus and CA3, while layer III neurons are innervating the CA1 region and the subiculum. Inputs from the hippocampus are impinging on the deeper layer V of the EC.

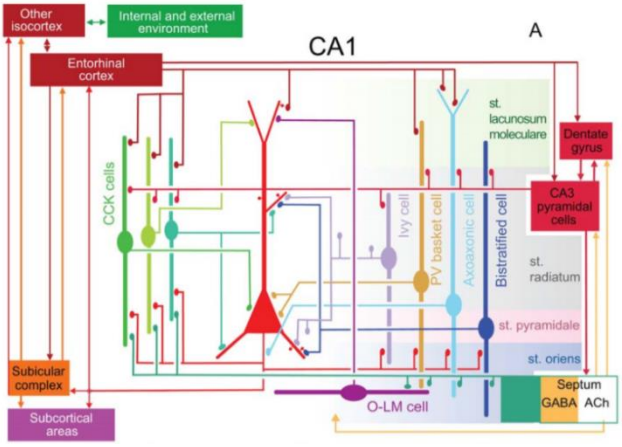

Figure 2.2 Schematic of the main synaptic connections of pyramidal cells *(red, middle), three types of CCK-expressing cells (basket cell, perforant path-associated cell, Schaffer collateral-associated cell), ivy cells and PV-expressing basket, axo-axonic, bistratified and O-LM interneurons (from Buzsáki 2015).*

2.1.5 Organization of local circuit connections

Local circuits in the hippocampus are comprised of excitatory connections from principal cells (which form the major output pathway from hippocampal subregions) to interneurons and mainly inhibitory interneuronal connections onto principal cells(see **Figure 2.2**). Interneurons are considerably less abundant (10%) than spiny principal neurons, such as granule and mossy cells in the dentate gyrus and pyramidal neurons in the CA1 and CA3 areas. In short, it has, as yet, proved impossible to find a set of physiological parameters that allows a meaningful classification scheme of hippocampal interneurons to be established.

The pattern of local connectivity is diverse and represents a rich tapestry of prospective strategies for modifying initial responses to inputs and post hoc responses to continued input activity on the basis of previously generated outputs.

The diverse profile of anatomical, pharmacological, and electrophysiological properties of local circuit connections can, to some extent, be reduced to a few basic properties. First, afferent activity invariably co-activates not only local principal cells but also local inhibitory interneurons. This organizing principle offers a mechanism by which any initial input can organize the response to any subsequent input, with the specific temporal profile being a consequence of the kinetics of interneuronal synaptic postsynaptic responses and their compartmental localization onto principal cells. Second, efferent activity also co-activates local inhibitory interneurons. There is some (but by no means complete) overlap between interneurons receiving feedforward and feedback signals. This organizing principle allows local circuits to modify responses to afferent activity further on the basis of whether an output is generated. Third, interconnectivity within either principal cell populations or local interneuron populations provides a mechanism by which spatially discrete patterns of input (and subsequent output) may influence populations of neurons outside the active area. Local circuits provide a substrate for converting blanket (relatively unstructured) inputs into specific spatiotemporal profiles of output on the basis of the history of each principal neuron in the target population.

2.2 SYNAPTIC PLASTICITY

One of the most studied properties of hippocampal synapses is their ability to respond to specific patterns of activation with long-lasting increases or decreases in synaptic efficacy. The term "synaptic plasticity" was introduced by the Polish psychologist Jerzy Konorski to describe the persistent, activity driven changes in synaptic efficacy. A formal hypothesis embodying this idea was advanced by the Canadian psychologist Donald Hebb in 1949: when an axon of cell A is near enough to excite a cell B and repeatedly or persistently takes part in firing it, some growth process or metabolic change takes place in one or both cells such that A's efficiency, as one of the cells firing B, is increased.

In 1973, Tim Bliss and Terje Lømo reported that long-lasting changes in synaptic efficacy (see **Figure 2.3**) at performant path-granule cell synapses in the hippocampus could be induced by brief tetanic stimulation(Bliss and Lømo 1973). Lømo noticed that after episodes of high frequency stimulation of the perforant path lasting a few seconds the responses evoked by subsequent stimuli could remain enhanced for many tens of minutes. The discovery of what has come to be known as "long-term potentiation" (or LTP) emerged. Subsequently, Bliss and Tony Gardner-Medwin (1973) found that tetanus-induced potentiation could persist for many days in the unanesthetized rabbit with chronically implanted electrodes. Analysis of input/output curves suggested that only the synaptic inputs that had actually been tetanized were potentiated, a phenomenon called "input specificity" (Bliss and Gardner-Medwin 1973).

Introduction of the living brain slice as a physiological preparation by Henry McIlwain during the 1960s stimulated the development of the transverse hippocampal slice preparation in the Oslo laboratory (Skrede and Westgaard 1971). This preparation allows ready access to all pathways of the dentate gyrus and hippocampus, provides mechanical stability for intracellular recording, and makes possible rapid pharmacological manipulation of the extracellular environment. Using this preparation, LTP was revealed at two other hippocampal pathways: the mossy fiber projection to CA3 pyramidal cells and the interleaved commissural and Schaffer collateral fibers from CA3 to CA1 pyramidal cells (Schwartzkroin and Wester 1975). Tetanic stimulation of both these pathways results in a rapid, persistent increase in synaptic responses, whether recorded intracellularly or extracellularly. LTP can be followed for many hours in both the slice preparation and the anesthetized animal and for days, weeks, or months in animals with implanted electrodes. Although it makes possible a range of

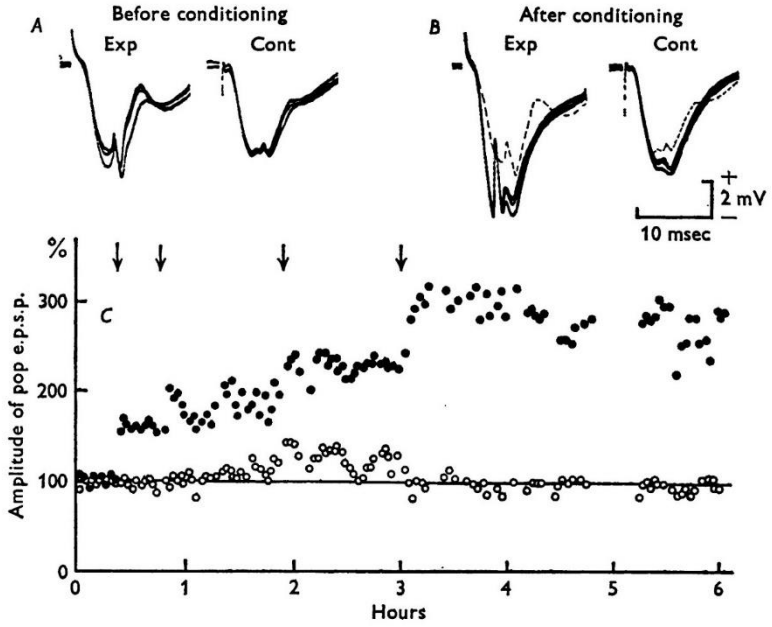

Figure 2.3 Discovery of Long term potentiation. *(**A**) EPSP Response before and after(**B**) high frequency stimulation. (**C**) Graph showing the amplitude of population E.P.S.P for the experimental pathway(filled circles) and the ipsilateral control pathway(open circles) as function of time. Conditioning trains were given through a medially placed conditioning electrode at the times indicated by the arrows (from Bliss and Lømo 1973).*

physiological and pharmacological experiments that would not otherwise be feasible, a full understanding of the mechanisms and significance of hippocampal synaptic plasticity cannot be reached by *in vitro* studies alone.

Graham Collingridge and colleagues showed that D-2-amino-5-phosphonopentanoic acid (DAP5), a highly specific antagonist of the NMDA blocks the induction of LTP in area CA1 while having little or no effect on synaptic responses recorded at low rates of stimulation. The NMDA channel is unusual for a ligand-conducted ionophore in that its conductance is both ligand- and voltage dependent. At near-resting membrane potentials, the channel is blocked by Mg2, and substantial depolarization is required to drive Mg2 from the channel (Ault et al. 1980; Mayer, Westbrook, and Guthrie 1984; Nowak et al. 1984). Activation of the NMDA channel requires the temporal coincidence of activity in presynaptic terminals to release transmitter plus adequate depolarization of the postsynaptic membrane. Three major properties of LTP can be defined: cooperativity, input specificity and associativity.

A wide range of stimulus protocols can induce LTP. In most cases, it is probably true to say that the choice of protocol favoured by a particular laboratory relies more on tradition than any clearly demonstrated superiority. But, what is the function of LTP? Is it a physiological phenomenon that engages the same neural mechanisms that are responsible for some forms of learning and memory? Or is it a laboratory curiosity of no functional significance? A version of these questions was posed at the end of the first article on LTP (Bliss and Lømo 1973), but the debate has been with us ever since. This debate has moved on from merely recognizing certain analogies between LTP and learning to specific ideas about how the mechanisms of induction and expression of synaptic plasticity-related to the multiple types and processes of memory that we now know to exist. The pioneering studies implicating LTP in memory were correlational. Researchers (Barnes 1979; Barnes and McNaughton 1985) observed, in the course of work on aging, that the persistence of LTP over time was statistically correlated with the rate of learning and/or the degree of retention of spatial memory in a circular arena task. The “synaptic plasticity and memory” (SPM) hypothesis (Martin, Grimwood, and Morris 2000) assert that activity-dependent synaptic plasticity is induced at appropriate synapses during memory formation, and is both necessary and sufficient for the information storage underlying the type of memory mediated by the brain area in which that plasticity is observed.

2.3 OSCILLATIONS: BEHAVIORAL NEURAL CORRELATES

Since the early days of human neurophysiology, scientists have been fascinated by the variety of mesoscopic events that can be recorded from the scalp as EEG and directly from within the brain as local field potential (LFP; cf.,). Many of these events are periodic and the different frequency bands identified over the years are designated by Greek letters (δ, θ, α/μ, β, λ, ε).

In the waking rat, LFP activity of the CA1 region is dominated by theta oscillations (6–10 Hz) during preparatory behaviors, such as ambulation, exploration, rearing and sniffing (Vanderwolf 1969).In contrast, during consummatory behaviors, such as immobility, drinking, eating and grooming, theta is replaced by irregularly occurring sharp waves (SPW). Gamma oscillations (30–120 Hz) or "fast waves" (Stumpf 1965)are present during both theta state and SPW state, but gamma amplitude is small although its amplitude variability is much larger in the absence of theta (Csicsvari et al. 2003).SPWs are large amplitude negative polarity deflections (40–100 ms) in CA1 stratum radiatum that are most often, but not always, associated with a short-lived fast oscillatory pattern of the LFP in the CA1 pyramidal layer, known as "ripples" (110–200 Hz). SPW-Rs have been observed in the hippocampus of every species investigated so far. Hippocampal theta oscillation versus SPW-R dichotomy reliably reflects the brain-state categories of voluntary-preparatory and consummatory-terminal behaviors (Vanderwolf 1969; Buzsáki 2005). The theta-SPW-R electrophysiological dichotomy is also present during sleep; REM sleep is characterized by theta (Grastyan and Karmos 1961; Jouvet 1999), whereas non-REM sleep (i.e., slow wave sleep) by SPW-Rs.

The observation of spikes or spike bursts of individual pyramidal cells does not allow for the identification of SPWs, no matter how long the observation period is. In contrast to single neurons, recordings from large cell assemblies can instantaneously identify SPW-Rs because of the strong synchrony of neurons. The probability of pyramidal neuron participation and the fraction of neurons firing in each SPW event show a strongly skewed, lognormal-like distribution (Buzsáki and Mizuseki 2014). During a typical SPW event, 50,000 to 150,000 neurons discharge in the CA3-CA1subicular complex and entorhinal cortex.

2.3.1 SPW-Rs supported memory consolidation

While the exact functions and mechanisms for the generation of SWRs are still elusive, it is known that they are involved in the formation and consolidation of new memories. According to the dominant theory in the field, i.e., the two-stage memory hypothesis (Buzsáki 1989) SWRs perform information transfer of memory traces that are temporally stored in the hippocampus to the distributed neocortical network. SPW-Rs thus may be a mechanism that allows cementing learned associations. The hypothesized two-stage routine for memory formation is:

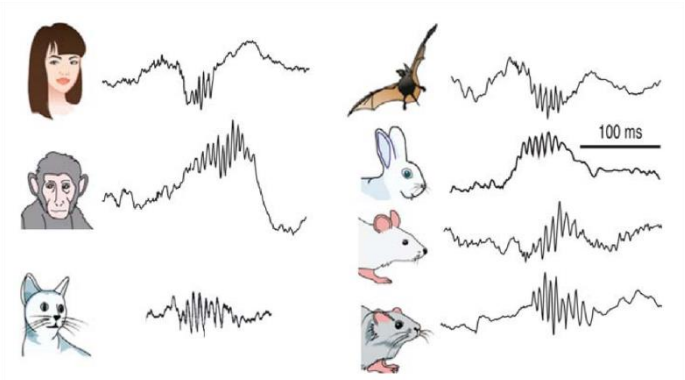

Figure 2.4 Preservation of SPW-Rs in mammals*. Illustrative traces of ripples recorded from various species (from Buzsáki 2014).*

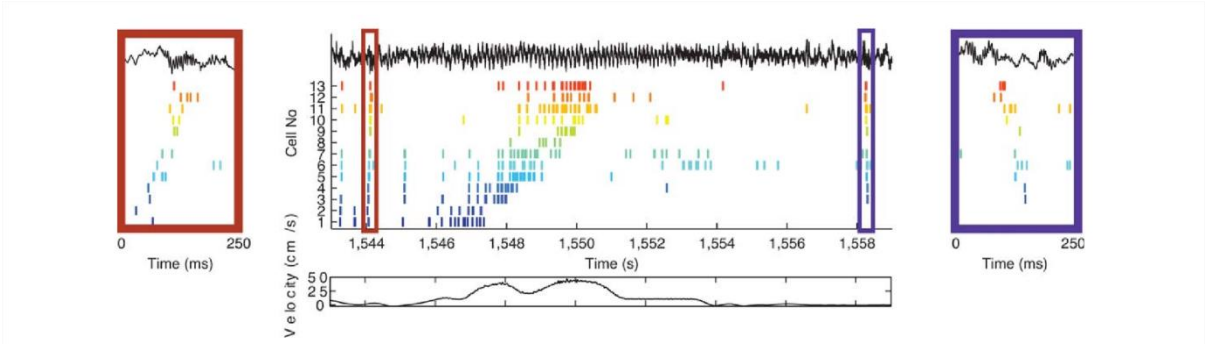

Figure 2.5 Place cell sequences experienced during behavior *are replayed in both forward (red box) and reverse (blue box) direction during awake SPW-Rs (from Buzsáki 2007).*

1. Labile form of memory trace. During learning, associated with theta brain state, afferent activity from the neocortex/ entorhinal cortex brings about a transient change of synaptic strengths in the CA3 hippocampal regions, where the learned information is temporarily held.
2. Long-lasting form of memory trace. During consummatory behaviors, including slow wave sleep, spontaneous SPW bursts are initiated in the CA3 recurrent network and the recurring SPW-Rs transfer the newly acquired hippocampal information to the neocortex and the repeating SPW-Rs continue to potentiate those same synapses which gave rise to the synaptic changes during the learning process.

The SPW event would in essence compress time and allow temporally distinct neuronal representations to be combined into a coherent whole. SPW-Rs reactivate the same subset of neurons in CA3 and CA1 precisely determined by the recent past of the neural network.
The supportive evidence for this hypothesis falls into three categories. First, spike sequences within SPW-Rs are related to the sequences present during the waking experience. Second, consolidation of episodic memories is correlated with several parameters of SPW-Rs, and perturbation of sleep events rich in SPW-Rs impairs memories in both humans and other animals. Third, specific and selective perturbation of SPW-Rs affects hippocampus-dependent memories. In addition, numerous recent experiments have also demonstrated that in addition to a retroactive, memory-assisting role, SPW-Rs also play a prospective role that may assist in route planning, recall and decision-making, perhaps due to the preexistence of a rich variety of SPW-R events before experience.

2.4 ELECTRODE NEUROTECHNOLOGIES FOR RECORDING BRAIN SIGNALS

In order to study bioelectrical signals and to study their dynamics at different spatial and temporal scale, among the different techniques, various types of electrode-based devices were developed. These devices can be classified based on the level of their invasiveness or on the signals that they acquire. Non-invasive techniques such as electroencephalography (EEG) measure macroscopic low frequency field potentials from large brain areas and are representative of synchronous activity generated by large population of neurons in different brain circuits. To increase the spatial and temporal information content on these signals toward single-cell spikes, invasive techniques that penetrate the brain tissue were developed. These invasive devices include electrodes for epi-cortical recordings (electrocorticography - ECoGs) and intra-cortical implantable electrodes (microwires, silicon probes, etc.). The later, implemented as single-electrode or as arrays of electrodes, can record extracellular local field potential and action potentials (or *spikes*) from neurons located near the electrodes. Finally, intracellular single neuron activity can be recorded with patch clamp electrodes, but this technique restricts experimentalists to the observation of only a single or a very few neurons. All these techniques exploit the large frequency bandwidth that electrodes can sense and span from recordings of single cell spikes to low frequency signals generated by large neuronal assemblies. However, the understanding of how single cell activity and low-frequency collective activity relate is still not totally understood. Importantly, improving the understanding of low frequency signals is particularly relevant for interpreting signals that can be acquired with non-invasive diagnostic devices. The concept of using groups of microelectrodes for recording from or stimulating neural tissue is as old as the observation that the monitoring of dynamic neural systems requires the simultaneous capture of multiple electrophysiological events. However, the lack of appropriate microelectronic techniques and the large data streams prevented systematic fabrications and application until the second half of the 20th century (Gross 2011).

In the next paragraphs, I will shortly review two major classes of devices used for *in vitro* electrophysiology. This includes “passive multielectrode arrays”, that were developed since the seventies using thin-film technologies, and more recent “active multielectrode arrays”, that were recently proposed by exploiting the integration of monolithic CMOS devices. It has to be noted that similar passive or active MEA devices were also developed for *in vivo* electrophysiology by structuring the electrode substrate as a thin and needle-like implantable structure.

2.4.1 Passive multielectrode arrays (MEA)

The first functional planar multielectrode array (MEA) was realized using photolithographed thin film conductors and was conceived and fabricated by (Thomas et al. 1972) with gold/nickel conductors on glass substrate. This device was first demonstrated for recording of action potentials from cardiac myocytes. The first recordings of action potentials from individual neurons was reported in 1977 using spontaneously active Helix pomatia (snail) ganglia(Gross et al. 1977; Gross 1979)The next major step forward was achieved by (Pine 1980) when the first signals from mammalian central nervous system cultures were obtained with a 16-electrode array. In addition to the early developments of passive planar arrays and subsequently, by commercial enterprises such as Multichannel Systems in Reutlingen, Germany, Panasonic USA, and Ayanda in Switzerland, the simplicity of photolithography has allowed various research groups to fabricate custom arrays suited to their research purposes. Given the MEMs fabrication constraints, these devices typically integrate 64 microelectrodes having separation in the range of hundreds of micrometers (Liu et al. 2012).

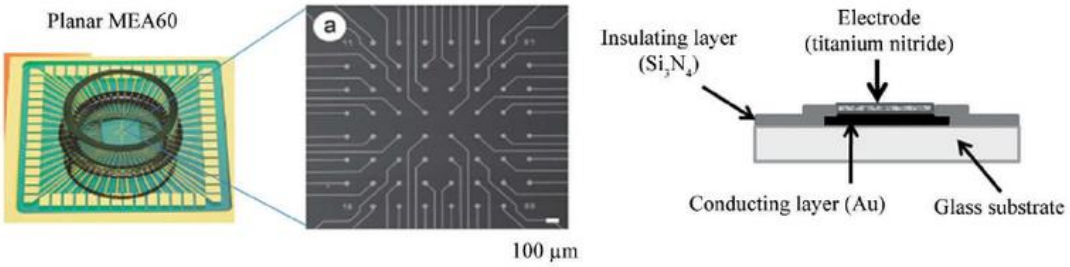

Figure 2.6 View of a widely-used passive MEA device. (**left**) *Example of a commercially available passive MEA with 60 electrodes (from Multichannel Systems, Germany), and (***right***) cross-sectional view of the thin-film materials structured to realize such device (from Liu et al. 2012).*

2.4.2 Active multielectrode arrays based on CMOS technology (CMOS-MEAs)

Recent efforts toward the development of large-scale electrode array devices have introduced a new generation of active high-density multielectrode arrays that is realized using complementary semiconductor–metal–oxide (CMOS) technology (Berdondini et al. 2014). The technological constraint of individually wiring each microelectrode to an amplifier is a major factor limiting the number of recording electrodes in passive electrode-array configurations. Thus, scaling up the number of electrodes faces the issues of routing the electrode interconnections and of managing the acquisition. As a first step to overcome this limitation, hybrid architectures consisting of CMOS-based application specific integrated circuits (ASICs) connected either on-chip or off-chip to passive electrode arrays were initially proposed (Dabrowski, Grybos, and Litke 2004; Blum et al. 2007; Bottino et al. 2009; Gunning et al. 2009; Gryboś et al. 2011). However, since this hybrid approach still relies on passive wiring of the electrodes, it is not a practical solution to drastically increase the number and density of microelectrodes over large recording areas of several square millimeters (Berdondini et al. 2014).

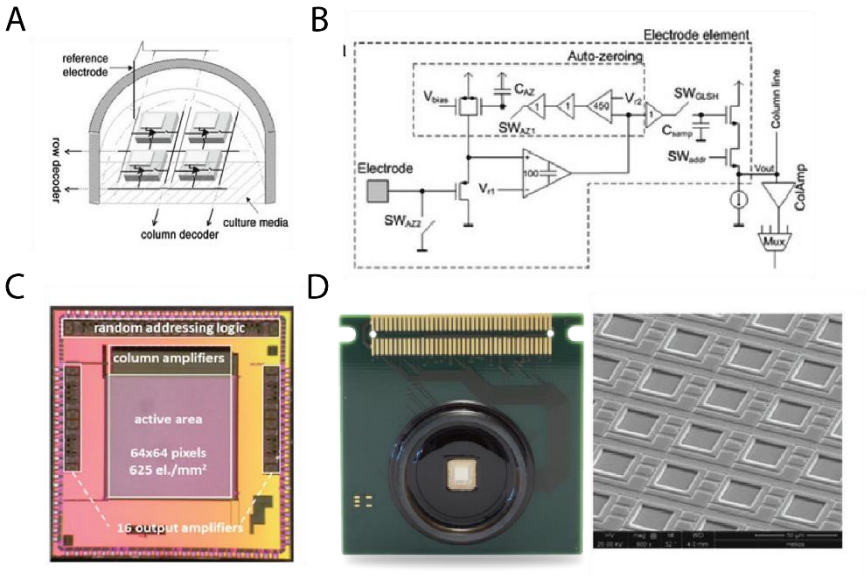

Figure 2.7 Overview of APS concept and implementation. *(**A**) Schematic representation of the APS-MEA circuit with in-pixel electrodes, amplifiers, and active circuits for the readout (**B**) Schematics of the signal amplification chain (providing a first stage under each electrode) and of the electrode readout(**C**) Micrograph of the CMOS chip. (**D**) APS-MEA providing 4,096 recording electrodes and SEM micrograph of an area of the electrode array. Electrodes are recessed by ~2 µm into the top insulation layer.*

The key advantage of integrating active electronic components on the same substrate as the actual electrodes is the possibility of integrating a much higher electrode density and a larger number of electrodes on active areas of several square millimeters. This concept was first introduced in 2001 (Berdondini 2001) by presenting the concept of active sensor pixel (APS) based MEA devices capable of whole-array recordings from thousands of electrodes(see **Figure 2.7**). For electrophysiological recordings, the original in-pixel circuitry of light sensing APS imaging devices was entirely redesigned to instead provide sensitivity to small extracellular charge variations resulting from the cellular activity. The active area of APS-based CMOS-MEAs is constituted by an array of "neuroelectronic pixels" (or electrode-pixels), each integrating a microelectrode and a circuit for the first-stage amplifier and low-pass filtering (filtering is mandatory in order to avoid aliasing issues in the following time-division multiplexing circuits). Due to the possibility of using active switches to time multiplex signals, integrated circuits make it feasible to transfer data from such high channel counts off chip and to overcome the connectivity limitation of passive devices. Additionally, such co-integration allows amplifying the signals with optimal quality, due to minimal parasitic capacitances and resistances. Two major classes of CMOS-MEAs devices were developed. The first is based on the APS concept for whole array recordings (Berdondini 2001), while the second (developed in the group of A. Hierlemann at ETH) adopts the strategy of recording from only a sub-set of electrodes in the array (Hierlemann et al. 2011). The later does not require integrating electrodes underneath each microelectrode and reduces constraints on the front-end design by enabling its integration outside of the active electrode array area. Finally, it has to be noted that CMOS-based electrode array based on FET-sensors rather than noble metal electrodes were also proposed (Hutzler et al. 2006; Stangl and Fromherz 2008; Eversmann et al. 2011). The respective dense microelectrode arrays (MEAs) with small electrode-pixels enable subcellular-resolution investigation of regions of interest in, e.g., neurobiological preparations, and, at the same time, the large number of electrodes allows for studying the activity of entire neuronal networks.(Hierlemann et al. 2011; Ferrea et al. 2012; Maccione et al. 2014; H. Amin et al. 2016).

The laboratory where I did this PhD is among the pioneers in the APS-based CMOS-MEA technology. This laboratory demonstrated these devices to enable high spatial and temporal resolution recordings of bioelectrical signals *in vitro* or ex-vivo (Berdondini et al. 2009; Ferrea et al. 2012; Maccione et al. 2014; Hayder Amin et al. 2016) as well as, more recently, *in vivo* (Angotzi et al. 2019). These devices consist of CMOS-based monolithic chips that integrate electrodes as well as amplification and analog multiplexing circuits designed to provide simultaneous extracellular recordings from thousands of microelectrodes. Planar devices are nowadays commercially available (3Brain AG, Switzerland) and can record from 4096 electrodes at a sampling rate up to 18 kHz (commercial version) per channel (see **Figure 2.7**). Each square electrode-pixel measures 21 × 21 µm and the 64 x 64 array is integrated with an electrode pitch (center-to-center) of 42 µm, thus providing a recording area of 7.22 mm^2 (electrode-pixel density of 567 pixel/mm^2). The three on-chip amplification stages provide a global gain of 60dB, with a 0.1–5 kHz band-pass filter. As previously shown, this bandwidth allows recording slow LFP signals as well as fast action potentials (APs) in brain slices (Ferrea et al. 2012)

3 HIGH-RESOLUTION CMOS-MEAS RECORDINGS OF ELECTRICALLY EVOKED RESPONSES IN CORTICO-HIPPOCAMPAL SLICES AND APPLICATIONS FOR COMPOUND TESTING

3.1 INTRODUCTION

Activity-dependent synaptic plasticity plays a vital role in sculpting synaptic connections during development. Although it plays a crucial role during critical periods of early development, it is also a fundamental process in the adult brain. For example, it is widely accepted that memory formation depends on changes in synaptic efficiency that permit strengthening or weakening associations between neurons. Further, activity-dependent synaptic plasticity at appropriate synapses during memory formation was suggested to be both necessary and sufficient for storing information (Lynch, 2004).

Unsurprisingly, an enormous effort in neuroscience was devoted to understanding the mechanism by which synaptic strength can be modulated. One of the phenomena underlying synaptic plasticity, widely recognized as one of the major cellular mechanisms that underlie learning and memory, is the long-lasting activity-dependent potentiation of synaptic strength, also known as long-term potentiation (LTP). This potentiation mechanism is considered at the base of memory (Schwartzkroin and Wester 1975; Yeckel and Berger 1998; Lomo 2003) The LTP can be obtained following high-frequency stimulation of chemical synapses and was first observed in studies on rabbits by Terje Lømo in 1966 in the laboratory of Per Andersen in Oslo (Lømo 1966). From the discovery of LTP until nowadays, a lot has been discovered, but this process sill remains only partially understood (Nicoll 2017). The quantification of electrically induced Long Term Potentiation (LTP) in acute cortico-hippocampal brain slices is also one among the gold standard electrical read-outs used to assess pharmacological and toxicological effects of compounds on synaptic transmission (Cho, Wood, and Bowlby 2007). Indeed, altered LTP is considered as a sign of potential neurotoxicity of a compound.

Electrical recordings to estimate synaptic efficacy and plasticity have been used for many years to measure neuronal function in brain slices. A typical protocol for LTP (**Figure 3.1**) consists in the use of two micro-positioned electrode wires to electrically stimulate the Schaffer collateral projections of CA3 hippocampal neurons and to record field potential responses from the efferent dendritic arborizations in CA1 (Schwartzkroin and Wester 1975). This circuitry involves two main ionotropic channels, namely NMDA and AMPA receptors. A well-accredited hypothesis of the mechanism underlying LTP sustains that potentiation occurs when strong excitation (such as obtained by means of a tetanic, high-frequency series of electrical stimuli) activates NMDA receptors whose, through an internal signal pathway, increase the recruitment of AMPAs at synapses, and consequently increase their excitability (Luscher and Malenka 2012).

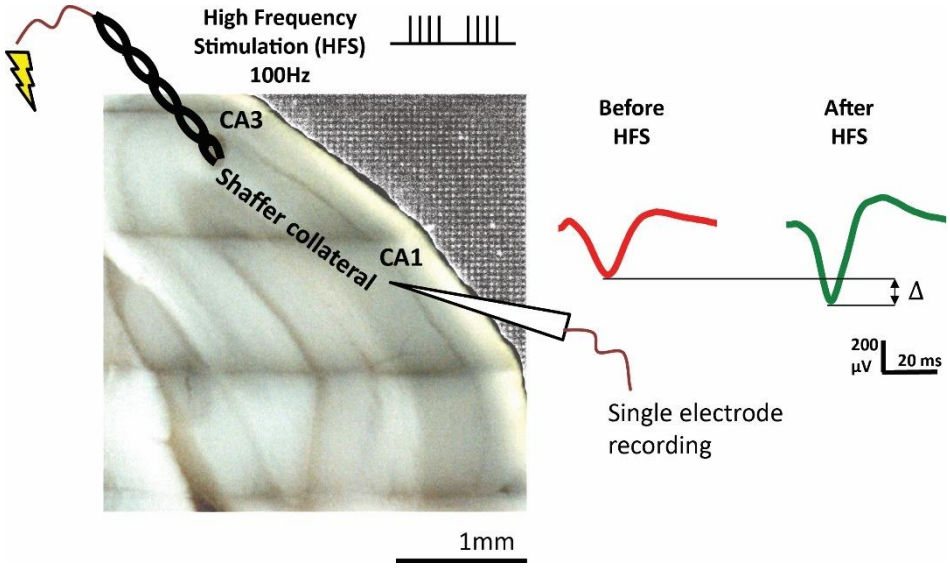

Figure 3.1 View of the typical protocol used for induced LTP*. (**A**) Example of hippocampal slice with stimulating and single recording electrode. (**B**) View of dendritic evoked activity in stratum radiatum pre and post high frequency stimulation as measured in one of my experiments.*

The critical event leading to the induction of LTP is considered to be the influx of calcium ions (Ca^{2+}) into the postsynaptic spine. It is commonly agreed that the elevation of postsynaptic calcium concentration is both necessary and sufficient for the induction of hippocampal LTP. In the majority of synapses that support LTP (in the hippocampus and elsewhere), the postsynaptic increase in calcium is mediated through activation of the NMDA receptor. Significantly, the characteristics of NMDA receptor activation eloquently explain the properties of LTP: the receptor activation leads to the opening of the associated calcium channel when occupied by glutamate and when the postsynaptic membrane is depolarized. The depolarization relieves the magnesium block of the NMDA receptor channel, allowing sodium, potassium and most importantly calcium to flow through the channel. Therefore, the NMDA receptor complex is dually regulated by ligand and voltage and thereby acts as a coincidence detector. Consistent with its pivotal role of NMDA receptors in LTP induction are numerous demonstrations showing that inhibition of NMDA receptors blocks LTP. The firsts of these demonstrations, in CA1 *in vitro* and in the dentate gyrus *in vivo,* were obtained using the specific competitive NMDA receptor antagonist AP5 (Davis, Butcher, and Morris 1992). The primary target of the rise in Ca^{2+} in dendritic spines is the calcium-calmodulin-dependent kinase II (CaMKII) which leads to increased recruitment and insertion into the membrane of AMPA receptors. The most powerful argument used to support the view that CaMKII is sufficient to induce LTP has been developed on the back of the “silent synapse” theory of LTP. A substantial number of hippocampal synapses are silent and lack of functional AMPA receptors, but they do contain a normal compliment of NMDA receptors. It was shown that LTP can rapidly un-silences these synapses with the all-or-none insertion of a population of AMPA receptors (Isaac, Nicoll, and Malenka 1995). We now know that activation of the NMDA receptor may be critical for the induction of many forms of LTP, but it is not necessary for all of them.

Motivations for high-resolution recordings in LTP experiments

As previously described, the conventional electrophysiological approach used to study LTP in brain slices consists in the use of two micro-positioned electrodes: one for delivering electrical stimuli and the second to record electrically evoked field potential responses before and after the delivery of high-frequency electrical stimuli (or tetanic stimulation). While manual electrode positioning can be a source of inter-trial variability, a major limitation of this approach for the study of potentiation mechanisms and for evaluating the effects of pharmacological compounds on LTP is the use of a single recording electrode. This hinders the possibility to record electrically evoked field potentials from the entire dendritic arborization and it assumes that the effects of a pharmacological compound that might alter LTP have homogenous effects on the entire area of the circuit under study. Furthermore, any induced response in other regions of the cortico-hippocampal circuit, such as the somatic layer of the CA1 area, are not monitored while they might provide additional information on the LTP process and on the effects of a compound.

To overcome this technology limitation in spatially mapping LTP, over recent years different laboratories have adopted the use of passive Multi Electrode Array (MEA) devices with a few tens of electrodes. These devices allow for multisite electrical recordings(Oka et al. 1999; Egert and Hämmerle 2002) and for measuring the induced potentiation at multiple locations (Ibi et al. 2010; Lu et al. 2014; Kim et al. 2016; Hamasaki et al. 2017; Schreurs, Sabanov, and Balschun 2017). Nevertheless, the low spatial resolution of conventional MEA devices having inter-electrode separation in the range of hundreds of microns does not provide spatially detailed recordings of the induced responses in specific sub-regions.

Here, we propose the use of active dense MEAs consisting in monolithic planar CMOS devices (CMOS-MEAs) that provide high-resolution extracellular recordings from an entire dense array of 4096 closely spaced (21 µm inter-electrode separation) microelectrodes (21 x 21 μm^2 electrodes) (Berdondini 2001; Berdondini et al. 2009). These devices are nowadays commercially available (from 3Brain AG, Switzerland) and were already demonstrated to provide detailed recordings from brain slices (Ferrea et al. 2012), with a sufficient spatial and temporal resolution for clustering pharmacologically induced epileptogenic-like activity patterns. In particular, in my work I explored the use of CMOS-MEAs in combination with electrical stimulation delivered by micro-positioned electrodes for LTP studies. As it will be described in the next paragraphs, after developing a protocol and validating the proposed approach in cortico-hippocamapl brain slices under untreated and pharmacologically treated conditions with a compound having well-characterized LTP effects, i.e. DAP5 (Davis et al. 1992), I investigated the effects of D-cycloserine (DCS) on LTP responses. This compound is a partial agonist of the NMDA receptors through the glycine binding site (Liu et al. 2016), but it also inhibits AMPA receptors (Rouaud and Billard 2003). It is considered as a potential candidate for alleviating the symptoms of schizophrenia (Goff 2016), but so far conventional electrophysiological read-outs have not determined a clear behavior of this compound on LTP.

These experiments aimed at evaluating the performances of the developed platform for compound testing and were performed in collaboration with 3Brain AG and a CRO (Aptuit, Verona) where I have implemented an experimental setup following my developments. In addition, a library of computational tools to automate the execution of these experiments and to quantify potentiated responses was developed in Python and licensed to 3Brain AG for the development of dedicated plug-ins for their BrainWave software.

3.2 MATERIALS AND METHODS

The next section summarizes the final material and methods developed to perform LTP experiments using CMOS-MEAs. Different materials (e.g. holders for brain slices) and methods (e.g. preparation and maintenance of brain slices) were tested and constantly optimized along with this thesis.

3.2.1 Brain slices preparation for acute electrophysiology

Adult male Sprague-Dawley rats (6 weeks old) were anesthetized with isofluorane, decapitated with a guillotine, and the brain was removed and placed in ice-cold vibratome solution. Brains were bisected along the mid-line and glued to the stage of a Vibroslice (Campden Instruments, Loughborough, UK). Sagittal hippocampal slices of 270 um in thickness were cut under cold (< 8 C), freshly-oxygenated artificial cerebrospinal fluid (ACSF) and transferred to a submerged recording chamber maintained at room temperature. The ACSF comprised (mm): 124 NaCl, 26 NaHCO3, 5 KCl, 2 CaCl2, 1.6 MgCl2 and 10 glucose, equilibrated with a 95% 02-5% CO2 gas mixture.

3.2.2 Recording of electrically evoked field-potential responses with high-resolution CMOS-MEA

Acute electrophysiological recordings of electrically evoked activity in brain slices were performed with 4096-CMOS-MEA (4096S+ biochip, from 3Brain AG). These devices provide a regular 64 x 64 electrode array on an active area of 2.8 by 2.8 mm^2 (electrode pitch 42 µm, electrode side 21 µm). For my experiments, I used an experimental platform providing a sampling frequency of 18 kHz/electrode for whole-array recordings. Brain slices were always positioned on the active area by taking care of positioning the CA3-CA1 circuit on the electrodes (Figure 3.3 panel A). After positioning, the tissue was held in place using a light, custom-made, harp weight and oxygenated ACSF media was continuously perfused at about 2mL/min (see inlet and outlet lines in Figure 3.3 panel B).

Electrical stimuli were delivered using a platinum-iridium concentric bipolar electrode (FHC Inc. www.fh-co.com) that was previously micro-positioned in order to touch the Schaffer collaterals of CA3 and connected to an external electrical stimulator (Dual Output square stimulator S88 from Grass technologies). The timestamps of the stimuli were recorded on the Biocam platform by connecting the input analog channel of the Biocam to the TTL line out of the stimulator.

The **LTP protocol** for electrophysiological recordings with CMOS-MEAs consisted of four phases (see schematics of **Figure 3.3** panel C):

i) **calibration phase**: responses to increasing stimulation signal amplitudes were recorded until reaching the saturation of the responses. Based on these data, amplitude of the stimulus used in next phases was set to the amplitude inducing 50% of the saturating response. The electrical stimuli consisted in biphasic voltage pulses of 100 msec in duration and amplitudes ranging between 10 V and 50 V.

ii) **stability phase**: responses to a low frequency stimulation train at 0.03 Hz (biphasic stimuli as defined in the calibration phase) were recorded for 30 min. to quantifying the baseline level of response of the brain slice.

iii) **high-frequency stimulation (HFS) phase**: delivery of tetanic stimuli aimed at inducing potentiation. The HFS consisted of: 2 trains of 100 stimuli at 100 Hz, separated by a pause of 20 sec.

iv) **stability phase**: recordings as performed in *ii*) to quantify the effects of the electrically induced potentiation.

For compound testing, each brain slice was recorded both under control conditions (i.e. ACSF only) and upon chemical manipulation, either by adding to the perfused ACSF solution 50 µMol of DAP5 or 100 µMol of DCS as tested in these experiments.

3.2.3 Monitoring the execution of the experiment, data extraction and analysis

Because of the software controlling the CMOS-MEA platform (BrainWave, 3Brain AG) did not provide integrated algorithms to monitor online the execution of the protocol described above for an LTP experiment, I implemented a software tool in Python™ (https://www.python.org/) that analyzes the recorded raw data, extracts the relevant parameters and visualizes the data in a way that enables a pseudo real-time monitoring of the course of the experiment. To do so, and to minimize the volume of data for each experiment, the BioCam system was not operated by continuously recording electrical activity, rather it was continuously recording periods of 33 sec every minute (in order to ensure containing one stimulus for each period). During the minute of pause among recording periods, the custom Python™ was designed to access and process the recordings to provide a continuously updated visualization of the experiment to the user. The software tool (**Figure 3.2**) that I developed consists of an analysis framework integrating all the on-line, but also off-line algorithms for a single brain slice experiment, as well as statistical methods to aggregate different experiments to compare multiple brain slices, such as controls (CTRL) with respect to those treated with pharmacological compounds. During an experiment, the software tool detects the occurrence of stimuli using a hard threshold detector applied on the channel recording the stimulation time-stamps. Successively, the evoked responses are extracted after low-pass filtering (cut-off frequency at 400Hz) the raw signal on the time-window following the stimuli. Next, for each extracted wave, it computes different feature parameters, such as the minimum and maximum peak intensity, the slope of the signal and the temporal delay of the response calculated as the interval between the stimulus and the higher peak of the waveform. The same software tool also controls the external electrical stimulator as required to execute the four experimental phases of an LTP experiment and to tune the amplitude of the electrical stimuli in the initial calibration phase.

3.2.4 Shape- and temporal-based waveform classification

An automatic classification procedure was designed to organize the waveforms of the electrically induced responses accordingly to their shape (this procedure can be manually corrected and re-launched also off-line using the same software tool). To discriminate between EPSPs (Excitatory Post Synaptic Potentials), PSs (Population Spikes) and noise, the clustering procedure relies on the maximum to minimum peak ratio (MMR) of the waveforms (here referred as *shape-based waveform classification*). Indeed, as illustrated in the example of **Figure 3.3** panel D, EPSPs have prominent negative envelope corresponding to the dendritic responses MMR > 2.2; PSs, instead, being relative to the somatic compartment typically show a tri-phasic shape with an MMR < 1. Waveforms with a MMR between 2.2 and 1 generally show a “mixed” behavior and were not considered for further analysis (classified as “noise”). Waveforms with very low amplitude (< 80 μV) were also classified as noise. These threshold values of MMR were defined empirically.

Notably, even though the classification is based on a simple decision rule and empirically defined threshold values, it is able to cluster channels defining spatially continuous areas. Indeed, as shown in **Figure 3.3** panel D top left, this is also confirmed by the shapes of the responses (top right) collected along the dashed line that moves from the radiatum to the pyramidal layer. Furthermore, PS and EPSP clusters are well confined and match specific anatomical regions as observed with superimposed slice images. The algorithm was also able to finely discriminate the “mixed” area in between the EPSPs and the PSs (see orange cluster in **Figure 3.3** panel D top) that is characterized by the integration of dendritic and somatic signals. However, this mixed area was not considered in our successive analysis.

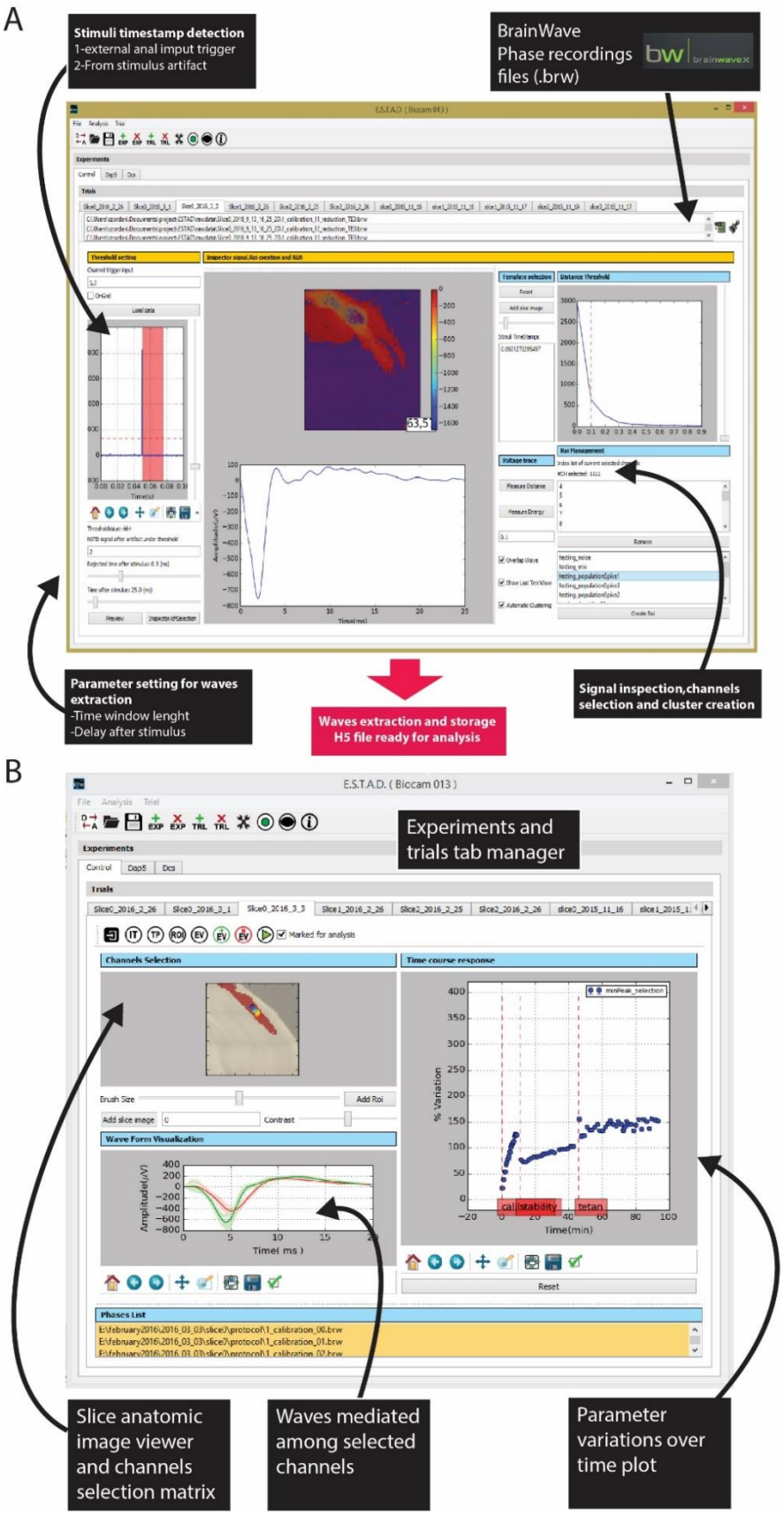

Figure 3.2 View of GUI of the software tool that I implemented in Python for detection, inspection and analysis of evoked activity by electrical stimulation. *(**A**) Detection from the BRW file of recording from BrainWave software where the user can set different parameters. (**B**) View of the analysis windows where the user can inspect the data and analyze multiple experiments.*

I also developed a further classification of the EPSP cluster in order to identify differences in the potentiation of the dendritic responses (here referred to as *temporal-based waveform classification*). Such cluster was subdivided into proximal, medial and distal regions with respect to their relative location with the stimulating electrode. This sub-classification is based on the delay of the electrically evoked response (see **Figure 3.3** panel D bottom left panel). The bottom right panel shows in differents colors waveforms collected after one stimulus for each one of the identified clusters. Such waveforms were collected along the dotted line, moving toward the stratum molecular layer. It can be noted that the signal propagates from proximal to distal areas with a decreasing of the amplitude and increasing time to peak of the response. Therefore, an alternative way to cluster the responses in the dendritic area could be based on the distance from the stimulating electrode position, rather than the delay.

Importantly, this two-steps classification of the evoked field-potential waveforms allowed to determine sub-regions that are consistent among different cortico-hippocampal brain slices. In this way, it has been possible to analyze data from different experiments and to compare responses under different experimental conditions regardless of the position of the brain slice on the array, the inter-animal heterogeneity, or the variability induced by the slice cut.

3.2.5 Statistical analysis of the data from multiple samples and conditions

Because the data analysis procedure leads to clusters defining a slice-related area with specific characteristics, I exploited this method to investigate the effects induced on LTP by different chemical compounds in each region by analyzing data from multiple brain slice samples. In order to analyze different parameters (e.g. min-max peak, slope, etc.), I computed normalized differences as percentage variations before and after potentiation. Specifically, the averaged value of each parameter computed from data acquired in the stability phase after HFS was normalized with respect to its averaged value computed from data recorded from the last five stimulations (at the stable and reliable plateau) before the HFS. An illustrative example of the color-coded variation for a given parameter (e.g. the min peak amplitude) with respect to its baseline and calculated on all the channels along all the phases of an experiment is shown in **Figure 3.3** panel C.

After normalization, I averaged the responses before and after tetanus for each electrode. The calculated pairs of averaged values for all channels are used to obtain two distributions: the first representing the distribution of the baseline, the second representing the potentiation induced by the HFS electrical stimulation. The difference between the two distributions for each sample represents the variation of the responses before and after the tetanus in a given experiment.

Given the heterogeneity of behaviors among channels in different experiments, the statistical difference between samples (such as control and pharmacologically treated slices) was evaluated based on the distribution of the normalized variation difference by using a Kolgoromov-Smirnov test. Importantly, to take into account the slice-to-slice variability, I defined a threshold for our tests using a standard bootstrapping method. In particular, I first constructed a vector of p-values considering all the possible pairs of distributions for control samples. Then, I choose as threshold the minimum p-value, which represents the maximum distance within the distributions of the control samples. Finally, for the sake of clarity, I displayed into a single boxplot the normalized difference distributions for samples under each experimental condition (i.e. control or treated).

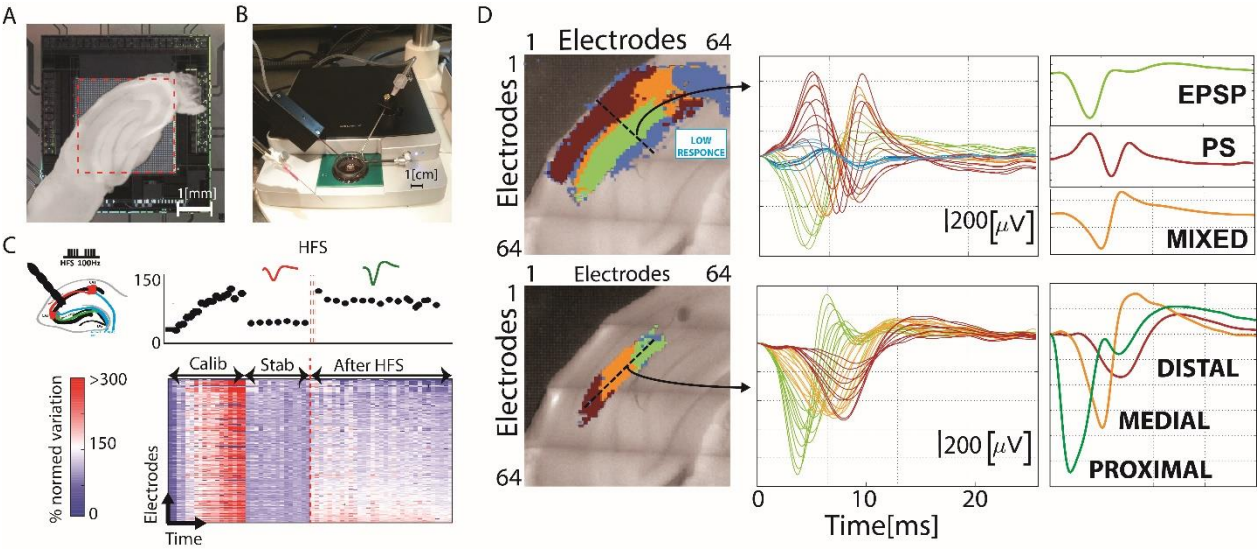

Figure 3.3 CMOS-MEA platform developed for LTP read-outs. *(**A**)View of a cortico-hippocampal brain slice lying on the CMOS-MEA chip. The red square indicates the electrode array area integrating 4096 continuously recording electrodes. (**B**) View of the experimental setup composed by Biocam system (3Brain AG, Switzerland); an external stimulation electrode mounted on a micro positioning system and connected to a Dual Output square stimulator S88 from Grass technologies ; a perfusion inlet/outlet with temperature heater; and a pseudo reference electrode immerged in the solution. (**C**) Top: schematic view of the experimental protocol composed by a calibration phase, a stability phase, delivery of high-frequency stimuli (HFS) and a phase to quantify the induced response variations. Bottom: corresponding normalized variation of the responses for the different phases and for different channels. (**D**) Shape- and temporal-based waveform classification. For a typical experiment, (top) visualization based on a first clustering algorithm (spatial) that subdivides the electrodes in four groups, namely PS, EPSP, Mixed and Noise; (bottom) visualization based on a second clustering algorithm (temporal) that subdivides the EPSP cluster in proximal, medial and distal areas from the stimulation site. The right plots show in different color for each cluster the waveform of the response to one stimuli (one for each electrode) and the mean response.*

3.3 RESULTS

3.3.1 Spatially-resolved LTP with multielectrode high-resolution recordings and waveforms clustering

In the first series of experiments, the potentiation of field potential responses to electrical stimuli delivered in the Shaffer collaterals of CA3 was quantified under two experimental conditions. This consisted of a group of untreated cortico-hippocampal brain slices and in a second group treated with an antagonist of NMDA receptors (D-AP5, 50 µM). While LTP is expected for untreated samples, those treated with the D-AP5 drug should not show any form of NMDA-mediated potentiation. For each sample, I quantified the level of potentiation by analyzing the induced field potential waveforms recorded by multiple nearby electrodes, with respect to pre-stimulation evoked responses. Nearby electrodes were clustered based on the similarity of the recorded evoked waveforms and the electrode position was associated with specific regions of the hippocampal circuit using optical microscopy images acquired from each brain slice mounted on chip.

The **Figure 3.4** panel A shows an example of the multielectrode mean waveform responses recorded before and after tetanus, for two samples under untreated and D-AP5 treated conditions. Under both conditions, these recordings show different mean response waveforms in different regions of CA1 that indicate field excitatory postsynaptic potentials (fEPSPs) and population spike (PS) responses, respectively. While a potentiation of the responses is observed in both CA1 regions of untreated samples, as expected, the D-AP5 drug blocked the NMDA-mediated potentiation. The effect of the HFS stimulation on brain slices under control conditions consisted of an increase of the response amplitude peaks and in a reduction of the response delays in both CA1 sub-regions. On the contrary, the post-tetanus responses for tissues treated with D-AP5 did not differ from pre-tetanus responses.

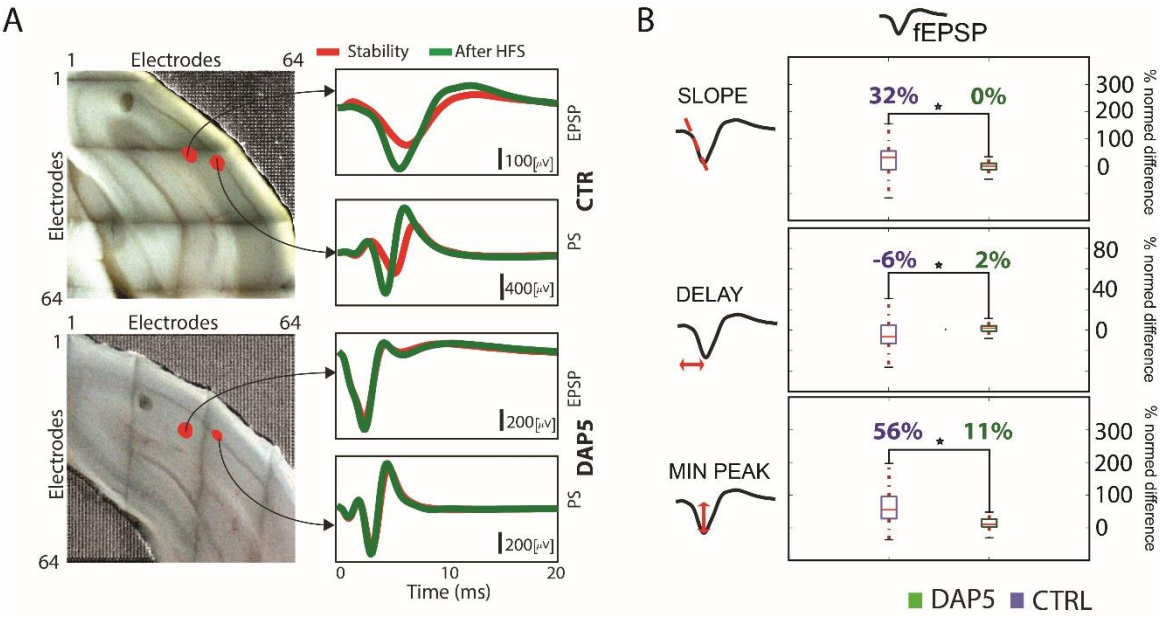

Figure 3.4 DAP5 results. *(**A**) Example of mediated response among two manually selected area in stratum radiatum(fEPSP) and pyramidal layer(PS). On top, the control condition is clearly visible the potentiated amplitude. Instead in DAP5 condition (bottom) there is no clear difference. (**B**) Three parameter (slope, delay, min-peak) are analyzed in fEPSP area. The response of ctrl trials is compared with the D-ap5 treated trials. Each boxplot represents the distribution of normed variation between before and after tetanus.*

To quantify the level of potentiation across samples for both untreated (n=4) and treated (n=4) samples (**Figure 3.4** panel B), I analyzed the variation of three parameters computed from the recorded waveforms. The computed parameters included the slope of the first decreasing phase of the waveform (slope), the delay of the response to the stimulus (delay) and the amplitude of the negative response peak (min peak). This analysis shows that all these parameters reveal statistically significant differences for samples treated by D-AP5 that do not show potentiated responses in both regions, with respect to untreated control brain slices.

3.3.2 Quantifying compound effects on LTP by clustering responses based on time-delay

In the second series of experiments, I investigated the capabilities of active dense recordings to determine the effects of D-cycloserine (DCS), which is a drug candidate under investigation for schizophrenia by acting on NMDA and AMPA receptors. It is important to highlight that conventional electrophysiological read-outs have so far failed in determining the clear effects of this compound on LTP. Differently than previous results obtained with D-AP5, read-outs obtained with the same procedure showed less evident effects on LTP for DCS-treated samples (n=4) with respect to control samples (n=4). The only significant change was a decrease in the minpeak of the response, mainly in the region expressing fEPSPs.

I was able to reveal significant differences between DCS-treated and untreated samples by exploiting the high spatial resolution of our multielectrode array recordings to distinguish effects induced in sub-

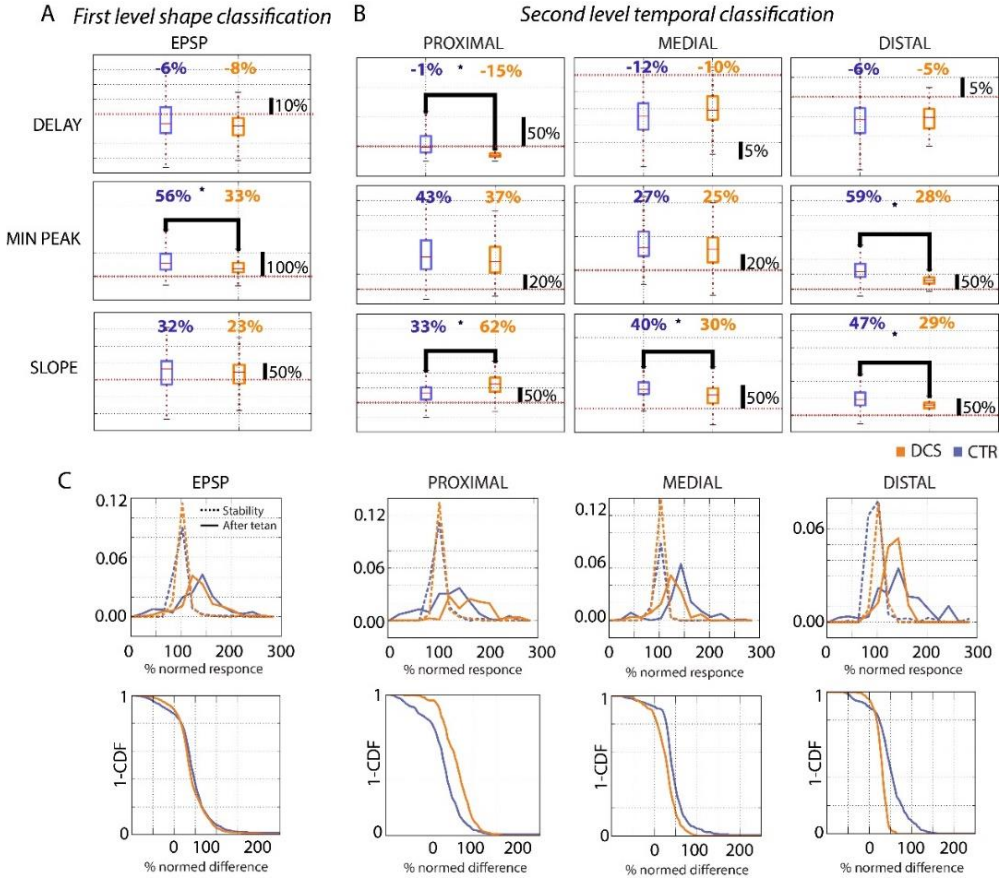

Figure 3.5 Comparison between control and DCS treated slices. ***(A)*** *For three parameters each boxplot show the potentiation in EPSP area (n=4).* ***(B)*** *With the second clusterization based on the delay we compare the potentiation along the longitudinal axis. Notice that for the slope parameter, there is no statistical significance difference if we consider all the electrodes of EPSP area(panel* ***A****). After the separation in proximal to distal region we found that there is an increase in proximal region and decrease of potentiation in the medial and distal region;(****C****) The probability density function (PDF) and the inverse of Cumulative density function are show for the slope parameter.*

areas of the fEPSP expressing region (**Figure 3.5** panel B). This was obtained by clustering the electrodes based on the time-delay of the pre-tetanus responses, thus allowing identifying groups of nearby electrodes located in proximal, medial and distal sub-regions with respect to the position of the stimulation electrode. In this way, by spatially and temporally resolving the evoked responses in DCS treated samples with respect to untreated slices, I found that the difference of the delay parameter was significant for the proximal region, while it was not significant for the medial and distal sub-regions. Additionally, the slope showed a significant increase in the proximal area and a significant decrease in the medial and distal regions. The "min peak" showed a significant decrease in the distal region and a trend similar to the other two parameters in the proximal and medial regions, but without significant differences with respect to untreated samples.

In **Figure 3.5** panel C I report the plots of the probability density function (PDF) and of the cumulative distribution function (1-CDF) computed using the two clustering approaches for the slope parameter and for all possible pairs of control (CTRL, blue line) and DCS-treated (DCS, orange lines) samples. As shown, clear separated trends between treated and untreated samples are obtained when electrodes in the fEPSP expressing region were divided into sub-compartments. On the contrary, when considering all electrodes the averaging of the opposite effects of DCS on the proximal (DCS increases potentiation) and on the distal region (DCS decreases potentiation) impairs the read-out.

Overall, these results demonstrate that high-resolution recordings allow assessing the effects of the DCS drug that were hidden when performing these experiments using conventional two-electrode systems or by analyzing the mean of the responses of all the electrodes in the entire fEPSPs expressing region without sub-dividing it in different areas.

3.3.3 Identification of highly potentiated "silent" regions

As shown in the previous section, high-resolution electrical recordings allow identifying different levels of potentiation in sub-compartments of the same region and elucidating the effects on LTP for compounds that conventional two-electrodes system was unable to determine. Also, the CMOS-MEAs used in this work record extracellular signals from a large active area. This offers the possibility to investigate at the same time the effects of the high-frequency stimulation and of pharmacological compounds in multiple regions of the cortical-hippocampal circuit.

By exploiting this recording feature, in all our experiments under untreated and DCS-treated samples we observed the presence of a strongly potentiated area that was almost silent (typical response amplitude < 100 μVolt) before delivering the tetanic stimulation. An illustrative example of this effect is reported in Fig 3.4 panel A, which shows the false-color map of the percentage variation of the "min peak" parameter. As shown, this analysis reveals a spatially confined region with an average potentiation higher than 280%. The average pre-/post-tetanus evoked signal waveforms computed for all the electrodes overcoming the 280% in change upon potentiation revealed a typical response that corresponded to a population spike and that was almost silent before tetanus.

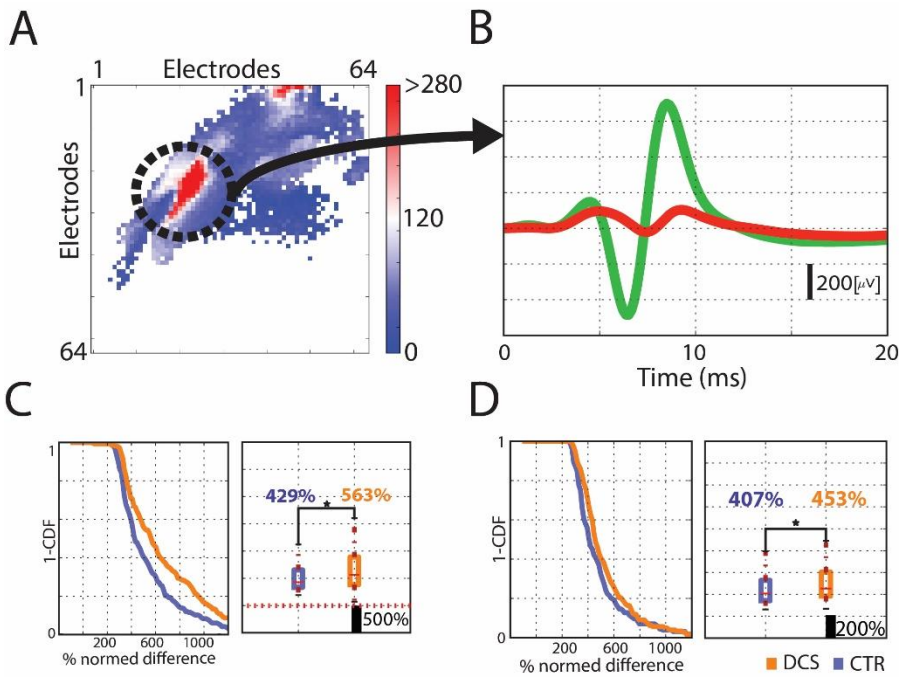

Figure 3.6 Highly potentiated "silent" region reveal by high density recordings. *(**A**) Spatial map of color coded potentiation. (**B**) Averaged trace before and after tetanic stimulation(**C,D**) min peak and maximum peak statistics comparison between DCS and CTR experiments selecting in each slice the highly potentiated region.*

This correspondence was further confirmed by imaging the brain slices. Indeed, even if we observed slightly different locations in different brain slices, these areas identified by the analysis of electrically evoked field potential responses anatomically matched with part of the pyramidal layer of CA1 (data not shown). Interestingly, these areas were not observed in recording from samples treated with D-AP5. This suggests that this sub-region is probably mostly driven by NMDA receptors that are strongly inhibited by D-AP5. Considering that DCS is known to act as a partial agonist of NMDA receptors, this is also confirmed by quantifying changes in the "min peak" parameter (**Figure 3.6** panel C) and in the difference between "max-min peaks" that indicate a significantly stronger potentiation for DCS-treated samples than control samples.

3.4 Discussion

In this first part of my PhD, I developed and demonstrated a platform exploiting the recording capabilities of CMOS high density MEAs to execute LTP experiments on cortico-hippocampal brain slices routinely and to quantify the effects of different compounds on LTP by analyzing data from multiple brain slice samples.

In particular, this allowed demonstrating two unique features of these recording devices. First, high-resolution recordings analyzed by automatic clustering algorithms of the recorded field potential waveforms are able to distinguish the different anatomical areas and let to compare and aggregate data from different slices and experimental groups. Further, this allowed identifying sub-compartments of the same circuit characterized by different levels of potentiation. This was useful for determining the clear effects of D-cycloserine (DCS) on LTP that could not be determined using conventional two-electrode systems. Indeed, experimental data show the opposite effect of potentiation along the proximal-distal longitudinal axes. It is therefore unsurprising that the micro-positioning of the recording electrodes (as in conventional systems) leads to a large variability hampering a precise characterization of the compound's effects. Second, by monitoring activity

changes in large active areas, this allowed monitoring effects induced by the high-frequency stimulation and compounds in multiple circuits simultaneously. By exploiting this feature, I was able to identify an area part of the pyramidal layer of CA1 that was almost silent before delivering the tetanic stimulation, and that was potentiated by 280%.

It has to be noted that with respect to classical single electrode recordings, the amplitude of the extracellular signals recorded on CMOS-MEAs is lower. This is most likely due to the 2D planar geometry of the microelectrodes and to the presence of a dead-cell layer in direct contact with the electrodes (it has also to be noted that recordings of spiking activity in these experimental conditions were quite rare). The recording quality might be improved either by optimizing tissue adhesion or by using new generations of CMOS-MEAs with 3D electrodes penetrating the tissue (not available for the platform used in this work). Many different approaches for enhancing cell and/or tissue adhesion have been devised, which include the use of adhesion proteins and chemical matrices (Hayder Amin et al. 2016). The slicing procedure affects the viability of those cells located at the border of the slice and leads to edema. Dead cells release intracellular potassium and neurotransmitter that can mediate neurotoxicity. In order to overcome the dead-cell layer problem, the most widely used solution is the organotypic slice culture technique, where the dead cells at the border of the tissue slice are eliminated during a culture period of about two weeks. Another possibility to overcome the dead-cell layer problem is to penetrate the slice with recording electrodes in order to reduce as much as possible the distance between recording electrodes and active cells. This can be achieved by using three-dimensional electrode arrays. An example of 3D electrode technology is reported using standard passive MEAs(Thiébaud et al. 1997; Heuschkel et al. 2006)

Finally, data dimensionality when using high-resolution CMOS-MEAs requires the development of adapted computational tools. In this context, an LTP protocol as implemented here typically involves recordings of evoked responses in more than 1000 electrodes and each test requires multiple slices. The software tool that I developed for this study allows us to store only the evoked responses and to restrict the analysis by selecting the same region in different slices for a good comparison. The experimenter can select by hand the areas of interest, but this procedure can be very user-dependent. Alternatively, in this study, I was able to propose a simple automated method to separate different anatomical areas (**Figure 3.3** panel D) consistently.

What I developed here is a first step to deal with the analysis and management of data in this type of experiment. However, given the increasingly higher volume of electrophysiological data that can be nowadays acquired with active dense electrode arrays, this is a field that requires strong efforts in the shortcomings. Importantly, as I attempted in my work, the development of software tools need to be usable by experimental researchers and have to implement efficient graphical user interfaces tuned to the specific experimental needs as here developed for LTP experiments. In this respect, I would like to highlight that the software developed here was used independently by the CRO involved in this project to run other pilot experiments.

4 MAPPING *IN VITRO* SHARP WAVE RIPPLES WITH HIGH RESOLUTION ELECTRODE ARRAY RECORDINGS

4.1 INTRODUCTION

The CMOS-MEAs high-density electrical recording technology and my interest in the process of memory and in the cortico-hippocampal circuit brought me to investigate the potential application of this technology for studying the spatial and temporal evolution of Sharp Wave Ripples (here referred as SPW-Rs). The physiological nature and properties of these oscillatory low-frequency events were already introduced in Chapter 2. However, it has to be remembered that these events can also be investigated ex-vivo on brain slices preparations. This *in vitro* method creates favorable technical conditions to finely study these events and offers unique advantages of experimental control to study the cellular and network mechanisms underlying distinct and isolated elements of cooperative population activities. Despite that, it is important to highlight that an active debate persists on whether *in vitro* recorded events can capture essential features of *in vivo* SPW-Rs or whether they largely reflect epileptic or other pathological events (Karlócai et al. 2014).
Similar to SPW-Rs recorded *in vivo*, *in vitro* SPW-Rs are typically initiated in the CA3 region and spread to CA1 and subiculum(Papatheodoropoulos and Kostopoulos 2002; Kubota et al. 2003; Maier, Nimmrich, and Draguhn 2003; Nimmrich et al. 2005; Wu et al. 2005). The depth profiles of SPWs and ripples in both CA1 and CA3 regions are similar to those observed in the intact brain (Kubota et al. 2003; Maier et al. 2003; Hájos et al. 2013; Hofer et al. 2015). These *in vitro* events can be recorded by placing a planar multielectrode array on the surface of a hippocampal brain slice, perpendicularly to the pyramidal or granule cell layer. However, an objective comparison between SPW-Rs *in vivo* and SPW-R-like events *in vitro* is difficult because of the high variability of the patterns across the *in vitro* models.

Most pharmacological experiments on SPW-Rs have been performed *in vitro*. SPW-Rs offers a testbed for examining the effects of various drugs not only on synaptic transmission of single cells but to assess the effects on network excitability. The *in vitro* slice preparation offers unique advantages of experimental control for studying the distinct pharmacological, neurotransmitter/modulator mechanisms of SPW-R control (Papatheodoropoulos 2007). In this respect, the technological advancement in high density recordings is providing new possibilities to researchers. Many factors, however, can affect the emergence and various aspects of SPW-Rs *in vitro*. This includes, among others, species differences, age of the animal model, slice cuts from the dorsal or ventral hippocampus, horizontal, transverse or coronal slices, temperature, and ionic composition of the bathing solution, thickness of the brain slice, and setup conditions such as the use of interface or submerged chambers (Hájos et al. 2009; Maier et al. 2012; Aivar et al. 2014)). For the latter, it was shown that specialized chambers with “ideal” flow-profile conditions, small-volume to enhance oxygen supply of the slices, increase ACSF flow and tissue viability, as well as pre-incubation conditions can dramatically improve the recording conditions and detectability of SPW-R (Hájos et al. 2009; Maier et al. 2012)

Therefore, setting up adequate experimental conditions to apply CMOS-MEAs to study SPW-Rs in brain slices was the first important research activity of my work. This included multiple experimental trials to optimize the brain slice preparation, tissue maintenance and experimental protocols to record spontaneously generated SPW-Rs. Besides, I evaluated alternative methods presented in the literature that could allow recording SPW-Rs more reliably. Successively, I focused on implementing and

evaluating data analysis algorithms in order to exploit the capabilities of high-density electrode array recordings for studying differences in the spatiotemporal features of SPW-Rs.

It has to be reminded that the majority of methods for the study of local-field potentials (LFPs), such as SPW-Rs, were initially derived from methods originally developed for the analysis of EEG signals. Local field potentials are composite signals that receive contributions from multiple neural sources. Yet, interpreting their nature and significance may be hindered by several concurrent factors and technical limitations. The main factor defining the amplitude of LFPs is the geometry of the current sources, over and above the degree of synchronization or the properties of the media (Herreras 2016). The geometry of these sources has been experimentally inaccessible until intra-cortical multisite recordings enabled to reveal the spatiotemporal co-activation of multiple sources. Without being able to access such detailed spatial information, interpretation of these signals was difficult and it was relying only on temporal cues, such as the timing of an event-related potential and signal frequency bands. However, still nowadays the exact extrapolation of the population of neurons giving rise to specific low-frequency voltage profile remains challenging. Ionic currents of multiple cellular sources may not only sum up, but they may also cancel out. Furthermore, ionic currents generated by single or populations of neurons give rise to field potentials that do not remain local, but rather extend unevenly throughout the volume far from their sources.

Consequently, any combination of synaptic currents raises an LFP that has a different amplitude and possibly a distinct polarity at different sites (Herreras 2016). Despite all these issues in interpreting LFPs, an important hypothesis in neuroscience considers that synchronized oscillations between different nodes of a network may facilitate the flow of neural information (Womelsdorf et al. 2007). In this way, the brain can dynamically coordinate the flow of information among circuits by changing the strength, pattern, or the frequency by which different brain areas engage in oscillatory synchrony (Bastos and Schoffelen 2016). Therefore, in neuroscience, a multitude of metrics has been developed to quantify oscillatory interactions (Wang et al. 2014; Bastos and Schoffelen 2016).

In my work, I aimed at exploring data analysis tools to study SPW-Rs. In particular, I was interested in quantifying differences and similarities among SPW-R propagations that might allow us to sort them in different clusters. This part of my work also faced the problem of the high dimensionality of CMOS-MEAs recordings already highlighted in the previous Chapter. In this respect, different methods might be used to overcome the dimensionality course of these data. Therefore, I first evaluated different approaches such as classical Principal Component Analysis (PCA), Factor Analysis (FA), Independent Component Analysis (ICA) and Non Negative matrix factorization(NNMF) (Hyvärinen and Oja 2000; Lee and Seung 2001). Upon discussions with partners and colleagues, I decided to focus on the use of the NNMF method. Briefly, other methods such as PCA can be understood as factorizing a data matrices with different constraints. Depending on the utilized constraints, the resulting factors can be shown to have very different representational properties. However, methods such as the PCA enforce only a weak orthogonality constraint, resulting in a very distributed representation that uses cancellations to generate variability. In this context, non-negativity is considered a useful constraint for matrix factorization that can be used to learn a representation of the data (Lee and Seung 2001). In particular, I used this decomposition approach to compute a distance matrix that allowed me to separate different types of event clusters (i.e. different origin locations). I then built spatial maps using analytical methods that measure the phase synchronization between all the channels. Similarly, as in the work of (Berényi et al. 2014), this allows observing the separation of different clusters and their anatomical relations, such as for events that follow the lamina profile of the hippocampus. Finally, I also explored the potential use of algorithms derived from the image-processing field, that were able

to present data describing field potential propagations from a different point of view. This latter approach is included in the perspective section as a possible direction for future research.

4.2 MATERIAL AND METHODS

To implement this study on Sharp Wave Ripples (SWRs) recorded *in vitro* from cortico-hippocampal brain slices, I implemented a dedicated experimental setup that took advantage of some of the developments already presented in the previous chapter. To do so, I also optimized the preparation and maintenance of the tissue in order to improve the reliability in recording these events from planar, unperforated silicon devices.

Briefly, the experimental setup is composed by a custom Biocam system (3Brain AG, Switzerland) for high-resolution CMOS-MEA recordings, a twisted nickel-chromo electrode wire controlled by a micromanipulator and connected to an external stimulator (PLexStim from Plexon Inc., USA), a perfusion system that was optimized (see **Figure 4.1** panel A) for maintaining the tissue during recordings, a microscope for collecting optical images of the brain slice lying on the chip, and by a PC running the BrainWave software (3Brain AG, Switzerland) for data acquisition as well as a custom software tool (written in Python) for controlling the stimulator and the waveform extraction. Finally, computational tools for data analysis were implemented in Matlab (from MathWorks) and were used to characterize the spatiotemporal dynamics of the recorded events. In the next section, I will summarize the methods and experimental conditions used to implement this study.

4.2.1 Brain slices preparation for acute electrophysiology

Horizontal brain slices (300 µm in thickness) that include the hippocampus and the entorhinal cortex were obtained from male C57BL6 mice aged 8-9 weeks. All experiments were carried out in accordance with the guidelines established by the European Community Council (Directive 2010/63/EU of September 22nd, 2010) and experimental protocols were approved by the Italian Ministry of Health.

To prepare brain slices, animals were anesthetized with isofluorane prior to decapitation. After decapitation, brains were rapidly removed and placed in cold (1–4 C) oxygenated sucrose artificial cerebrospinal fluid (ACSF) containing (in mM): 205 Sucrose, 2.5 KCl, 5 MgSO4, 0.5 CaCl2, 10 glucose, 1.25 NaH2PO4, 26 NaHCO3, saturated with carbogen (95% O2/5% CO2, pH 7.4 at 34 C). Brain slices were cut using a vibratome slicer (Leica VT1000S), then transferred into a submerged chamber (Gibb and Edwards 1994) filled with standard ACSF (in mM: 126 NaCl, 3.5 KCl, 1.2 MgSO4, 1.8 CaCl2, 10 glucose, 1.25 NaH2PO4, 26 NaHCO3, saturated with carbogen (95% O2/5% CO2) and equilibrated at pH 7.4 at 34°C. Before recordings, the tissues were incubated at 35°C for 30-60 minutes and for another hour at room temperature. Each experiment involved the preparation of fresh solutions to ensure reliable recordings.

It has to be noticed, that many different protocols were tested and the one reported here is the one that provided the best recordings in our experimental conditions.

4.2.2 Recording of SPW-R events with high-resolution CMOS-MEA: spontaneous and electrically induced events

For recordings, brain slices were positioned on the active area of CMOS-MEAs by taking care of positioning with a brush the CA3-CA1 circuit on the electrode area. After positioning, the tissue was held in place by a custom-made light harp weight. Oxygenated ACSF media was continuously perfused as soon as the brain slice was on the chip. In order to succeed with these experiments, it has been important to optimize the conditions to maintain the tissue once placed on the chip. Indeed, given the small volume chamber of the CMOS-MEAs (developed initially for cell-cultures), it required to optimize

the perfusion flow rate and the position of the inlet/outlet of the continuously perfused ACSF solution in the recording chamber. Indeed, because of the CMOS-MEA geometry, I could not use an interface chamber, as reported in many other works that have reported this approach for achieving better preservation of the tissue. However, the solution that I have figured out ensures that fresh ACSF could flow through the slice tissue lying on the chip (see **Figure 4.1** panel A). Remarkably, this allowed increasing the number of spontaneous events, from 7 events/min as recorded in initial experiments without optimizing the perfusion, to 20 events/min after this optimization. It has to be noted that I used the same ACSF solution both for cutting and recording, thus avoiding sucrose in ACSF. In fact, it was reported that slicing in sucrose may tip the excitation-inhibition balance in brain slices toward inhibition and thus to the lack of spontaneously expressed field potentials (Kuenzi et al. 2000).

I have investigated two conditions to record SPW-Rs: *spontaneously expressed SPW-Rs* and *electrically-induced SPW-Rs* (Behrens et al. 2005). While spontaneous SPW-Rs were recorded from the slices without any pharmacological or electrical manipulation, the latter were obtained upon delivering trains of high frequency stimuli as used in the previous chapter for LTP (in the next sections I will refer to them as SPW-Rs-LTP). To do so, a bipolar nickel-chrome twisted electrode connected to an external stimulator was used for stimulating the Schaffer collateral fibers by delivering every five minutes, until the expression of spontaneous events, three tetanic stimuli at 100 Hz, separated by 20 seconds. The main motivation for investigating alternative methods to ensure the recordings of SPW-Rs is due to the fact that spontaneously generated SPW-Rs were not reliably observed in all brain slices and, if observed, they were mostly expressed in ventral horizontal slices. On the other side, electrically-induced SPW-Rs (or SPW-Rs-LTP) were routinely recorded and therefore offered an easier way for implementing systematic experimental studies on ex-vivo brain slices.

4.2.3 Anatomical reconstruction and immunostaining

All brain slices that were recorded were also imaged while lying on the chip by using a Leica Z16 APO optical microscope(Leica Microsystems, Germany). This allowed reconstructing the anatomical position of the tissue respect to the position of the electrodes. In addition, after experiments, some slices were imaged by fluorescence confocal microscopy. To do so, the tissue was incubated in paraformaldehyde (4% in PBS-1X) at 4 °C overnight. After fixation, the slices were washed 4 times with 0.1% Triton in PBS-1X(PBST) and incubated for 15 min in the dark at room temperature with the nuclear marker Hoechst 33342 (1:300) diluted 1:1 in PBS (ThermoFisher Scientific, Italy). Images were acquired and visualized with 20X objective lenses using Leica SP5 upright confocal microscope (Leica Microsystems, Germany).

4.2.4 Data analysis

Following the development of the experimental conditions, a major activity of my work was to develop and evaluate different approaches for the spatiotemporal analysis of spontaneous and electrically induced SPW-Rs. At first, the custom software tool developed in Python for the analysis of LTP experiments (see Chapter 2) was adapted for filtering the raw data (low-pass filter with a cut-off frequency of 500 Hz) and detecting SPW-Rs events. Given the large amplitude and high synchronicity of these field potentials (typically up to 1-2mV in amplitude), this can be implemented with a simple threshold detector. Instead of applying a detection for each channel, I computed for each sample the minimum amplitude among the channels, thus obtaining a single signal of “minimum values”. A threshold (set manually from the software) is used for detecting the time position of each event. I then extract from the raw data the same window for all the channels(pre and post size can be set from the software), centered around each time event position computed from the “minimum values” signal. It has to be noted that this detection tool was also used for a quick visual inspection of the recorded raw data. A view of an averaged signal superimposed to the anatomical image of a recorded

brain slice is reported in **Figure 4.1** panel B. Once detected, the waveforms of all events were exported for successive analysis in Matlab, as described below and schematically illustrated in **Figure 4.1** panels E and F.

4.2.4.1 Current source density (CSD) analysis

During all types of neuronal activity, currents flow through the cell membranes. Viewed at a macroscopic scale from the extracellular space, membrane currents of multiple neurons are sinks (inward currents) and sources (outward currents) that give rise to field potentials. As established in many works (Mitzdorf 1985; Csicsvari et al. 2003; Maslarova et al. 2015; Kim et al. 2016; Vivar, Peterson, and van Praag 2016), sink and source distributions can be estimated from the recorded extracellular field potentials using the method known as the Current Source Density (CSD) analysis.

The high-frequency content of the extracellular signals contains information about the firing of neuronal action potentials. Action potentials are detected at a distance in the range of 0.1 mm around each recording electrodes (Buzsáki 2004; Pettersen and Einevoll 2008). On the other side, the low-frequency signal content of extracellular recordings, referred to as local field potentials (LFPs), are thought to be generated by synaptic inputs and their dendritic return currents. These low-frequency signals have a more extensive spatial spread due to volume conduction (Mitzdorf 1985; Pettersen and Einevoll 2008; Xing, Yeh, and Shapley 2009) and can modulate neural excitability in different circuits (Sirota et al. 2003).

In a first approximation, the Poisson equation provides the connection between the extracellular potential Φ and the current source density C under the assumption of a passive spread in a homogeneous and isotropic volume:

$$\sigma \, \Delta\Phi = -C$$

where Δ is the Laplace operator. To estimate C, as also done in other works, I developed an algorithm using the numerical second derivative in place of the Laplace operator. This is implemented by convolving the extracellular potential with a Laplacian of gaussian filter (kernel = 5 ,σ= 2). A subsequent convolution with a gaussian filter (σ=2) is then applied for denoising. The view of the spatial difference between the recorded initially extracellular potential (Potential) and the outcome of the CSD analysis is reported for a putative example in the **Figure 4.1** panels C, D respectively.

The algorithm used here is a conventional and fast method to compute the CSD. However, CSD algorithm development is an active domain of research and more sophisticated algorithms were presented. Therefore, the outcome of my analysis was also compared with the result obtained using another method, named kernel CSD or kCSD (Potworowski et al. 2012). Results from this comparison are reported in the discussion.

4.2.4.2 Events clustering

The aim of this procedure is to identify peculiar differences and similarities among spatiotemporal propagations of SPW-Rs upon the CSD analysis. A schematic representation of the analysis chain that I have developed is reported in the **Figure 4.1** panel E. To reduce the dimensionality of the data and extract salient features of SPW-Rs by separating time and space dimensions, I first used the method of the non-negative matrix factorization (Lee and Seung 2001). After this step, I quantified differences in the reduced data by computing a distance matrix between all the events recorded in a single brain slice. Successively, I clustered all events by using a hierarchical tree algorithm (Rokach, Lior 2005). The number of clusters that had the best consistency between the events was evaluated using a silhouette function.

When considering the events in the form of a matrix C (CSD computed for a time-window around the event and for all the electrodes) we can then use the non-negative matrix factorization to approximately factorized this matrix as the product of two matrices as:

$$C \approx S \times T$$

where C is the CSD matrix of size *e x t* (*e* is the number of electrodes and *t* is the number of time points); S is the space matrix of size *e x r* (*r* is the new reduced dimension) and T the time matrix of size *r x t* . Usually, *r* is chosen to be smaller than *t*. This results in a dimensionally reduced version of the original data matrix *C* (Lee and Seung 2001).

Therefore, for each recorded event, I computed the CSD with the approximation of the second derivative. Because here I was interested only in oscillations under 500 Hz, with a recording sampling frequency of 7022 Hz, I down sampled the data by a factor of ten. This still permitted to catch oscillation up to 700 Hz. All events were concatenated in a single matrix for the non-negative matrix factorization. This allowed obtaining the same spatial components (r) for all the recorded events. I chose arbitrarily a value of r=20. Successively, I computed a distance matrix $D_{i,j}$ representing the difference in the T matrices among all events as:

$$D_{i,j} = \sum_{r,t}(T_j - T_i)^2$$

Finally, an agglomerative hierarchical tree algorithm was used for clustering all the events based on the $D_{i,j}$ matrix.

4.2.4.3 Spatial Synchronization Map

In addition to the clustering analysis of the spatiotemporal patterns of the recorded SPW-Rs, I also implemented an analysis chain to compute spatial synchronization maps (**Figure 4.1** panel F). The rationale behind these maps considers that two brain areas showing the activity of different oscillators should express, in the case of connectivity between these regions, oscillation properties (i.e. phase or frequency) that are related (Bruña, Maestú, and Pereda 2018). Therefore, in a similar way as presented in (Berényi et al. 2014), using this analysis I attempted to cluster the field potentials recorded by multiple electrodes in different spatial locations. Using the phase information allows mapping the levels of synchrony among regions of the recorded cortico-hippocampal brain slices.

To do so, I computed the CSD and filtered in different frequency bands the averaged potentials calculated for each cluster determined as described above. The Phase Lag Index (PLI) was computed between all the channels and is a similar measure than the Coherence and Phase Lock Value (PLV) (Wang et al. 2014; Bastos and Schoffelen 2016). Specifically, the PLI measures the asymmetry in the phase difference distributions. The fundamental idea consists in disregarding phase locking that is centered around the null phase difference in order to exclude volume conduction effects (at the risk of ignoring true instantaneous interactions). This also applies to phase locking at π, 2π and so on. Mathematically, the PLI is expressed as:

$$PLI = \|sign[\Delta\varphi(t\ )]\|$$

where φ is the instantaneous phase of Hilbert transformation at time t . After computing the PLI matrix, I used an interacting energy-based clustering algorithm to identify electrode areas that might be related to anatomical regions. This approach is similar to (Berényi et al. 2014), but instead of using the measure of the coherence, here I used the PLI. This is because computing the PLI is faster than computing the coherence. In this computation, every site served as a reference against all other electrode sites. The resulting values were clustered using a gradient-descent algorithm (Berényi et al. 2014) so that each site was merged into a cluster for which the resulting PLI gain after merging was

the largest. Starting from random initial assignments, the interactive clustering algorithm formed a few stable clusters corresponding to a local energy minimum. In this analysis, the energy of a cluster A is defined as:

$$E^A = \frac{-1}{N^A} \sum_{i,j \in A} PLI_{ij}$$

where PLI_{ij} is the phase lag index between i[th] and j[th] sites and N^A is the number of recording sites in cluster A. The energy gap between two different assignments of an electrode *i* to clusters A and B is therefore defined as:

$$\Delta E_i^{AB} = \frac{1}{N^B} \sum_{j \in B} PLI_{ij} \; - \; \frac{1}{N^A} \sum_{k \in A} PLI_{ik}$$

If the energy gap is positive, the site *i* is assigned to the cluster B. Otherwise, it remains in cluster A. Clustering consistency was verified by repeating the process several times (n=100). It has to be noted

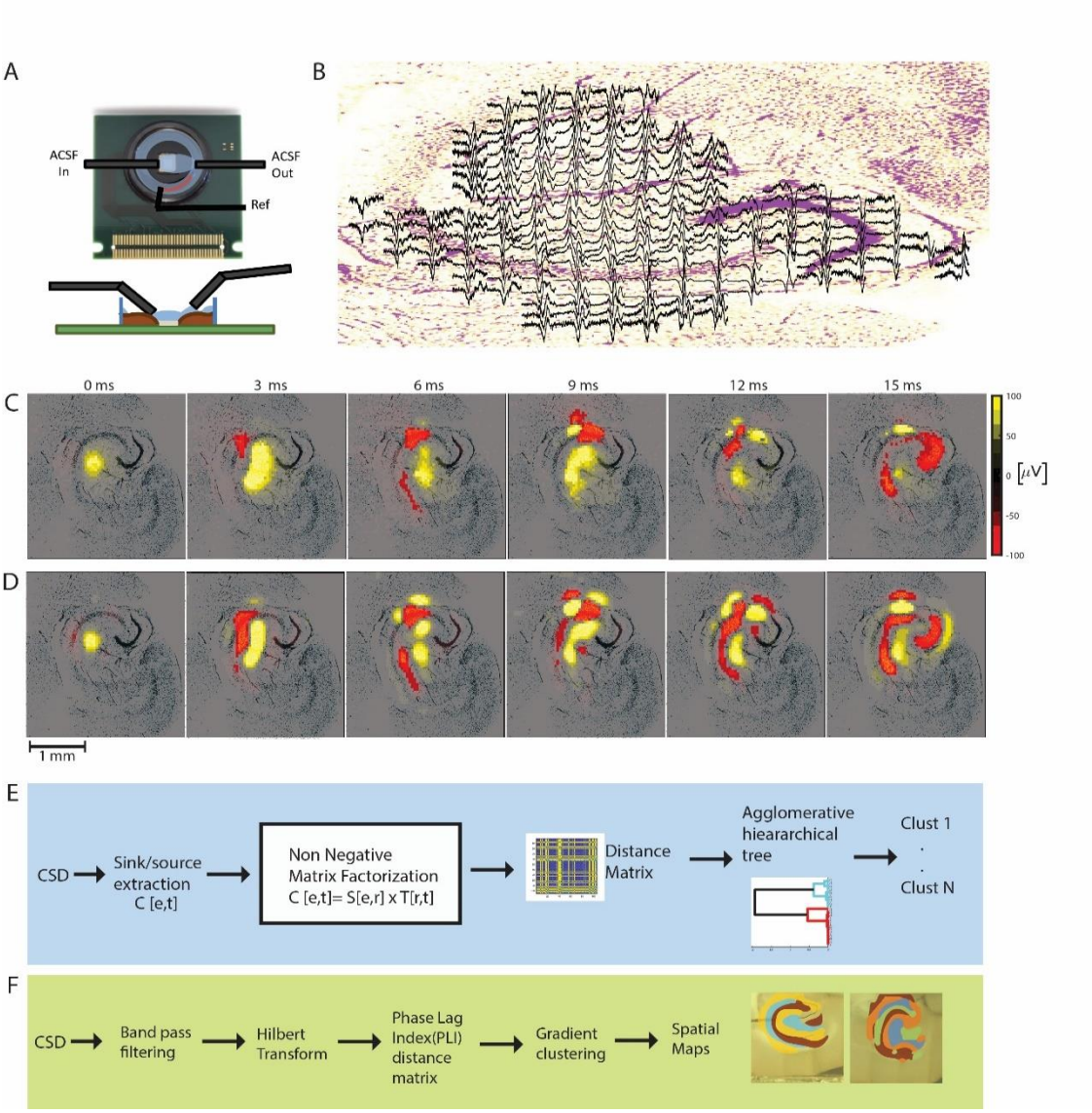

Figure 4.1 Recording SPW-Rs events with high density recording. *(**A**) Optimization of the ACSF flow through the slice on the CMOS chip. (**B**) Hoechst anatomical image with overlap averaged normalized signals(first 40 ms) take from a subgrid of electrodes. (**C**) False color map of the potential for different time point of the initial propagation of SPW-Rs (**D**) Current source density (CSD). (**E**) Clustering methods based on reduction with Non negative matrix factorization(NNMF) used to separate different type of events. (**F**) Phase Lag Index method used for computing spatial synchronization maps separating different anatomical layer.*

that only channels that were the most active were considered in the gradient-descending algorithm. A simple threshold, usually around 4 times the standard deviation of the signal noise, was used for selecting active channels.

4.3 RESULTS

4.3.1 Revealing different spatiotemporal patterns of SPW-Rs from high-resolution recordings

In order to study the spatial and temporal evolution of SPW-Rs and differences among the acquired events, here I report results obtained by using the above-mentioned methodologies. This allowed to extract and classify different spatiotemporal features of the recorded events. NNMF was used (see methods 4.2.4.2) to analyzed both SPW-Rs (**Figure 4.2**) and SPW-Rs-LTP (**Figure 4.3**) events. In all the recorded brain slices, I was able to separate different types of events forming at least two distinct clusters.

4.3.1.1 Spatiotemporal patterns of spontaneously expressed SPW-Rs in brain slices

In **Figure 4.2** I summarize the identified clusters for each brain slice expressing spontaneous SPW-Rs. In Panel A I show the distribution of the recorded events in time for each cluster. Panel B reports a histogram that quantifies the number of events in each cluster, while Panel C reports the distance matrix computed from the NNMF. Three over the six brain slices reported here show clear and distinct clusters that were also confirmed by visually inspecting the averaged potentials for these events (looking at the evolution of the potentials it was also possible to appreciate the different origins and propagations among clusters). To illustrate these differences, in Panel D I report an example of different propagations for well-separated clusters. In this plot, the *r* component of the two T matrix

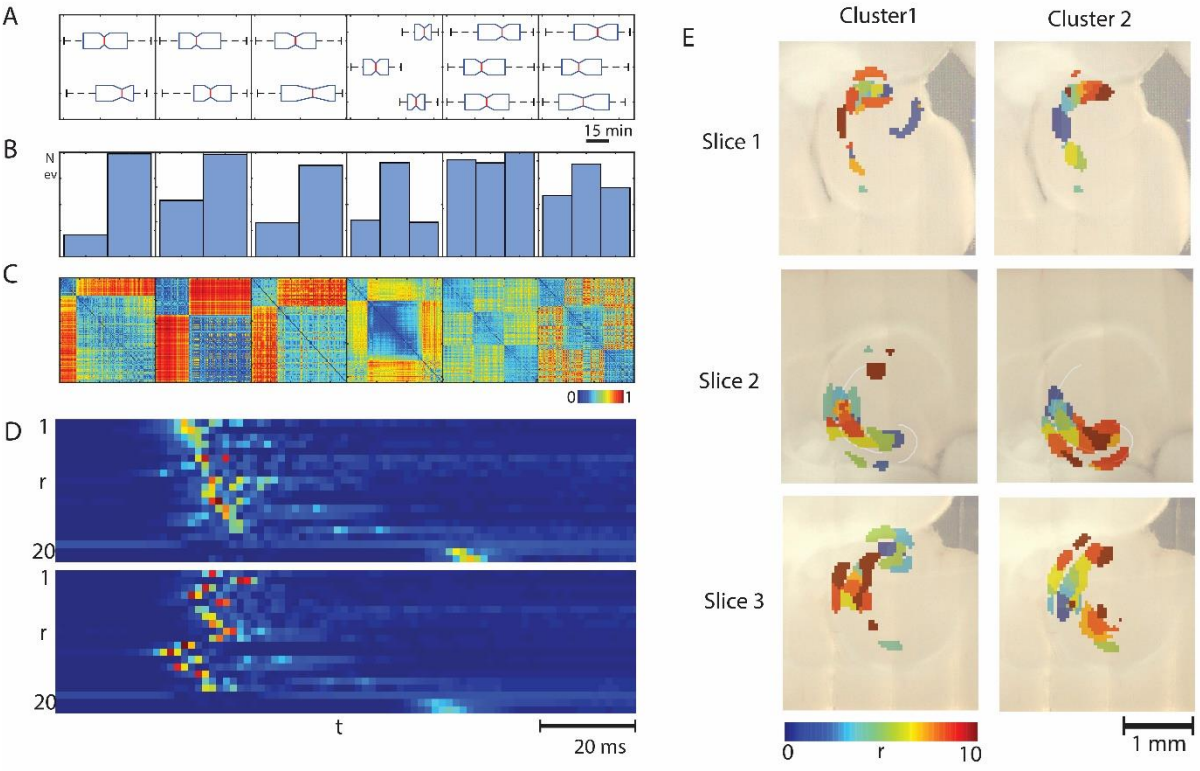

Figure 4.2 Clustering of spontaneous SPW-Rs events *(**A**) distribution of clustered events along time for different slices (**B**) histogram of number of events for each cluster (**C**) the distance matrix computed from NNMF reduction. (**D**) for one trial, NNMF T matrix of the two clusters with components ordered respect the first cluster (**E**) for tree slice the first 10 spatial component are color coded respect the ordering in the T matrix*

obtained by the NNMF is sorted over time. For the sake of clarity, I also built time colored maps superimposed on the anatomical microscopy image of the brain slices that are shown in Panel E. These data correspond to the clusters identified for the first three brain slices (counting from the left side) reported in Panels A-C. Each component in space is ordered with respect to the T matrix and colors represent different time bins (the first component is colored in blue). As illustrated in these maps, it is possible to see how one cluster propagate from the CA3 area. Instead, the second cluster has an origin in a region that seems to be the CA2 region. It is interesting to highlight that the debate about the origin of SPW-Rs events is still open. Among them, some researchers claim that they originate from the CA2 area, consistently with the second cluster identified here (Oliva et al. 2016).

4.3.1.2 Spatiotemporal patterns of electrically induced SPW-Rs in brain slices

In **Figure 4.3** I report the analysis results on electrically induced SPW-Rs (or SPW-Rs-LTP). As shown in the Figure, differently from the spontaneous SPW-Rs, these originate from the same region. However, the clustering method can still separate different spatiotemporal clusters. In Panel D I show the T

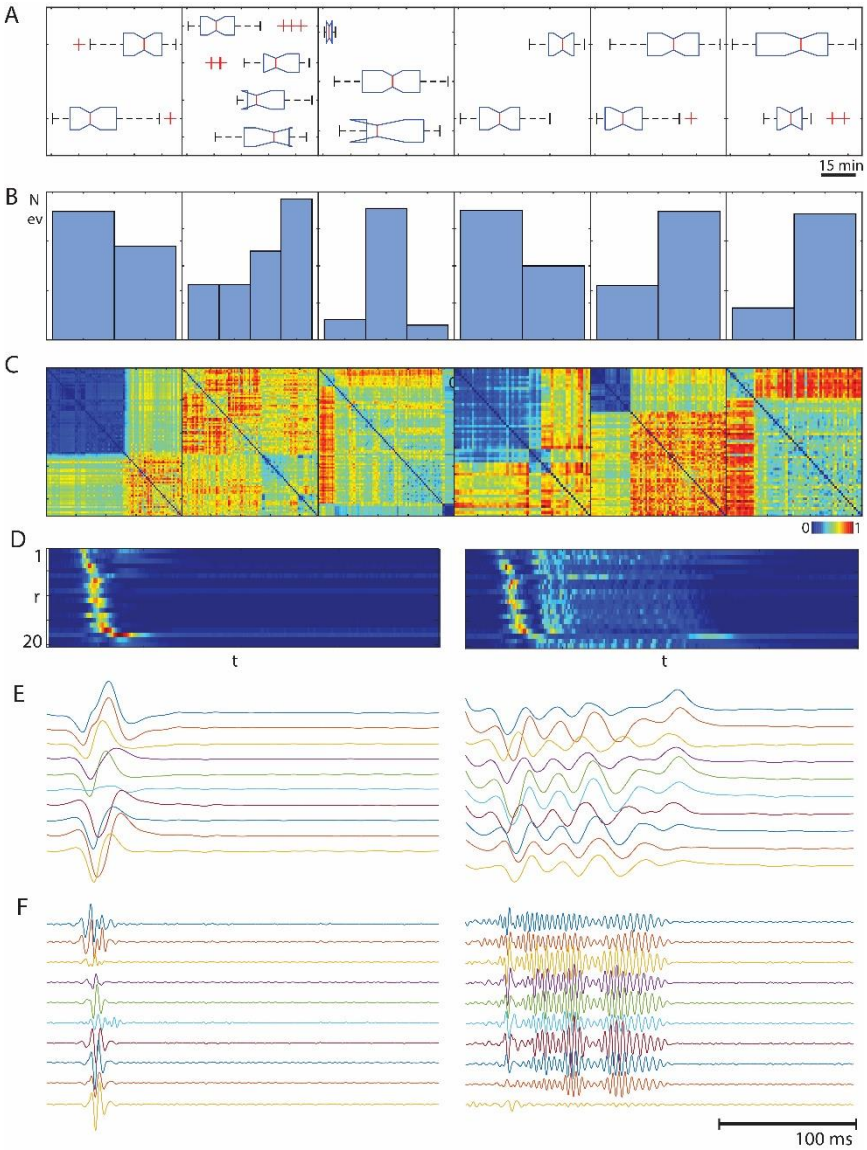

Figure 4.3 Classification of LTP induced SPW-Rs. ***(A)*** *Distribution in time of the events for each cluster. (**B**) Histogram of the number of events for each cluster. (**C**) Distance matrix compute from NNMF. (**D**) Example of ordered T matrix for each cluster .(**E-F**) For the first 10 spatial components I compute the average waveform filtered with a low-pass at 50 Hz (**E**) and pass-band 50-300 Hz (**F**).*

averaged matrix for two clusters detected in a typical brain slice subjected to the tetanic potentiation. The first cluster (on the left) is similar in duration to the propagation of spontaneous SPW-Rs. The second cluster (on the right) has a higher and much longer ripple activity. In panel E and F I report for the first ten components the averaged signal filtered with a low-pass (cut at 50 Hz in panel E) and band-pass (50-300 Hz in panel F) filter, respectively. These events look like the Clustered Sharp-wave ripples already observed in Papatheodoropoulos 2010, in which authors claim that this type of events generally occur when brain slices are maintained at a temperature similar to the rat body temperature.

In my experiments on spontaneously active brain slices (mouse animal model at ambient temperature) I never experienced spontaneous events similar to these ones. However, they appeared upon potentiation as SPW-Rs-LTP. The features that emerge from the clustering are clearly defined: ordering each channel in relation to the maximum amplitude peak or by merely looking at their duration, is enough for observing the difference in the propagation. One should also note that the algorithm identifies even other clusters that, instead, cannot be easily identified by simply looking at the raw recorded data.

4.3.2 Spatial synchronization maps reveal anatomical layers from electrical recordings

The Phase Lag Index (PLI) reflects the strength of the coupling between the signals expressed in different anatomical regions. This parameter is expected to be less sensitive to the influence of common sources and amplitude effects. This metric is based on the idea that the existence of a consistent, nonzero phase lag between two times series cannot be explained by volume conduction from a single strong source and, therefore, renders true interactions between the underlying systems rather likely. Such consistent, non-zero phase lags can be determined from the asymmetry of the

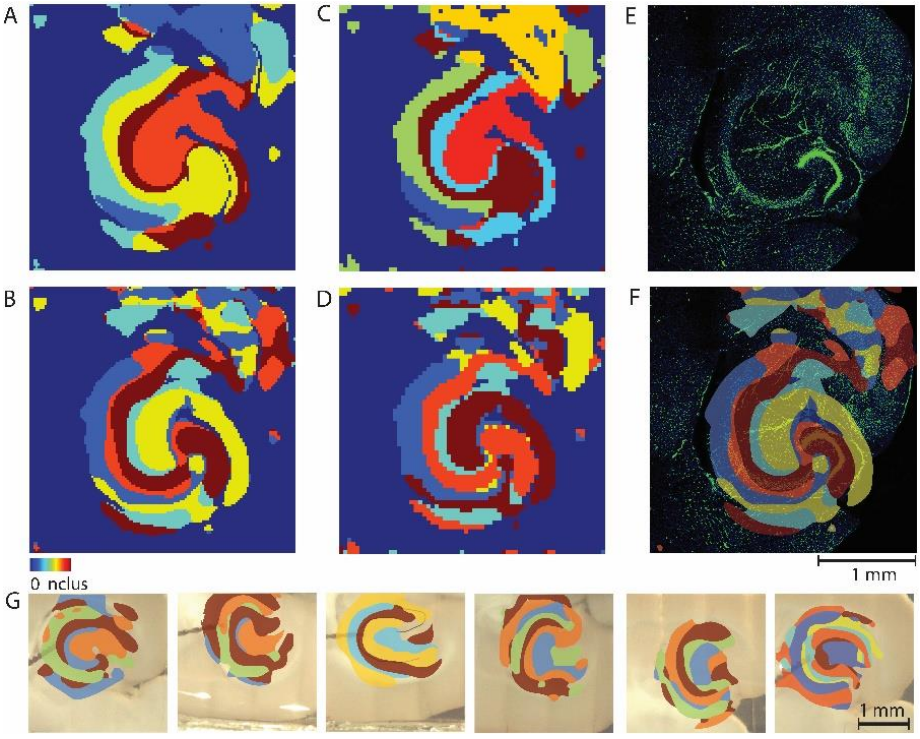

Figure 4.4 Spatial synchronization maps. *(**A,C**) Maps computed from interpolated and normal potential averaged events. (**B,D**) Computed from CSD. (**E**) Hoechst staining that show the structure of the nuclei of the recorded corticol-hippocampal slice. (**F**) Spatial synchronization map show in B superimposed to the anatomical image. (**G**) Example of Spatial synchronization maps applied to the CSD computed for other brain slices.*

distribution of instantaneous phase differences between two signals (Stam, Nolte, and Daffertshofer 2007). The central idea of this method is to discard phase differences that center around 0 mod π.

By applying this analysis, I was able to compute the spatial synchronization maps reported in **Figure 4.4** for a typical recording in which the activity also spread to the cortex. The same analysis was applied to both the extracellular recorded potential (panel A,C) and to the result of the CSD analysis (panel B,D). For computing maps shown in panel A and B, data were interpolated to increase the number of points from 64 x 64 to 120 x 120. Further, the potential and CSD were filtered in the low frequency band 10-40 Hz, before computing the PLI matrix. It has to be noted that filtering in other frequency bands was not giving any kind of the clear clustering results. Following this analysis, I compared the clustering results with the anatomical microscopy image of the recorded brain slice (see 4.2.3).

As shown in panel F the PLI map indicates that the profile of the different clusters follows the lamina profile of the hippocampus. As it can be appreciated, the brown cluster follows the pyramidal layer and the granule cell layer of dentate gyrus; the red and blue clusters are localized over the stratum oriens; the light blue cluster on the stratum radiatum and the yellow cluster on the molecular layer. Other examples of PLI map results from other brain slices are reported in panel G and are consisted with the first example.

4.4 DISCUSSION

Electrophysiological experiments on brain slices have a great advantage that they can be accurately controlled. The extracellular drug, ionic and modulatory concentrations can be precisely set and varied. Virtually any part of the brain can be accessed and targeted under visual guidance, and the *in vitro* preparation can be used in absence of anesthetics, which can distort the interpretation of data in many *in vivo* experimental situations. However, neuronal networks in brain slices are limited to local connections only. Indeed, these *in vitro* studies are limited due to the simple fact that the brain is reduced down to a slice. The physiology of the *in vitro* brain slice is maintained artificially, and the degree to which the 'normal' physiological state is recreated will determine the validity and quality of the data obtained from it. It is therefore important to ensure that the brain slice is kept under optimal conditions during *in vitro* experiments. The optimization of these conditions was an important part of my work that allowed me, finally, to successfully implement my experiments and the analysis of data presented here.

High resolution CMOS-MEA technology has an incredible potential to unveil how the brain process the information. However, the amount of data that these devices generate is a challenge per se. Indeed, the computational cost of algorithms tends to escalate with the square of the number of signals evaluated. Following the outcomes presented in the previous chapter, in which I developed a strategy to minimize the amount of recorded data by controlling the non-continuous recording of the evoked activity only, here I investigated the use of a data reduction method (the non-negative matrix factorization or NNMR) to catch salient features in space and time dimensions of sharp-wave ripples (SPW-Rs) recorded in cortico-hippocampal brain slices. Overall, my results show that computing the non-negative matrix factorization from CMOS-MEA recordings and measuring the difference in the Time matrix allows separating events that differ for their propagation (as in the case of spontaneous SPW-Rs) and duration (as in the case of SPW-Rs-LTP). From the acquired data, one can appreciate that there are some apparent differences between spontaneous SPW-Rs and SPW-Rs-LTP. The longer events found in SPW-Rs-LTP are very similar to the clustered SPW-Rs reported in (Papatheodoropoulos 2010). The fact that in spontaneous SPW-Rs I could not observe this kind of event is very likely due to the fact that these experiments were performed at room temperature without heating the ACSF solution.

In my study, I used the Current Source Density (CSD) analysis. This method provides an index of the location, direction, and density of transmembrane currents that arise with synchronous activation of neural tissue and that generate a potential profile in the extracellular environment. In all my experiments I estimated the CSD with the convolution of a Laplacian of Gaussian (LoG), which is a second-order derivative filter. However, many limiting factors should be considered, such as the geometry of the array or the distance of the electrodes to the tissue. In the last few years, a new method for CSD estimation has been developed: the inverse CSD (iCSD) method (Pettersen et al. 2006). The main idea behind iCSD is to assume a specific parametric form of CSD generating the measured potentials (e.g., spline interpolated between the grid nodes) and to calculate the LFP in a forward-modeling scheme in order to obtain the values of CSD parameters (e.g., CSD values at the nodes) by matching the experimental data with the computed values. The iCSD framework requires the assumption of a specific geometry of contacts requiring new calculations for each distribution of electrodes. Alternatively, the kernel CSD method (kCSD)(Potworowski et al. 2012)uses some basic facts from the theory of reproducing kernel Hilbert spaces used in machine learning. In this case, the assumption of a regular electrode arrangement is not necessary and kCSD can be applied to recordings from electrodes distributed at any position, including one-, two-, and three-dimensional sets. Moreover, the kCSD is a general non-parametric framework for the CSD estimation that also includes all the previous variants of iCSD methods as special cases (Potworowski et al. 2012).

In order to evaluate if the kCSD could have been providing a better estimation of sink and sources in my experiments, in ***Figure 4.5*** I compare the results obtained using the CSD method based on the Log filter (Panel C) and the kCSD method (Panel D). As one can notice, results of these two methods do not show astonishing differences on high-resolution electrical recorded data. However, computationally these two methods are very different. Indeed, due to the high computational cost and the need of tuning different parameters for the kCSD method, in my work I therefore decided to

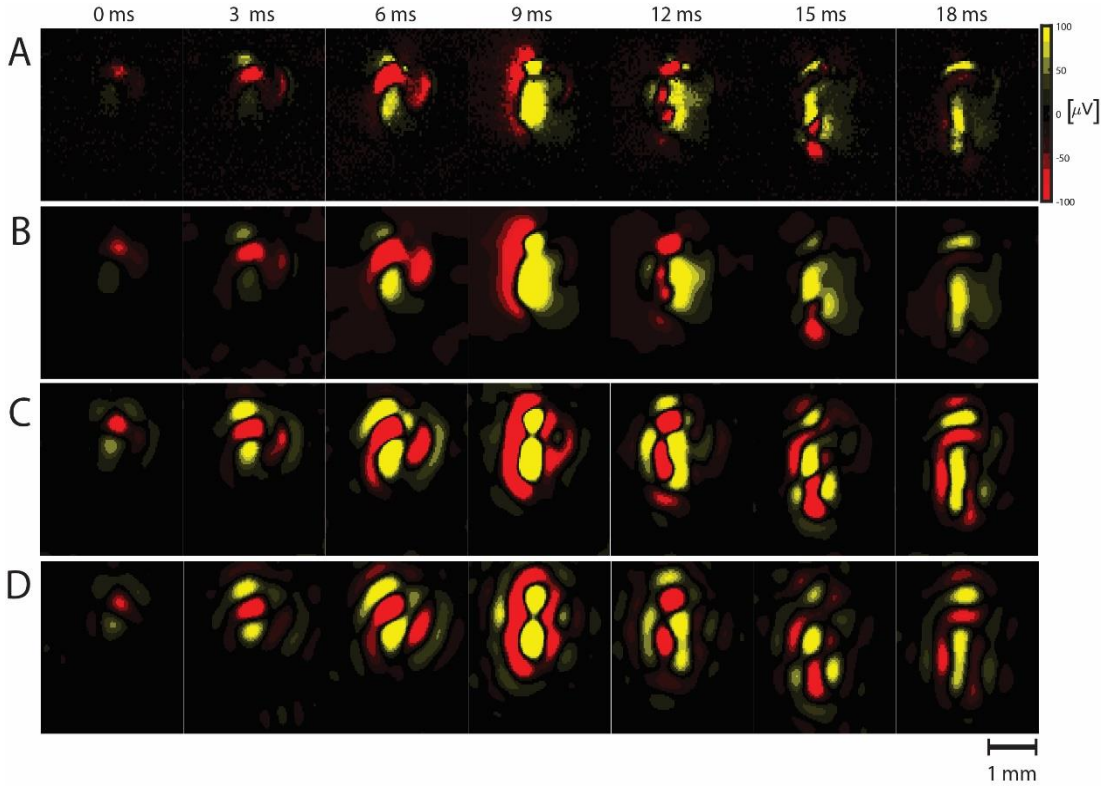

Figure 4.5 Comparison of potential and current source density methods. *(**A**) View of the voltage potential profile in space at different timepoints; (**B**) potential smoothed with a gaussian filter(sigma=2) (**C**) Csd computed with LOG filter (**D**) Kernel Csd method.*

focus on the use of the simple convolution with Log filter. Definitively, more detailed studies are needed to understand whether complex modeling as implemented in the kCSD is really useful for high-resolution electrical recordings (my laboratory collaborates with Prof. Daniel Wójcik on this topic).

The different clusters of events that emerge from the NNMF analysis of high-resolution reflect different origins and trajectories of propagation of SPW-Rs. For these results, one could ask whether the recording resolution might be relevant for this type of analysis. To answer this question, I analyzed the same data presented in this Chapter by spatially downsampling the recordings, thus mimicking the case of recordings from classical passive MEAs with low-density arrays of 64 electrodes. For this analysis, I selected a sub-set of 64 electrodes by considering a layout consisting of a regular grid with electrodes spaced by 300 µm. In ***Figure 4.6*** I report results by comparing the clusters obtained with high resolution (panel A) and low-resolution recordings (panel B). Overall, what emerges is that the analysis of spatially downsampled data is sufficient to identify the same clusters of SPW-Rs. This reflects the high synchronicity and spatial widespread in the entire hippocampal circuit of this type of field potential propagation. However, while the latency and of the propagating activity is maintained, high-resolution recordings allow to finely localizing these events in space (see the bottom of ***Figure 4.6***) and appreciate how they follow the laminar profile when observed by overlying the anatomical view of the recorded brain slices. Indeed, the strength of high-resolution recordings is the possibility of correlating LFPs with anatomical structural data. This could be better appreciated on results obtained by analyzing the phase synchronicity of the SPW-Rs. By computing spatial synchronization maps I have shown the possibility of extrapolating the anatomical information from the synchronicity between extracellular signals recorded from electrodes located in different sites of the cortico-hippocampal circuit. The method that I used to create these maps is very similar to the method used by (Berényi et al. 2014), differing from the use of the Phase Lag Index (PLI) matrix, and similar to an

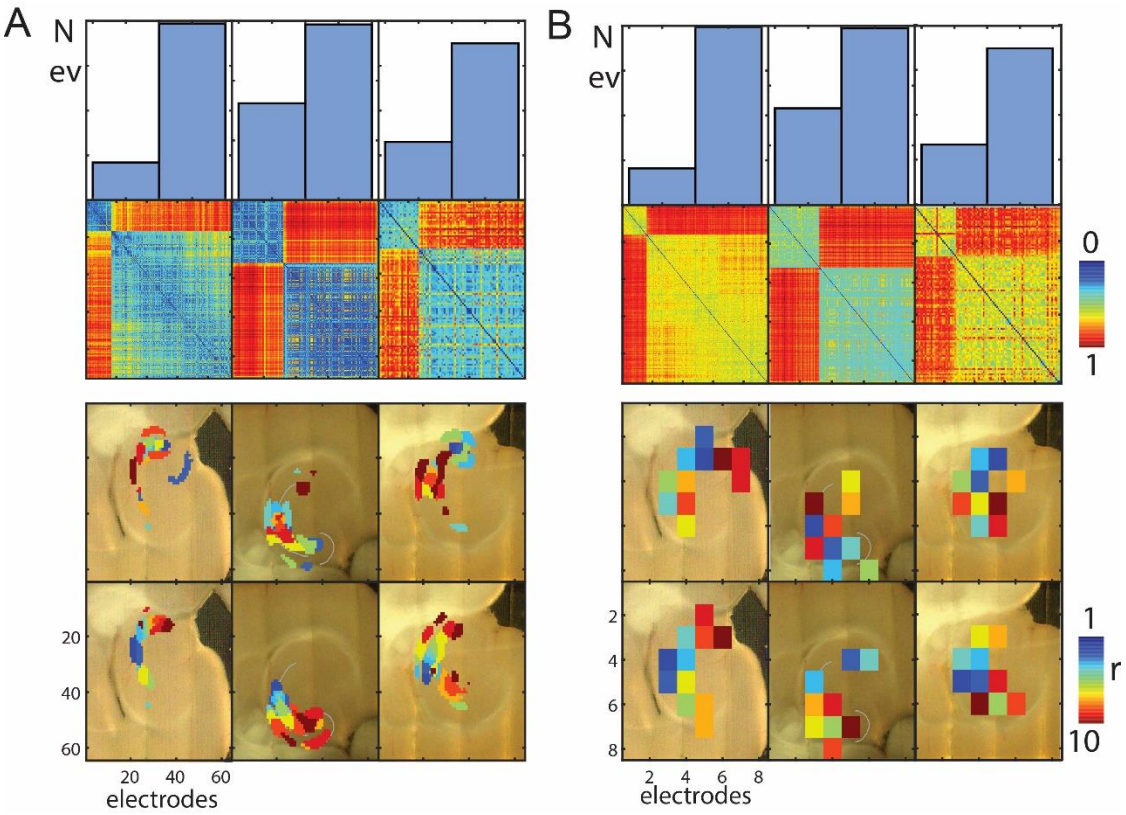

Figure 4.6 Comparison of NNMF method between high density recording (panel A) and low density down sampling (panel B). *Histogram of the number of events for each cluster (Top); distance matrix (Middle); first 10 spatial component color coded respect order in T matrix*

implementation that was recently presented (Bruña et al. 2018). Notably, this algorithm allows the direct calculation of all source pairs at once, with negligible memory increase. In addition, the implementation removes the need for using a for-loop over the signals. The distance matrix generated scale up very quickly with the number of electrodes. Applied to many events this fast implementation prevented the distance matrix storage, thus keeping it in the memory and applying directly the gradient algorithm for clustering. The maps generated using this method show that the recorded events tend to follow the laminar profile. This can be expected since these events reflect the highly synchronous activation of the stratum radiatum of the hippocampus during sharp waves. However, this co-localization is still not very precise and this because it most likely requires a better estimation of the current sources.

Given the development of these algorithms, I also investigated the use of the same data analysis developed in this chapter for SPW-Rs to analyze the evoked activity in LTP experiments presented in Chapter 3. Interestingly this method allows distinguishing very well the events recorded before and after potentiation as induced by the tetanic electrical stimulation (**Figure 4.7** panel A,B). Panel C shows the spatial synchronization maps obtained from the averaged potential after potentiation computed for each slice.

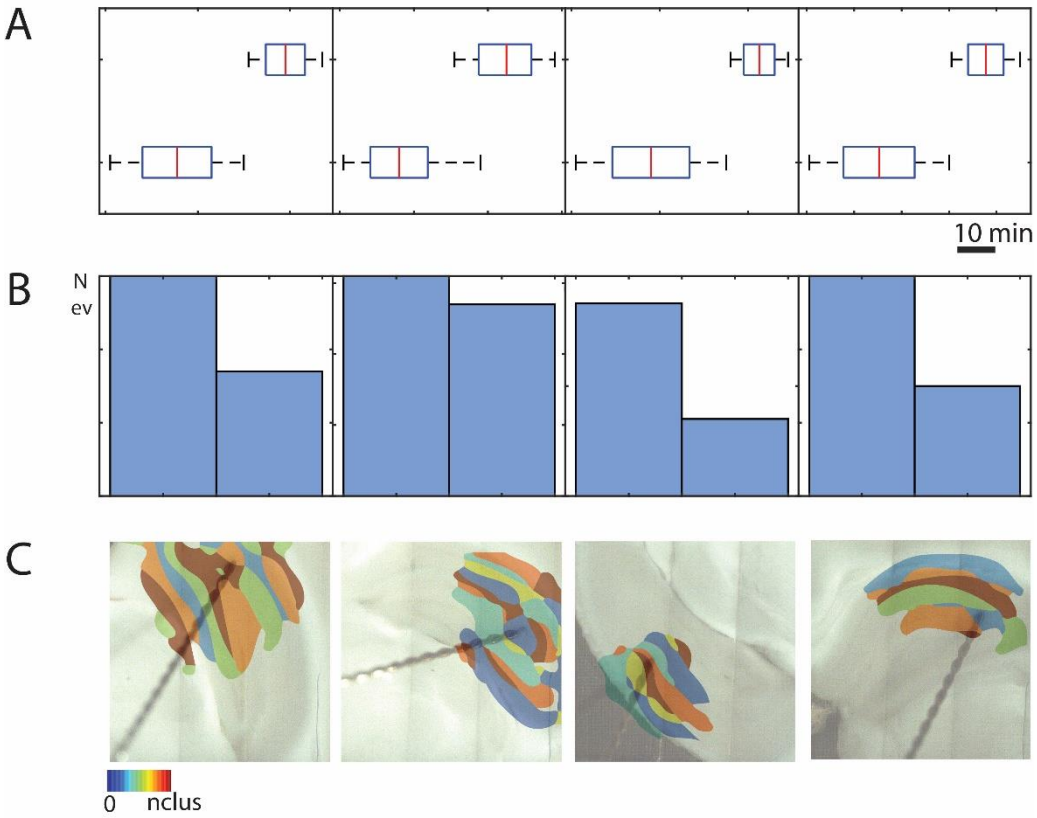

Figure 4.7 NNMF analysis clusterization and spatial synchronization maps applied to LTP experiments. *(**A**) Distribution in time of events for each clusters in four slices. (**B**) Histogram of number of events for each cluster. (**C**) PLI maps of averaged evoked activity*

4.5 PERSPECTIVES

My study on SPW-Rs recordings from *in vitro* brain slices introduce the CMOS-MEA technology for these studies. However, there are many aspects that could be further investigated on this platform. Additionally, something that I did not perform, but it would be interesting to try, is to extend the analysis presented in this Chapter to other types of activity patterns generated in the hippocampal-cortical circuits, such as gamma waves induced by carbachol *in vitro* (Wójtowicz et al. 2009)(Pálhalmi et al. 2004). More interesting should be the use of optogenetics to stimulate different populations of neurons. (Schlingloff et al. 2014) have shown that in the hippocampal slice preparation, strong optogenetic stimulation of parvalbumin-expressing (PV) interneurons was sufficient to trigger SPW-Rs. In contrast with these experiments (Stark et al. 2014) has shown that the stimulation of the same PV-interneuron is sufficient to abolish SPW-Rs *in vivo*. The contradiction is explained with the different numbers of cells that were modulated in the two experimental conditions (whole hippocampus *in vitro* and few cells *in vivo*). Recently, it was also shown that a weak focus and diffuse electrical stimulation is sufficient to induce SPW-Rs events (Jiang et al. 2018).

During my PhD I also attempted to implement optogenetic stimulation combined with the CMOS-MEA recording platform. Briefly, I attempted to modulate neural activity in the slice lying on the CMOS-MEA from the top using a laser HD projector (https://celluon.com/picopro-3/). To do so, I built an optical setup that permitted regulated the projection area on the CMOS-MEA active area (see **Figure 4.8**). A user-friendly interface was also implemented to deliver a different type of stimulus in multiple points of the projected area. I performed some pilot experiments using a transgenic mouse model (Thy1-ChR2-YFP https://www.jax.org/strain/007615). These mice express the light-activated ion channel, Channelrhodopsin-2 (from the green alga Chlamydomonas reinhardtii), fused to Yellow Fluorescent Protein (ChR2-YFP) throughout the brain, including in the cortex, hippocampus, thalamus, midbrain, brainstem, cerebellar mossy fibers and retinal ganglion cells. However, in this platform I encountered several issues and in particular, we had too much noise artifact that obscured the light-evoked response. Future improvement and control of the hardware acquisition parameter of CMOS-MEA are needed to perform experiments with direct high energy light exposure. Additionally, improvements in CMOS-MEAs devices (as those under development in our laboratory) might support better recording performances when combined with optogenetic stimulations.

On the data analysis side, I also preliminarily investigated the idea of deriving alternative methods using techniques developed in the optical image-processing field. As the number of channels scales up, we can start thinking about new kinds of analysis approaches. The concept of active pixel sensor (APS), on which CMOS-MEAs used for my experiments are based (Berdondini et al. 2009), comes from

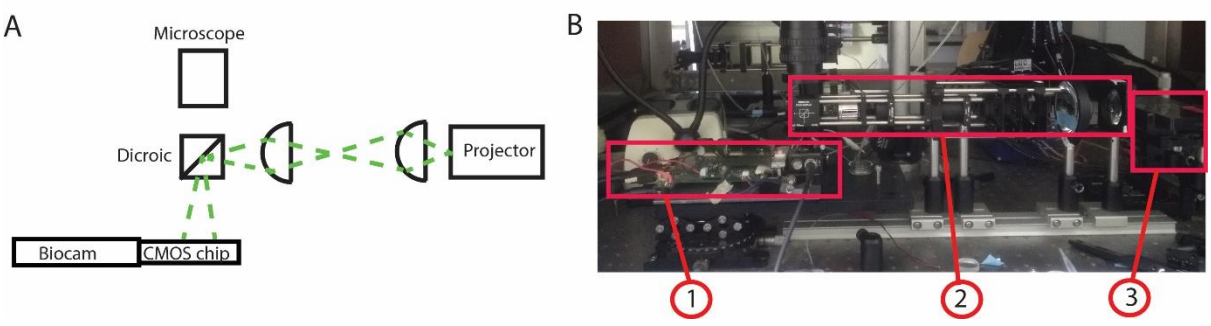

Figure 4.8 Overview of the setup implemented for optogenetic stimulation on CMOS-MEA platform. *(**A**) Schematic view of the optical pathway and (**B**) photo of the setup highlighting the biocam system (1), the optical pathway (2) and the laser projector (3).*

the field of image camera sensors. As shown here, these devices can literally image the electrophysiological activity of brain circuits.

As reported in paragraph 4.2.4.3, one of the main factors that determine the amplitude of the LFP is the geometry of the source that generates them and thanks to the high density electrode array technology we can nowadays analyze these events in a more reliable way. Usually, we are used to thinking about many signals (for each electrode recording in time) varying over time. However, nowadays, we can conceive treating our data as a sequence of images and analyze them by developing approaches exploiting concepts from the field of digital image processing. A wide range of algorithms has been developed with the aim of useful extract information from visual imaging data (Szeliski 2010). These algorithms range from simpler methods of image processing convolving the images with a different type of filters (like the log filter that I used for computing the CSD) to more complex algorithms like the analysis of segmentation or optical flow with the aim of tracking the motion of objects based on pixel intensities.

To illustrate this concept, I explored the use of a simple technique used for edge detection in computer vision (Canny 1986). During my PhD I spent a lot of time watching the SPW-Rs potentials propagating along with the hippocampus. Before the reducing approach, that let me to deal with the high dimensionality of these data, I was trying to track the center of the dipoles of sink and source regions along time. The aim was to build a trajectory for each event (see **Figure 4.9**). The problem was that at a certain time the shape of the propagation become very complex, and a linear propagation was not anymore sufficient to describe the data. Therefore, I explored the use of edge detection to analyze these propagations in an alternative way. Considering a single event as a sequence of frames in time, one can compute for each frame the edge of the CSD distributions. Thus, for each frame, I obtained a binary image in which the computed lines represent the edges between positive and negative regions. In other words, these are regions in which the current changes sharply (see **Figure 4.10** panel A).

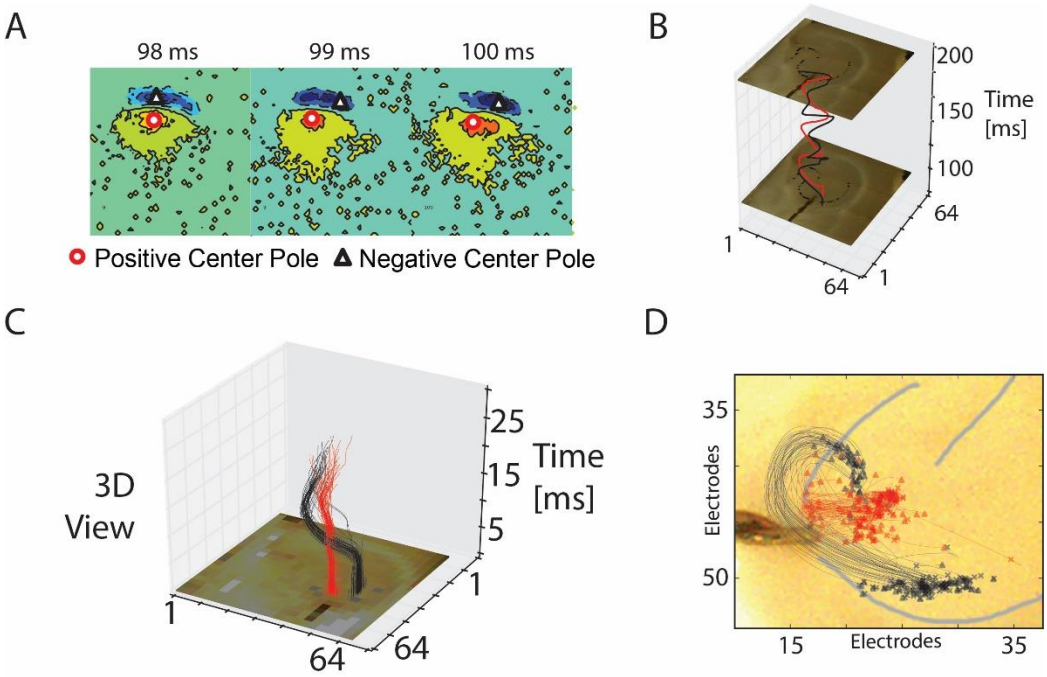

Figure 4.9 Overview of the analysis for computing potential dipole trajectories. *(**A**) Examples for three timepoints of the potential dipoles center position (**B**) 3d view of positive and negative trajectories for one event (**C**) 3d view of the initial trajectories for many events (**D**) Projection of trajectories shown in C (triangle and cross are the first and last timepoints)*

Finally, I superimposed all the detected edges to obtain an intensity map that shows the regions in which the dipole of the detected sink and sources activates the most. This map provides a spatial view on where the activity propagates for all the recorded events, with a higher intensity where it remains for more time. In the examples of the intensity maps shown in **Figure 4.10** panel B I report the results for three different brain slices that expressed spontaneous SPW-Rs. It can be observed how the higher intensities overlap with the pyramidal layer of CA3. The other most active layer corresponds to the edge of the molecular layer. This active area seems reflecting the recurrent connection present in the CA3 area.

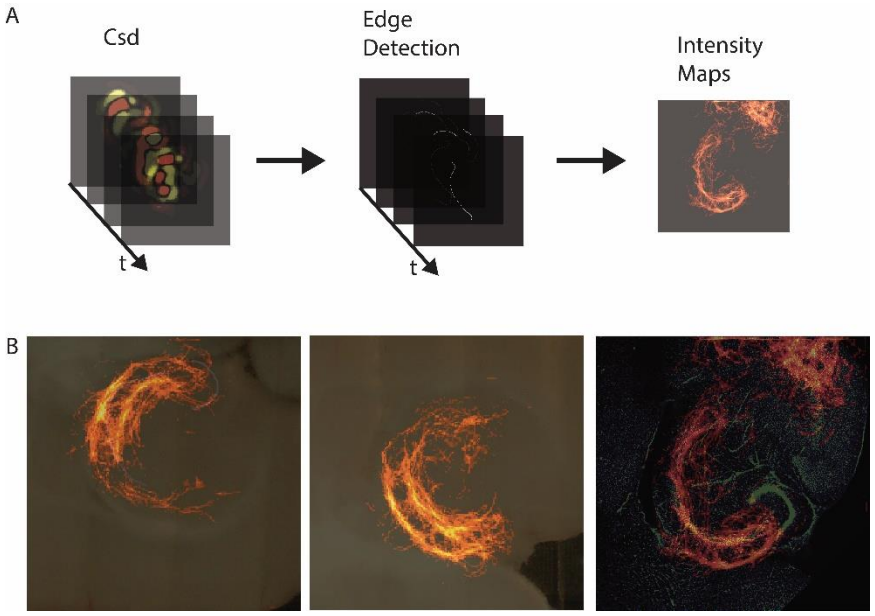

***Figure 4.10 Perspective of image processing techniques applied to high density LFP activity data (A**) Illustration of the alternative approach of analysis using canny edge detector applied to CSD data **(B)** Examples for tree slices of intensity maps computed with edge detection technique superimposed to anatomical image of the slices**.

5 SOFTWARE DEVELOPMENT FOR SINAPS PROBE

5.1 INTRODUCTION

In the previous chapters, I have been focusing on brain slice recordings using planar high-density CMOS-MEA devices and, specifically, in setting up the experimental conditions and computational methods to analyze high-dimensional electrophysiological data. Here, I report on my contribution to the development of a platform for high-resolution electrical recordings *in vivo*.

The IIT-NetS^3 laboratory in which I did this PhD is currently developing a cutting-edge technology for implantable active dense electrode array probes that is grounded on similar concepts as previously developed for planar devices. Indeed, these neural probes exploit the Active Pixel Sensor concept (APS) to integrate a dense array of active microelectrodes with underneath front-end circuits for signal conditions and on-probe multiplexing and addressing circuits. The technology that was developed to design these probes is referred to as SiNAPS, or Simultaneous Neural recording Active Pixel Sensor technology (www.sinapsprobes.eu). CMOS-probes with single (Angotzi et al. 2019) or multiple shanks (Boi et al. 2019) integrating thousands of closely spaced microelectrodes (electrode size 15 × 15 μm^2, pitch of 28 μm,) with whole array readout capabilities were designed and fabricated to map neural activity across and within large brain circuits. Acute *in vivo* recordings performed on different animal models (mice, rats and, non-human primates) demonstrated broad-band, whole-array read-outs capabilities at 25 kHz/channel, and show a measured input referred noise in the action potential band (300-7000 Hz) of 6.5 ± 2.1 μV_{RMS}, and a power consumption <6μW/electrode-pixel.

During the last period of my PhD I participated to preliminary experiments in awake behaving mice (performed in Munich in collaboration with Prof. Anton Sirota) using a 1024 electrode-pixels, 4-shank CMOS-probe and, as a first step, I worked on the development of a Graphical User Interface for controlling the acquisition and visualization of neural recorded data. Furthermore, I started to investigate ways to apply *in vivo* the data analysis methods for high resolution electrophysiological recordings that I developed during my PhDS to study LFPs in brain slices.

In this chapter, I will first introduce the SiNAPS probes technology and the current experimental platform that was adapted and validated for 4-shanks probes. Successively, I will describe the experimental data that were collected *in vivo* and report on the software implementation that I developed to operate this platform.

5.2 SINAPS PROBES

The 4-shanks SiNAPS probe is based on the power efficient analog front-end module that was also used in the single shank SiNAPS device previously described in (Angotzi et al. 2019). As illustrated in **Figure 5.1** panel A, these devices rely on the integration of electrode array modules. A single SiNAPS module comprises 32 electrode-pixels, with each electrode-pixel providing in situ amplification and low-pass filtering (Gain = 46 dB, f_{-3dB} = 4 kHz). These 32 electrode-pixels are time-division multiplexed to a second stage variable gain amplifier (up to a 7-fold gain) before off-chip analog to digital conversion (12 bit resolution, up to 25 ksamples/s per electrode-pixel).

An active feedback circuit shared in a time division multiplexed fashion among the 32 electrode-pixels of the analog front-end periodically and automatically adjusts the operating point of the in-pixel low-noise amplifiers. This is needed to avoiding the saturation of the first-stage amplifier by inevitable DC drifts arising at the tissue electrode electrode-pixel interface. This DC offset correction procedure was deemed favorable as it negates the need for additional circuit elements such as RC components or

large feedback capacitors that are subject to mismatch that can degrade the input impedance and may lead to signal attenuation by creating voltage dividers. Therefore, this circuit solution is based on DC front-ends and it allows for minimally sized front-ends that can be integrated underneath each electrode. As illustrated in Figure 1A-B, in the current implementation of the 4-shanks probes the 32 electrode-pixels comprising the analog front-end module are arranged with a 28 µm pitch in two rather than three columns as for the single shank SiNAPS probe, thus reducing the cross-sectional width of the shanks from 120 µm to 80 µm. Each shank integrates eight of such modules, and achieves a total number of 256 active recording sites over an active length of 3.58 mm. Finally, the inter-shank separation is of 560 µm and was specifically set to target spatially distributed recordings in the hippocampus of rodents. The overall CMOS area needed to fabricate each multi-shanks SiNAPS probe (base + shanks) is <12 mm^2, with an electrode-pixel density of ˜90 pixels/mm^2.

5.3 SiNAPS ACQUISITION SYSTEM ARCHITECTURE

An overview of the current SINAPS platform, from the probe to the acquisition system, is shown in **Figure 5.1** panel C. The acquisition system is composed by an interface board for analog to digital conversion (ADC Box), an FPGA-based acquisition unit (Opal Kelly ZEM4310 integration module based on an Altera Cyclone IV FPGA) and a Cameralink interface for real-time, high-rate data transmission to a PC equipped with a frame grabber. The interface board integrates 32 ADCs, one for each one of the 32 electrode-pixels of a module of the SiNAPS probe. The acquisition unit implements a controller for the ADCs, an input memory buffer, a bank of programmable band-pass digital filters and a bidirectional interface for communication with the CMOS-probe. The PC runs a data acquisition software (in the first phase of the project this was a modified version of BrainWave, from 3BrainAG, Switzerland) for data visualization and storage which is currently limiting to a maximum acquisition rate of about 16 ksample/s. For technical detail see (Angotzi et al. 2019). As it will be described in the next session, I contributed to the development of dedicated control software that is replacing the originally used BrainWave software.

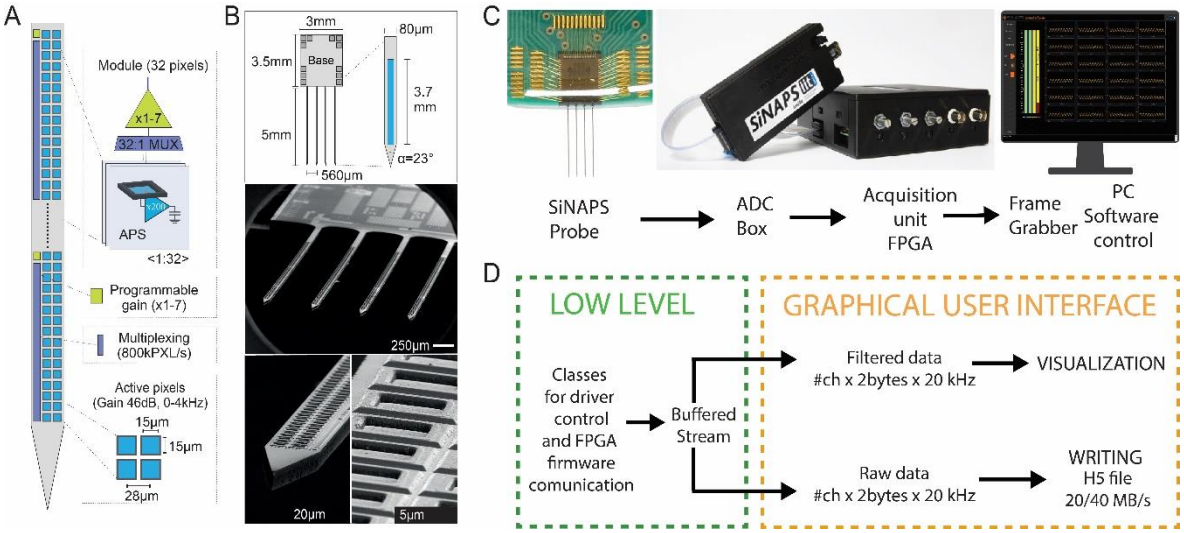

Figure 5.1 Overview on the Synapsis probe, acquisition system and data management. *(**A**) Architecture and dimensions of the implantable CMOS-probe: multiple modules comprising 32 active electrode-pixels that are time division multiplexed to a variable gain amplifier are arranged over a 80µm wide shank for a total of 256 electrode-pixels per shank (pitch 28µm, electrode pad size 15×15µm2). (**B**) Scanning Electron Micrographs showing a structured 4-shanks SiNAPS at different magnification levels. Shanks are 5mm long, with active sensing of 3.6mm in length, and 560µm shanks separation (**C**) Schematic chain of the complete acquisition system (**D**) Schematic view of the data flow.*

5.4 PRELIMINARY EXPERIMENTS

The overall aims of the preliminary experiments reported here were to evaluate the recording performances of 4-shank CMOS-probes. These were required in order to implement the full platform for specific research studies that are ongoing.

5.4.1 Surgical procedures and acute *in vivo* recordings

Three adult male mice were prepared for these experiments, but only data from a single mouse are shown in this work. Mice were first habituated to human handling after which surgical procedures were administered. Anaesthetization was induced using midazolam, medetomidine and fentanyl pharmacological cocktail. Mice were then head-fixed within a stereotaxic frame and oxygenated air was supplied at 1l/min throughout the surgical procedures. Anesthesia maintenance was achieved with 0.5-1% isoflurane, which was administered through a vaporizer. After rostral skin incision and clearance of the skull from any connective tissue, several screws were implanted around the location of the craniotomy destined to serve as ground and reference screws. Two of these were found on the occipital bone above the cerebellum, while a third was implanted very close to the point of insertion of the SiNAPS probes (medial shank coordinates AP: -2 mm, ML: +0.9 mm). We did not observe differences in the signal quality when using any of these reference screws. To enable a stable head fixation of the animal during behavioral recordings, a custom-designed head post was implanted onto the posterior bone plate. An additional wire was inserted into the olfactory sensory epithelium allowing recordings of respiration rhythm. All screws and headpost were secured onto the skull using dental acrylic cement. Finally, a cranial window was drilled above the dorsal hippocampus, the dura was carefully retracted and the craniotomy was sealed with two components artificial dura that was easily penetrable using multi-shank probes. A further layer of a silicon elastomer (quick seal) was added above but not in contact with the artificial dura.

After a week of post-operative recovery, mice were water-deprived and trained to run on a running disk for water reward. To record electrophysiological signals, the SiNAPS probe was mounted on a micromanipulator, aligned to the craniotomy and lowered down to 3.4 mm from the brain surface (insertion speed 0.2 µm/s). After 15 minutes of resting, in which the animal calmed down in complete darkness, we acquired from the multi-shanks SiNAPS probe broadband neural activity from cortical, hippocampal and thalamic structures. After recordings, the probe was extracted from the mouse brain and rinsed in distilled water to be reused in the next experimental sessions. All procedures were performed in accordance with the European Communities Directive 2010/63/EC and the German Law for Protection of Animals (TierSchG), and were approved by local authorities (ROB-55.2-2532.Vet 02-16-170). All efforts were made to minimize the number of animals used and the incurred discomfort. The **Figure 5.2** show some examples of data recorded with SiNAPS probe. In panel B are shown some traces for one shank of LFPs.

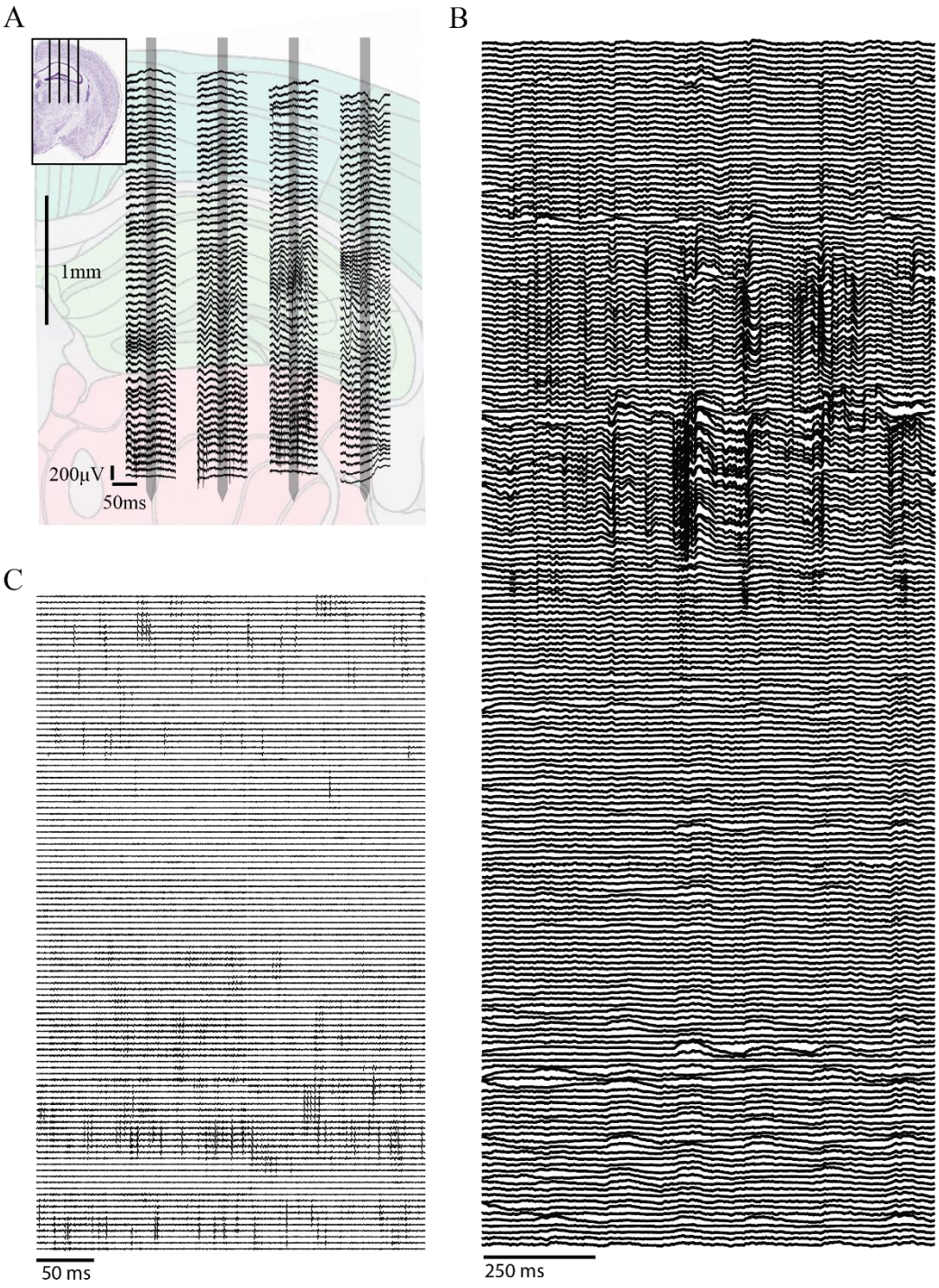

Figure 5.2 In vivo recording with multi-shanks SiNAPS probe. (A) *Approximate probe position during experiments superimposed to Allen Mouse Brain Atlas (-2 mm AP from bregma) with, for each shank, 100ms of the broadband neural signals collected from a representative subset of the 1024 available channels* ***(B,C)*** *Example of band pass filtered (1-300 Hz,300-5000 Hz) neural data collected from a portion of one of the shank.*

5.5 CONTROL SOFTWARE DEVELOPMENT

The control software has been developed in C# through Visual Studio 2017 environment. Its architecture is composed by two main core components:

1. *low level libraries* implementing a driver interface with the FPGA-based acquisition system (developed by Luca Berdondini).
2. *high level libraries* implementing the Graphical User Interface (GUI) for data storage and visualization that I developed during the last part of my PhD.

5.5.1 Low level Libraries

Low level libraries are used for bi-directional communication with the FPGA-based acquisition system. Two distinct physical channels are available: a low-data rate serial interface for system initialization through a set of user defined parameters (these include among others the sampling rate and the probe type (single or 4-shank)); a high data-rate cameralink communication channel for reading-in the recorded neural data with a typical rate of about (~40Mb/s). More in detail, from the FPGA, two data streams are sent to the PC (**Figure 5.1** panel D): a raw data stream and a filtered data stream (real-time filtered on the FPGA). The former is useful to characterize the working performances of the system and for precise post recording reconstruction of the full band signal (see paragraph 5.2) while the latter is produced by real-time processing module implemented in the FPGA to correct unwanted artifact intrinsically related to the on-probe circuits.

5.5.2 The GUI Interface

In **Figure 5.3** panel A I report a view of the GUI that I developed for monitoring the CMOS-probe recordings. On the left side, different control buttons give access to distinct pup-up menus (panel B) in-which the user can set different parameters:

- Setting Panel: permits to set the operating mode of the probe;
- File Panel: defines the destination of the recording file, the name and the duration;
- Plot Panel: defines all the control parameter for data visualization (see below);

On the middle, the user-control buttons allow to control the data acquisition:

- Play button: starts data acquisition and (only) visualization;
- Rec button: starts data acquisition, visualization and storage to file;.
- Stop button: stops both play or recording modes.

In the “Recording” mode the raw data is stored in an HDF5 file with a hierarchical structure that includes, besides recorded data, all the parameters used for the recording.

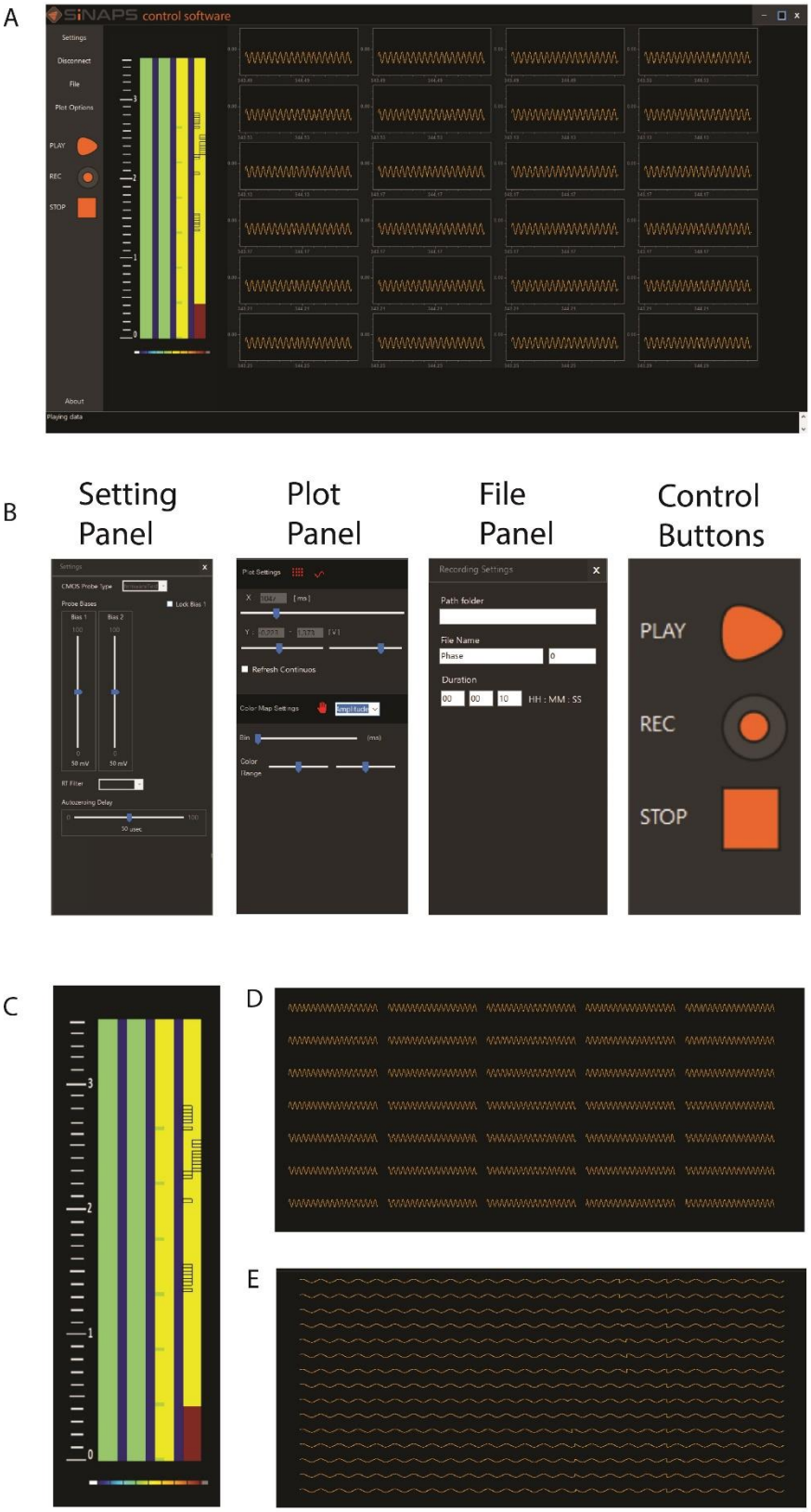

Figure 5.3 Graphical User Interface of the control software developed for the SiNAPS platform. *(**A**) Overview of the interface during a recording. (**B**) Different panels for parameters setting. (**C**) Color map that integrate continuously the activity from all the channels (**D,E**) different modalities for distributing single signal plot of the selected channels from the color map.*

Notably, a color map generated by integrating the activity for each electrode over a user-defined time-bin provides real-time information on the overall neural activity recorded from the whole probe (**Figure 5.3** panel C). Different types of integrations can be computed and set (such as max-min amplitude and variance, among others). A millimeter scale bar on the left of the same map is added to provide the experimenter a feedback about the position of the probe inside the brain. Furthermore, multiple channels can be selected from the color map to be plotted as voltage vs time traces, with a user selected layout (stacked in vertical or in a square matrix, see Panel D,E in **Figure 5.3)**

5.5.3 Future implementations and improvements

The control software is still at its initial stage of development and is on the way to be tested during experimental recordings. Upon its testing, we aim at integrating different other functionalities, including:

- Offline visualization of previously recorded files
- Writing and conversion of data in other formats for compatibilities with other third party software
- A Library of offline/online data analysis tools (e.g. spikes detection and spectrum visualization for LFP)

5.6 PERSPECTIVES

During the last period of my PhD, I started to analyze the data recorded in this preliminary experiment by applying some of the methods that I have previously developed and used for *in vitro* experiments. However, in these first and preliminary trials, we were not able to record SPW-Rs events. Additionally, we also faced minor issues on the signal quality of signals in the low frequency band. This problem is now fixed and we need new experiments to move forward with this analysis. Besides that, I tried to compute the CSD with the Log filter presented in the previous Chapter. For the data recorded with the 4-shank probe, due to the spatial distance between the shanks, I used a vertical kernel (size of [2,5] with a sigma of 2) on data that were previously smoothed with a Gaussian filter (sigma=2). Some examples of the potential and CSD results are reported in **Figure 5.4** panel A,B respectively. Finally, I also computed the spatial synchronization map at different time bins and by filtering the LFP at different frequency bands. This was applied to the potential and CSD data (**Figure 5.4** panel C,D). In this figure, the superimposed anatomical image is only indicative. As shown, this method is likely able to separate different clusters, but further studies require the acquisition of more experimental data.

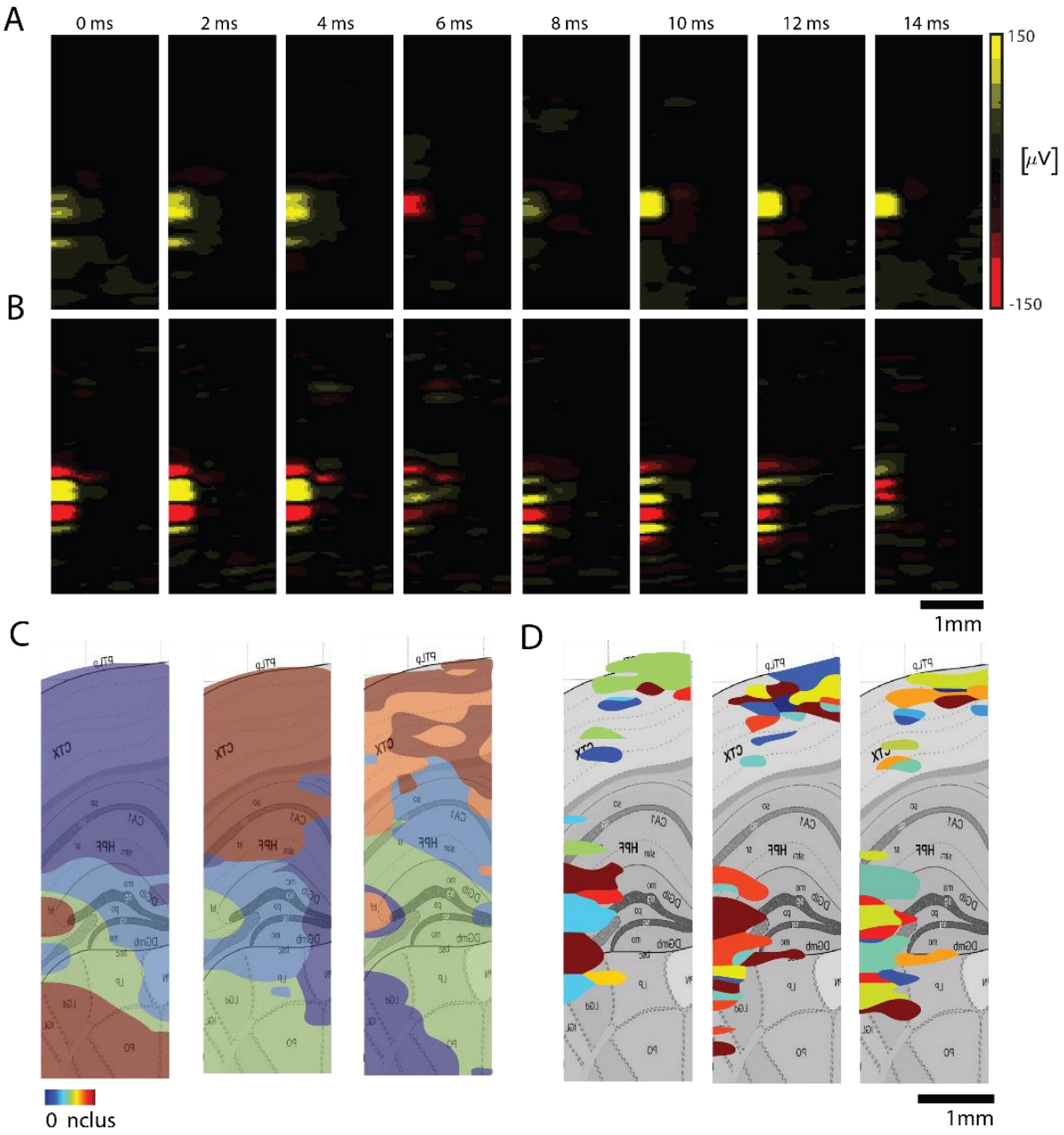

Figure 5.4 Preliminary analysis of LFP recorded with SiNAPS system. *(**A**) Smoothed electrical potential with a gaussian filter (**B**) Current source density computed with Log filter (**C**) Examples of Spatial synchronization maps computed from a bin of 1 of the potential filtered at different bands(from left to right 4-300 Hz, 120-280 Hz,280-300 Hz) (**D**) Examples of Spatial synchronization maps computed from a bin of 1 of the CSD filtered at different bands(from left to right 4-300 Hz, 120-280 Hz,280-300 Hz). The superimposed anatomical image is taken from the Allen Mouse Brain Atlas (-2 mm AP from bregma) and is only indicative.*

6 OVERALL CONCLUSION

In my PhD I investigated the application of high-resolution electrode array devices and computational methods to characterize low-frequency electrophysiological signals recorded from the cortico-hippocampal circuit. As I described, planar devices for *in vitro* electrophysiology, and very recently also implantable CMOS-based devices with dense active electrode-pixels are increasingly used in neuroscience research and will very likely increase their impact for functional studies on brain circuits in the incoming years. In this context, a major motivation in using and developing these devices consists in exploiting the small inter-electrode separations and a large number of recording electrodes to scale up current capabilities for identifying a large-number of single-units. However, as introduced in Chapter 2, low-frequency bioelectrical signals (or low-frequency field potentials, LFPs) play a fundamental functional role in the brain. This consideration motivated the studies that I have implemented in my PhD thesis, with the aim of contributing to advancing the characterization of these signals and in developing potential applications.

In particular, my work started by focusing on the development of a platform for pharmacological electrical read-outs from acutely recorded brain slices. This work was developed in collaboration with a CRO and 3Brain AG and is reported in the Chapter 3. By implementing a software tool to execute experimental protocols of long-term potentiation (LTP) and data analysis, my results show the potentiality of high-density recordings for revealing the effects pharmacological compounds on synaptic plasticity in different spatial regions of the cortico-hippocampal circuit. These spatiotemporally resolved recordings from the entire cortico-hippocampal slice provide a detailed overview of the effects induced by high frequency stimulation on electrically evoked potentials, and allowed identifying significant effects of a pharmacological compound (D-cycloserine DCS, a partial agonist of the NMDA receptors and an inhibitor of AMPA receptors). Such significance was not observed by testing its effects using conventional electrophysiological read-outs reported in the literature. While already in this first experimental Chapter I had to deal with the large volume of data that these devices are generating (the software tool that I developed allows to record only electrically evoked responses to minimize the volume of data), this is an aspect that I further investigated in Chapter 4. Indeed, I aimed at investigating a different type of computational approaches for the analysis of spontaneous SPW-Rs and LTP induced SPW-Rs. With Non Negative Matrix Factorization, I was able to separate different event clusters corresponding to events with different spatiotemporal features. This revealed differences in propagations for SPW-Rs and durations for LTP SPW-Rs. However, the major advantage of high-resolution recordings is not related to the capability of clustering SPW-Rs, rather in finely resolving this type of electrical activity to correlate it with anatomical structures. Indeed, one of the strengths of high-resolution recordings that I observed is the possibility to implement a fine analysis of the phase of these rhythms to investigate their synchronicity among brain circuit areas. Following a previously reported and slightly modified data analysis methodology to compute synchronicity maps, I have shown the possibility to link the recording of low-frequency electrical activity with the anatomical circuit organization. Following these results, I had planned to implement optogenentic experiments that would have allowed advancing in dissecting functional effects involved in the generation and propagation of SPW-Rs. Unfortunately, I encountered several technical difficulties related to the CMOS-MEA system that I was using that impeded the implementation of these experiments. In particular, because we were using a commercial platform, this could not be modified to investigate its performances under light stimulation. On this, the full in-house SiNAPS technology currently under development in our laboratory might be used in the near future to investigate alternative solutions to overcome this issue.

During the final period of my PhD, I had the chance to participate in some preliminary experiments *in vivo* using implantable high-resolution SiNAPS probes. I have shown in Chapter 5 some of the preliminary recordings and analyses of these data as obtained by applying similar methods that I did develop for *in vitro* experiments. In the future, it will be fascinating to advance the development of analytical tools for LFPs recorded *in vivo* with high-resolution devices as well as to combine some of the outcomes of this work with the analysis of single-unit activity that can be simultaneously recorded in multiple brain circuits (such as thalamus, hippocampus and cortex).

Besides the experimental research work and experience, during this PhD I developed several software tools using Python, Matlab and C#. These software tools, available at IIT for further studies, can help in a semi-automatic way the experimenter in monitoring the execution of experimental protocols and in the data analysis. Following my contribution to the development of a basic SiNAPS control software (Chapter 5), these tools might be integrated in the near future for the routine analysis of *in vivo* electrophysiological data.

7 PUBLICATIONS

7.1 PAPERS

1) **S. Zordan**, A.Maccione, A. Ugolini, C. Virginio, M. Corsi, D. Lonardoni, M. Gandolfo L. Berdondini.**"** Quantifying LTP in cortico-hippocampal slices with high-resolution CMOS-MEAs for compound testing." (In preparation for submission)

2) M.Marrese, D. Lonardoni, F.Boi, H.Hoorn, A. Maccione, **S. Zordan**, D.Ianuzzi, L.Berdondini. 2019. "Investigating the Effects of Mechanical Stimulation on Retinal Ganglion Cell Spontaneous Spiking Activity." *Frontiers in Neuroscience*.DOI: 13. 10.3389/fnins.2019.01023.

3) F. Boi, N.Perentos, A. Lecomte, G. Schwesig, **S. Zordan**, A. Sirota, L. Berdondini, G.N. Angotzi 2019. "Multi-shanks SiNAPS Active Pixel Sensor CMOSprobe: 1024 simultaneously recording channels for high-density intracortical brain mapping". *Biorxiv* . DOI: 10.1101/749911.

4) D. Lonardoni, H. Amin, **S.Zordan**, F.Boi,A. Lecomte ,G.N. Angotzi, L. Berdondini. 2019. "Active High-Density Electrode Array Technology and Applications in Neuronal Cell Cultures*" Adv Neurobiol*. DOI: 10.1007/978-3-030-11135-9_11.

5) H. Amin, A. Maccione, F. Marinaro, **S. Zordan**, T. Nieus, L. Berdondini. 2016. "Electrical responses and spontaneous activity of human iPS-derived neuronal networks characterized for three-month culture with 4096- electrode arrays." *Front. Neurosci.* DOI: 10.3389/fnins.2016.00121

6) A. Maccione, M. Gandolfo, **S. Zordan**, H. Amin , S. Di Marco, T. Nieus, G. N. Angotzi, L. Berdondini Microelectronics, 2015. "Bioinformatics and neurocomputation for massive neuronal recordings in brain circuits with large scale multielectrode array probes." *Brain research bulletin*. DOI: 10.1016/j.brainresbull.2015.07.008

7) G. N. Angotzi, F. Boi, **S. Zordan**,A. Bonfanti, A. Vato. 2014. "A programmable closed-loop recording and stimulating wireless system for behaving small laboratory animals." *Scientific Reports* . DOI: 10.1038/sre p05963

7.2 CONFERENCES

1) **S. Zordan**, D. Lonardoni, A. Maccione, L. Berdondini. 2018. "Mapping low-frequency field potentials in cortico-hippocampal brain slices with high-resolution CMOS-MEAs". *Frontiers in Cellular Neuroscience*. DOI: 12. 10.3389/conf.fncel.2018.38.00117.

2) **S. Zordan**,M. Zanotto , T. Nieus,S. Di Marco,H. Amin, A. Maccione, L. Berdondini. 2015. "A Scalable High Performance Client/Server Framework to Manage and Analyze High Dimensional Datasets Recorded by 4096 CMOS-MEAs" *7th Annual International IEEE EMBS Conference on Neural Engineering, At Montpellier, France*

3) H. Amin, A. Maccione, **S. Zordan**, T. Nieus, L. Berdondini. 2015. “High-density MEAs reveal lognormal firing patterns in neuronal networks for short and long term recordings”. *7th Annual International IEEE EMBS Conference on Neural Engineering, At Montpellier, France*

4) S. Di Marco, A. Maccione, L. Glavinskaya, G. Pruzzo, G. Hilgen, **S. Zordan**, O. Muthmann, M. Hennig, E. Sernagor , L. Berdondini. 2014. “Large-scale recording of light-evoked responses in the retinal ganglion cell layer of the explanted retina: a new HD experimental platform” *FENS 2014 Milan, Italy*

5) H. Amin, A. Maccione, T. Nieus, **S. Zordan**, L. Berdondini.2014. “High resolution microelectrode arrays (MEAs) for reliably studying an in-vitro neuronal network model of induced-Alzheimer’s Disease (AD)” *FENS 2014 Milan, Italy / Biosensors 2014 Melbourne, Australia*

6) G. N. Angotzi, F. Boi, **S. Zordan**, A. Vato. 2013. “A compact wireless multi-channel system for real-time intracortical microstimulation of behaving rodents” *Proceeding Neural Engineering (NER) 6th International IEEE/EMBS 1009 - 1012.*

Acknowledgments

First of all, I have to say thanks to all the colleagues of my lab Fabio, Gian, Lidia , Joao and all the people that left(Serena, Aziliz, Davide, Hayder, Ermanno, Sara, Mattia, Mario, Ale). They always helped me and bore all my existential crisis. A special thanks to Luca, that encouraged me and pushed me to see the half-full glass instead of the half-empty part, and gave me the opportunity to confront myself in the experimental research.

A special thanks to Alessandro M., that taught me a lot and pushed me to be better, supporting me for all my first period in iit.

Thanks to all the other friends of the iit (Roby, Fra, Sam, Loris, Isa, Lollo, Enrico, Annavera et al.) that transformed the sadness of my failures into a smile, sharing thought and happy moments.

Thanks to my family that always supported all my decisions and stood by my side from far away.

Thanks to my special cousins Gioia e Giulia, they were always there when I needed the most.

Thanks to the world wide web and all the technology that let me write this thesis.

8 CITED REFERENCES

Aivar, P., M. Valero, E. Bellistri, and L. Menendez de la Prida. 2014. “Extracellular Calcium Controls the Expression of Two Different Forms of Ripple-Like Hippocampal Oscillations.” *Journal of Neuroscience* 34(8):2989–3004.

Amin, H., A. Maccione, F. Marinaro, S. Zordan, T. Nieus, and L. Berdondini. 2016. “Electrical Responses and Spontaneous Activity of Human IPS-Derived Neuronal Networks Characterized for 3-Month Culture with 4096-Electrode Arrays.” *Frontiers in Neuroscience* 10(MAR).

Amin, Hayder, Alessandro Maccione, Federica Marinaro, Stefano Zordan, Thierry Nieus, and Luca Berdondini. 2016. “Electrical Responses and Spontaneous Activity of Human IPS-Derived Neuronal Networks Characterized for 3-Month Culture with 4096-Electrode Arrays.” *Frontiers in Neuroscience* 10(MAR).

Andersen, Per, Richard Morris, David Amaral, Tim Bliss, and John O’Keefe. 2007. *The Hippocampus Book*.

Angotzi, Gian Nicola, Fabio Boi, Aziliz Lecomte, Ermanno Miele, Mario Malerba, Stefano Zucca, Antonino Casile, and Luca Berdondini. 2019. “SiNAPS: An Implantable Active Pixel Sensor CMOS-Probe for Simultaneous Large-Scale Neural Recordings.” *Biosensors and Bioelectronics* 126(August 2018):355–64.

Ault, B., R. H. Evans, A. A. Francis, D. J. Oakes, and J. C. Watkins. 1980. “Selective Depression of Excitatory Amino Acid Induced Depolarizations by Magnesium Ions in Isolated Spinal Cord Preparations.” *The Journal of Physiology* 307(1):413–28.

Barnes, C. A. 1979. “Memory Deficits Associated with Senescence: A Neurophysiological and Behavioral Study in the Rat.” *Journal of Comparative and Physiological Psychology* 93(1):74–104.

Barnes, C. A. and B. L. McNaughton. 1985. “An Age Comparison of the Rates of Acquisition and Forgetting of Spatial Information in Relation to Long-Term Enhancement of Hippocampal Synapses.” *Behavioral Neuroscience* 99(6):1040–48.

Bastos, André M. and Jan Mathijs Schoffelen. 2016. “A Tutorial Review of Functional Connectivity Analysis Methods and Their Interpretational Pitfalls.” *Frontiers in Systems Neuroscience* 9(JAN2016):1–23.

Behrens, Christoph J., Leander P. van den Boom, Livia de Hoz, Alon Friedman, and Uwe Heinemann. 2005. “Induction of Sharp Wave-Ripple Complexes in Vitro and Reorganization of Hippocampal Networks.” *Nature Neuroscience* 8(11):1560–67.

Berdondini, Luca. 2001. “High-Density Microelectrode Arrays for Electrophysiololgical Activity Imaging of Neuronal Networks.” *Proceedings of the IEEE International Conference on Electronics, Circuits, and Systems* (1239–1242).

Berdondini, Luca, Alessandro Bosca, Thierry Nieus, and Alessandro Maccione. 2014. “Active Pixel Sensor Multielectrode Array for High Spatiotemporal Resolution.” Pp. 207–38 in *Nanotechnology and Neuroscience: Nano-Electronic, Photonic and Mechanical Neuronal Interfacing*.

Berdondini, Luca, Kilian Imfeld, Alessandro Maccione, Mariateresa Tedesco, Simon Neukom, Milena Koudelka-Hep, and Sergio Martinoia. 2009. “Active Pixel Sensor Array for High Spatio-Temporal Resolution Electrophysiological Recordings from Single Cell to Large Scale Neuronal Networks.” *Lab on a Chip* 9(18):2644–51.

Berényi, Antal, Zoltán Somogyvári, Anett J. Nagy, Lisa Roux, John D. Long, Shigeyoshi Fujisawa, Eran Stark, Anthony Leonardo, Timothy D. Harris, and György Buzsáki. 2014. “Large-Scale, High-Density (up to 512 Channels) Recording of Local Circuits in Behaving Animals.” *Journal of Neurophysiology* 111(5):1132–49.

Blackstad, T. W., K. Brink, J. Hem, and B. June. 1970. “Distribution of Hippocampal Mossy Fibers in the Rat. An Experimental Study with Silver Impregnation Methods.” *Journal of Comparative Neurology*.

Bliss, T. V. P. and T. Lømo. 1973. “Long-lasting Potentiation of Synaptic Transmission in the Dentate Area of the Anaesthetized Rabbit Following Stimulation of the Perforant Path.” *The Journal of Physiology*.

Bliss, T. V and a R. Gardner-Medwin. 1973. “Long-Lasting Potentiation of Synaptic Transmission in the Dentate Area of the Unanaestetized Rabbit Following Stimulation of the Perforant Path.” *The Journal of Physiology* 232(2):357–74.

Blum, Richard A., James D. Ross, Edgar A. Brown, and Stephen P. DeWeerth. 2007. “An Integrated System for Simultaneous, Multichannel Neuronal Stimulation and Recording.” *IEEE Transactions on Circuits and Systems I: Regular Papers* 54(12):2608–18.

Boi, Fabio, Nikolas Perentos, Aziliz Lecomte, Gerrit Schwesig, Stefano Zordan, Anton Sirota, Luca Berdondini, and Gian Nicola Angotzi. 2019. “Multi-Shanks SiNAPS Active Pixel Sensor CMOS Probe: 1024 Simultaneously Recording Channels for High-Density Intracortical Brain Mapping.” *BioRxiv* 749911.

Bottino, Emanuele, Paolo Massobrio, Sergio Martinoia, Giacomo Pruzzo, and Maurizio Valle. 2009. “Low-Noise Low-Power CMOS Preamplifier for Multisite Extracellular Neuronal Recordings.” *Microelectronics Journal* 40(12):1779–87.

Bruña, Ricardo, Fernando Maestú, and Ernesto Pereda. 2018. “Phase Locking Value Revisited: Teaching New Tricks to an Old Dog.” *Journal of Neural Engineering* 15(5):1–19.

Buzsáki, G. 1989. “Two-Stage Model of Memory Trace Formation: A Role for ‘Noisy’ Brain States.” *Neuroscience*.

Buzsáki, György. 2004. “Large-Scale Recording of Neuronal Ensembles.” *Nature Neuroscience* 7(5):446–51.

Buzsáki, György. 2005. “Theta Rhythm of Navigation: Link between Path Integration and Landmark Navigation, Episodic and Semantic Memory.” *Hippocampus* 15(7):827–40.

Buzsáki, György and Kenji Mizuseki. 2014. “The Log-Dynamic Brain: How Skewed Distributions Affect Network Operations.” *Nature Reviews Neuroscience* 15(4):264–78.

Canny, John. 1986. “A Computational Approach to Edge Detection.” *IEEE Transactions on Pattern Analysis and Machine Intelligence* PAMI-8(6):679–98.

Cave, Carolyn Backer and Larry R. Squire. 1992. “Intact Verbal and Nonverbal Short-term Memory Following Damage to the Human Hippocampus.” *Hippocampus*.

Cho, Seongeun, Andrew Wood, and Mark R. Bowlby. 2007. “Brain Slices as Models for Neurodegenerative Disease and Screening Platforms to Identify Novel Therapeutics.” *Current Neuropharmacology* 5:19–33.

Claiborne, Brenda J., David G. Amaral, and W. Maxwell Cowan. 1986. “A Light and Electron Microscopic Analysis of the Mossy Fibers of the Rat Dentate Gyrus.” *Journal of Comparative Neurology*.

Csicsvari, Jozsef, Darrell a Henze, Brian Jamieson, Kenneth D. Harris, Anton Sirota, Péter Barthó, Kensall D. Wise, and György Buzsáki. 2003. “Massively Parallel Recording of Unit and Local Field Potentials with Silicon-Based Electrodes.” *Journal of Neurophysiology* 90:1314–23.

Dabrowski, W., P. Grybos, and A. M. Litke. 2004. “A Low Noise Multichannel Integrated Circuit for Recording Neuronal Signals Using Microelectrode Arrays.” *Biosensors and Bioelectronics* 19(7):749–61.

Davis, S., S. P. Butcher, and R. G. Morris. 1992. “The NMDA Receptor Antagonist D-2-Amino-5-Phosphonopentanoate (D-AP5) Impairs Spatial Learning and LTP in Vivo at Intracerebral Concentrations Comparable to Those That Block LTP in Vitro.” *The Journal of Neuroscience : The Official Journal of the Society for Neuroscience* 12(1):21–34.

Egert, U. and H. Hämmerle. 2002. “Application of the Microelectrode-Array (MEA) Technology in Pharmaceutical Drug Research.” *Sensoren Im Fokus Neuer Anwendungen* 51–54.

Eversmann, Björn, Armin Lambacher, Thomas Gerling, Alexander Kunze, Peter Fromherz, and Roland Thewes. 2011. “A Neural Tissue Interfacing Chip for In-Vitro Applications with 32k Recording / Stimulation Channels on an Active Area of 2.6 Mm 2.” Pp. 211–14 in *European Solid-State Circuits Conference*.

Ferrea, E., a Maccione, L. Medrihan, T. Nieus, D. Ghezzi, P. Baldelli, F. Benfenati, and L. Berdondini. 2012. “Large-Scale, High-Resolution Electrophysiological Imaging of Field Potentials in Brain Slices with Microelectronic Multielectrode Arrays.” *Frontiers in Neural Circuits* 6(November):80.

Gaarskjaer, Frank B. 1978. “Organization of the Mossy Fiber System of the Rat Studied in Extended Hippocampi. II. Experimental Analysis of Fiber Distribution with Silver Impregnation Methods.” *Journal of Comparative Neurology*.

Gibb, Alasdair J. and Frances a Edwards. 1994. “Patch Clamp Recording from Cells in Sliced Tissues.” *Microelectrode Techniques, The Plymouth Workshop Handbook* 255–74.

Goff, D. 2016. “The Therapeutic Role of D -Cycloserine in Schizophrenia.” *Neuropsychopharmacology: A Tribute to Joseph T. Coyle* 76:39–66.

Grastyan, E. and G. Karmos. 1961. “A Study of a Possible ‘Dreaming’ Mechanism in the Cat.” *Acta Physiologica Academiae Scientiarum Hungaricae* 20:41–50.

Gross, G. W., E. Rieske, G. W. Kreutzberg, and A. Meyer. 1977. “A New Fixed-Array Multi-Microelectrode System Designed for Long-Term Monitoring of Extracellular Single Unit Neuronal Activity in Vitro.” *Neuroscience Letters*.

Gross, Guenter. 2011. “Multielectrode Arrays.” *Scholarpedia* 6(3):5749.

Gross, Guenter W. 1979. “Simultaneous Single Unit Recording in Vitro with a Photoetched Laser Deinsulated Gold Multimicroelectrode Surface.” *IEEE Transactions on Biomedical Engineering*.

Gryboś, Paweł, Piotr Kmon, Mirosław Zołądź, Robert Szczygieł, Maciej Kachel, Marian Lewandowski, and Tomasz Błasiak. 2011. “64 Channel Neural Recording Amplifier with Tunable Bandwidth in 180 Nm CMOS Technology.” *Metrology and Measurement Systems* 18(4):631–44.

Gunning, D. E., C. J. Kenney, A. M. Litke, and K. Mathieson. 2009. “High Spatial Resolution Probes for Neurobiology Applications.” *Nuclear Instruments and Methods in Physics Research, Section A: Accelerators, Spectrometers, Detectors and Associated Equipment* 604(1–2):104–7.

Hájos, Norbert, Tommas J. Ellender, Rita Zemankovics, Edward O. Mann, Richard Exley, Stephanie J. Cragg, Tamás F. Freund, and Ole Paulsen. 2009. “Maintaining Network Activity in Submerged Hippocampal Slices: Importance of Oxygen Supply.” *European Journal of Neuroscience*

29(2):319–27.

Hájos, Norbert, Mária R. Karlócai, Beáta Németh, István Ulbert, Hannah Monyer, Gábor Szabó, Ferenc Erdélyi, Tamás F. Freund, and Attila I. Gulyás. 2013. “Input-Output Features of Anatomically Identified CA3 Neurons during Hippocampal Sharp Wave/Ripple Oscillation in Vitro.” *Journal of Neuroscience* 33(28):11677–91.

Hamasaki, Yuuta, Natsumi Haba, Naoki Iwata, Yoshiki Uno, and Minoru Saito. 2017. “Simultaneous Measurement of Neural Activities of Acute Mouse Hippocampal Slices Using Multi-Electrode Array System and Laser Confocal Calcium Imaging.” *Journal of Behavioral and Brain Science* 07(02):68–78.

Herreras, Oscar. 2016. “Local Field Potentials: Myths and Misunderstandings.” *Frontiers in Neural Circuits* 10(DEC):1–16.

Heuschkel, Marc Olivier, Corina Wirth, Esther Marie Steidl, and Bruno Buisson. 2006. “Development of 3-D Multi-Electrode Arrays for Use with Acute Tissue Slices.” *Advances in Network Electrophysiology: Using Multi-Electrode Arrays* 69–111.

Hierlemann, By Andreas, Urs Frey, Sadik Hafizovic, and Flavio Heer. 2011. “Growing Cells Atop Microelectronic Chips : Interfacing Electrogenic Cells In Vitro With CMOS-Based Microelectrode Arrays.” 99(2).

Hirano, T., P. Best, and J. Olds. 1970. “Units during Habituation, Discrimination Learning, and Extinction.” *Electroencephalography and Clinical Neurophysiology*.

Hofer, Katharina T., Ágnes Kandrács, István Ulbert, Ildikó Pál, Csilla Szabó, László Héja, and Lucia Wittner. 2015. “The Hippocampal CA3 Region Can Generate Two Distinct Types of Sharp Wave-Ripple Complexes, in Vitro.” *Hippocampus*.

Hutzler, M., A. Lambacher, B. Eversmann, M. Jenkner, R. Thewes, and P. Fromherz. 2006. “High-Resolution Multitransistor Array Recording of Electrical Field Potentials in Cultured Brain Slices.” *Journal of Neurophysiology* 96(3):1638–45.

Hyvärinen, Aapo and Erkki Oja. 2000. “Independent Component Analysis : Algorithms and Applications.” 1(1).

Ibi, Daisuke, Atsumi Nitta, Kumiko Ishige, Xiaobo Cen, Tomohiro Ohtakara, Toshitaka Nabeshima, and Yoshihisa Ito. 2010. “Piccolo Knockdown-Induced Impairments of Spatial Learning and Long-Term Potentiation in the Hippocampal CA1 Region.” *Neurochemistry International* 56(1):77–83.

Isaac, John T. R., Roger A. Nicoll, and Robert C. Malenka. 1995. “Evidence for Silent Synapses: Implications for the Expression of LTP.” *Neuron* 15(2):427–34.

Jiang, Huiyi, Shicheng Liu, Xinling Geng, Adam Caccavano, Katherine Conant, Stefano Vicini, and Jianyoung Wu. 2018. “Pacing Hippocampal Sharp-Wave Ripples with Weak Electric Stimulation.” *Frontiers in Neuroscience* 12(MAR):1–10.

Jouvet, Michel. 1999. “Sleep and Serotonin: An Unfinished Story.” *Neuropsychopharmacology* 21:24S-27S.

Karlócai, Mária R., Zsolt Kohus, Szabolcs Káli, István Ulbert, Gábor Szabó, Zoltán Máté, Tamás F. Freund, and Attila I. Gulyás. 2014. “Physiological Sharp Wave-Ripples and Interictal Events in Vitro: What’s the Difference?” *Brain* 137(2):463–85.

Kim, Hyun Bum, Tong In Oh, Kelley M. Swanberg, Mun Bae Lee, Tae Woo Kim, Eung Je Woo, Ji Ho Park, and Oh In Kwon. 2016. “Microelectrode Array Analysis of Hippocampal Network

Dynamics Following Theta-Burst Stimulation via Current Source Density Reconstruction by Gaussian Interpolation." *Journal of Neuroscience Methods* 264:1–10.

Kubota, Don, Laura Lee Colgin, Malcolm Casale, Fernando A. Brucher, and Gary Lynch. 2003. "Endogenous Waves in Hippocampal Slices." *Journal of Neurophysiology* 89(1):81–89.

Kuenzi, F. M., S. M. Fitzjohn, R. A. Morton, G. L. Collingridge, and G. R. Seabrook. 2000. "Reduced Long-Term Potentiation in Hippocampal Slices Prepared Using Sucrose-Based Artificial Cerebrospinal Fluid [In Process Citation]." *J.Neurosci.Methods* 100(1–2):117–22.

Lacaille, J. C., A. L. Mueller, D. D. Kunkel, and P. A. Schwartzkroin. 1987. "Local Circuit Interactions between Oriens/Alveus Interneurons and CA1 Pyramidal Cells in Hippocampal Slices: Electrophysiology and Morphology." *Journal of Neuroscience* 7(7):1979–93.

Lee, Dd and Hs Seung. 2001. "Algorithms for Non-Negative Matrix Factorization." *Advances in Neural Information Processing Systems* (1):556–62.

Liu, Ming-Gang, Hu-Song Li, Wei-Guang Li, Yan-Jiao Wu, Shi-Ning Deng, Chen Huang, Oleksandr Maximyuk, Volodymyr Sukach, Oleg Krishtal, Michael X. Zhu, and Tian-Le Xu. 2016. "Acid-Sensing Ion Channel 1a Contributes to Hippocampal LTP Inducibility through Multiple Mechanisms." *Scientific Reports* 6:23350.

Liu, Ming Gang, Xue Feng Chen, Ting He, Zhen Li, and Jun Chen. 2012. "Use of Multi-Electrode Array Recordings in Studies of Network Synaptic Plasticity in Both Time and Space." *Neuroscience Bulletin* 28(4):409–22.

Lomo, T. 2003. "The Discovery of Long-Term Potentiation." *Philosophical Transactions of the Royal Society B: Biological Sciences* 358(1432):617–20.

Lømo, T. 1966. "Frequency Potentiation of Excitatory Synaptic Activity in the Dentate Area of the Hippocampal Formation." *Acta Physiologica Scandinavica* 68((suppl. 277)):128.

Lu, Yun Fei, Yan Wang, Ying He, Fu Kang Zhang, Ting He, Rui Rui Wang, Xue Feng Chen, Fei Yang, Ke Rui Gong, and Jun Chen. 2014. "Spatial and Temporal Plasticity of Synaptic Organization in Anterior Cingulate Cortex Following Peripheral Inflammatory Pain: Multi-Electrode Array Recordings in Rats." *Neuroscience Bulletin* 30(1):1–20.

Luscher, C. and R. C. Malenka. 2012. "NMDA Receptor-Dependent Long-Term Potentiation and Long-Term Depression (LTP/LTD)." *Cold Spring Harbor Perspectives in Biology* 4(6):a005710–a005710.

Lynch, M. A. 2004. "Long-Term Potentiation and Memory." 87–136.

Maccione, Alessandro, Matthias H. Hennig, Mauro Gandolfo, Oliver Muthmann, James van Coppenhagen, Stephen J. Eglen, Luca Berdondini, and Evelyne Sernagor. 2014. "Following the Ontogeny of Retinal Waves: Pan-Retinal Recordings of Population Dynamics in the Neonatal Mouse." *The Journal of Physiology* 592(7):1545–63.

Maier, N., V. Nimmrich, and A. Draguhn. 2003. "Cellular and Network Mechanisms Underlying Spontaneous Sharp Wave-Ripple Complexes in Mouse Hippocampal Slices." *The Journal of Physiology* 550(3):873–87.

Maier, Nikolaus, Genela Morris, Sebastian Schuchmann, Tatiana Korotkova, Alexey Ponomarenko, Claudia Böhm, Christian Wozny, and Dietmar Schmitz. 2012. "Cannabinoids Disrupt Hippocampal Sharp Wave-Ripples via Inhibition of Glutamate Release." *Hippocampus* 22(6):1350–62.

Martin, S. J., P. D. Grimwood, and R. G. M. Morris. 2000. "Synaptic Plasticity and Memory: An

Evaluation of the Hypothesis." *Annual Review of Neuroscience* 23(1):649–711.

Maslarova, Anna, Kristina Lippmann, Seda Salar, Anton Rösler, and Uwe Heinemann. 2015. "Differential Participation of Pyramidal Cells in Generation of Spontaneous Sharp Wave-Ripples in the Mouse Subiculum in Vitro." *Neurobiology of Learning and Memory* 125:113–19.

Mayer, Mark L., Gary L. Westbrook, and Peter B. Guthrie. 1984. "Voltage-Dependent Block by Mg 2+ of NMDA Responses in Spinal Cord Neurones." *Nature* 309(5965):261–63.

Mitzdorf, U. 1985. "Current Source-Density Method and Application in Cat Cerebral Cortex: Investigation of Evoked Potentials and EEG Phenomena." *Physiological Reviews* 65(1):37–100.

Nicoll, Roger A. 2017. "Review A Brief History of Long-Term Potentiation." *Neuron* 93(2):281–90.

Nimmrich, V., N. Maier, D. Schmitz, and A. Draguhn. 2005. "Induced Sharp Wave-Ripple Complexes in the Absence of Synaptic Inhibition." *J.Physiol* (0022–3751).

Nowak, L., P. Bregestovski, P. Ascher, A. Herbet, and A. Prochiantz. 1984. "Magnesium Gates Glutamate-Activated Channels in Mouse Central Neurones." *Nature* 307(5950):462–65.

O'Keefe, J. and J. Dostrovsky. 1971. "The Hippocampus as a Spatial Map. Preliminary Evidence from Unit Activity in the Freely-Moving Rat." *Brain Research*.

Oka, Hiroaki, Ken Shimono, Ryuta Ogawa, Hirokazu Sugihara, and Makoto Taketani. 1999. "A New Planar Multielectrode Array for Extracellular Recording: Application to Hippocampal Acute Slice." *Journal of Neuroscience Methods* 93(1):61–67.

Oliva, Azahara, Antonio Fernández-Ruiz, György Buzáski, and Antal Berényi. 2016. "Role of Hippocampal CA2 Region in Triggering Sharp-Wave Ripples." *Neuron* 91(6):1342–55.

Pálhalmi, J., O. Paulsen, T. F. Freund, and N. Hájos. 2004. "Distinct Properties of Carbachol- and DHPG-Induced Network Oscillations in Hippocampal Slices." *Neuropharmacology* 47(3):381–89.

Papatheodoropoulos, C. 2010. "Patterned Activation of Hippocampal Network (~10 Hz) during in Vitro Sharp Wave-Ripples." *Neuroscience* 168(2):429–42.

Papatheodoropoulos, Costas. 2007. "NMDA Receptor-Dependent High-Frequency Network Oscillations (100-300 Hz) in Rat Hippocampal Slices." *Neuroscience Letters* 414(3):197–202.

Papatheodoropoulos, Costas and George Kostopoulos. 2002. "Spontaneous, Low Frequency (Approximately 2-3 Hz) Field Activity Generated in Rat Ventral Hippocampal Slices Perfused with Normal Medium." *Brain Research Bulletin* 57(2):187–93.

Pettersen, Klas H., Anna Devor, Istvan Ulbert, Anders M. Dale, and Gaute T. Einevoll. 2006. "Current-Source Density Estimation Based on Inversion of Electrostatic Forward Solution: Effects of Finite Extent of Neuronal Activity and Conductivity Discontinuities." *Journal of Neuroscience Methods* 154(1–2):116–33.

Pettersen, Klas H. and Gaute T. Einevoll. 2008. "Amplitude Variability and Extracellular Low-Pass Filtering of Neuronal Spikes." *Biophysical Journal* 94(3):784–802.

Pine, Jerome. 1980. "Recording Action Potentials from Cultured Neurons with Extracellular Microcircuit Electrodes." 2:19–31.

Potworowski, Jan, Wit Jakuczun, Szymon Łeski, and Daniel Wójcik. 2012. "Kernel Current Source Density Method." *Neural Computation* 24(2):541–75.

Ranck, James B. 1973. "Studies on Single Neurons in Dorsal Hippocampal Formation and Septum in Unrestrained Rats. Part I. Behavioral Correlates and Firing Repertoires." *Experimental*

Neurology.

Rokach, Lior, and Oded Maimon. 2005. *Clustering Methods.Data Mining and Knowledge Discovery Handbook.* Springer US.

Rouaud, E. and J. M. Billard. 2003. "D-Cycloserine Facilitates Synaptic Plasticity but Impairs Glutamatergic Neurotransmission in Rat Hippocampal Slices." *British Journal of Pharmacology* 140(6):1051–56.

Schlingloff, D., S. Kali, T. F. Freund, N. Hajos, and A. I. Gulyas. 2014. "Mechanisms of Sharp Wave Initiation and Ripple Generation." *Journal of Neuroscience* 34(34):11385–98.

Schreurs, An, Victor Sabanov, and Detlef Balschun. 2017. "Distinct Properties of Long-Term Potentiation in the Dentate Gyrus along the Dorsoventral Axis: Influence of Age and Inhibition." *Scientific Reports* 7(1):1–10.

Schwartzkroin, Philip A. and Knut Wester. 1975. "Long-Lasting Facilitation of a Synaptic Potential Following Tetanization in the in Vitro Hippocampal Slice." *Brain Research* 89:107–19.

Sirota, A., J. Csicsvari, D. Buhl, and G. Buzsaki. 2003. "Communication between Neocortex and Hippocampus during Sleep in Rodents." *Proceedings of the National Academy of Sciences* 100(4):2065–69.

Skrede, Knut Kr and Rolf H. Westgaard. 1971. "The Transverse Hippocampal Slice: A Well-Defined Cortical Structure Maintained in Vitro." *Brain Research* 35(2):589–93.

Stam, Cornelis J., Guido Nolte, and Andreas Daffertshofer. 2007. "Phase Lag Index: Assessment of Functional Connectivity from Multi Channel EEG and MEG with Diminished Bias from Common Sources." *Human Brain Mapping* 28(11):1178–93.

Stangl, Christian and Peter Fromherz. 2008. "Neuronal Field Potential in Acute Hippocampus Slice Recorded with Transistor and Micropipette Electrode." *European Journal of Neuroscience* 27(4):958–64.

Stark, Eran, Lisa Roux, Ronny Eichler, Yuta Senzai, Sebastien Royer, and Gy??rgy Buzs??ki. 2014. "Pyramidal Cell-Interneuron Interactions Underlie Hippocampal Ripple Oscillations." *Neuron* 83(2):467–80.

Steward, Oswald and Sheila A. Scoville. 1976. "Cells of Origin of Entorhinal Cortical Afferents to the Hippocampus and Fascia Dentata of the Rat." *Journal of Comparative Neurology*.

Stumpf, Ch. 1965. "The Fast Component in the Electrical Activity of Rabbit's Hippocampus." *Electroencephalography and Clinical Neurophysiology*.

Swanson, L. W., J. M. Wyss, and W. M. Cowan. 1978. "An Autoradiographic Study of the Organization of Intrahippocampal Association Pathways in the Rat." *Journal of Comparative Neurology*.

Szeliski, Richard. 2010. *Computer Vision: Algorithms and Applications*.

Thiébaud, P., N. F. De Rooij, M. Koudelka-Hep, and L. Stoppini. 1997. "Microelectrode Arrays for Electrophysiological Monitoring of Hippocampal Organotypic Slice Cultures." *IEEE Transactions on Biomedical Engineering* 44(11):1159–63.

Thomas, C., P. Springer, G. Loeb, Y. Berwald-Netter, and L. Okun. 1972. "A Miniature Microelectrode Array to Monitor the Bioelectric Activity of Cultured Cells." *Experimental Cell Research* 74(1):61–66.

Vanderwolf, C. H. 1969. "Hippocampal Electrical Activity and Voluntary Movement in the Rat."

Electroencephalography and Clinical Neurophysiology.

Vivar, Carmen, Benjamin D. Peterson, and Henriette van Praag. 2016. "Running Rewires the Neuronal Network of Adult-Born Dentate Granule Cells." *NeuroImage* 131:29–41.

Volianskis, Arturas, Grace France, Morten S. Jensen, Zuner A. Bortolotto, David E. Jane, and Graham L. Collingridge. 2015. "Long-Term Potentiation and the Role of N-Methyl-D-Aspartate Receptors." *Brain Research* 1621:5–16.

Wang, Huifang E., Christian G. Bénar, Pascale P. Quilichini, Karl J. Friston, Viktor K. Jirsa, and Christophe Bernard. 2014. "A Systematic Framework for Functional Connectivity Measures." *Frontiers in Neuroscience* 8(DEC):1–22.

Wójtowicz, Anna Maria, Leander Den Van Boom, Arnab Chakrabarty, Nicola Maggio, Rizwan U. Haq, Christoph J. Behrens, and Uwe Heinemann. 2009. "Monoamines Block Kainate- And Carbachol-Induced. γ-Oscillations but Augment Stimulus-Induced γ-Oscillations in Rat Hippocampus in Vitro." *Hippocampus* 19(3):273–88.

Womelsdorf, Thilo, Jan Mathijs Schoffelen, Robert Oostenveld, Wolf Singer, Robert Desimone, Andreas K. Engel, and Pascal Fries. 2007. "Modulation of Neuronal Interactions through Neuronal Synchronization." *Science* 316(5831):1609–12.

Wu, Chiping, Marjan Nassiri Asl, Jesse Gillis, Frances K. Skinner, and Liang Zhang. 2005. "An in Vitro Model of Hippocampal Sharp Waves: Regional Initiation and Intracellular Correlates." *Journal of Neurophysiology* 94(1):741–53.

Xing, Dajun, Chun I. Yeh, and Robert M. Shapley. 2009. "Spatial Spread of the Local Field Potential and Its Laminar Variation in Visual Cortex." *Journal of Neuroscience* 29(37):11540–49.

Yeckel, M. F. and T. W. Berger. 1998. "Spatial Distribution of Potentiated Synapses in Hippocampus: Dependence on Cellular Mechanisms and Network Properties." *The Journal of Neuroscience : The Official Journal of the Society for Neuroscience* 18(1):438–50.